TECHNICAL REPORT

WAKES OF LIFTING PROPELLERS (ROTORS) IN GROUND EFFECT

By: F.A. DuWaldt

CAL No. BB-1665-S-3

Prepared for:

Air Programs
Naval Applications Group
Office of Naval Research
Washington, D.C. 20360

$1.00 .65 96 as

Final Report
ONR Contract No. Nonr 3691(00)
November 1966

CORNELL AERONAUTICAL LABORATORY, INC.
OF CORNELL UNIVERSITY, BUFFALO, N. Y. 14221

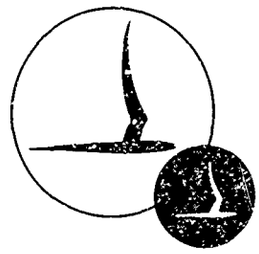

CORNELL AERONAUTICAL LABORATORY, INC.
BUFFALO, NEW YORK 14221

FINAL REPORT
WAKES OF LIFTING PROPELLERS (ROTORS) IN GROUND EFFECT

by

F. A. DuWaldt

CAL REPORT NO. BB-1665-S-3

ONR CONTRACT NO. Nonr 3691(00)

NOVEMBER 1966

Prepared for:

AIR PROGRAMS
NAVAL APPLICATIONS GROUP
OFFICE OF NAVAL RESEARCH
WASHINGTON, D. C. 20360

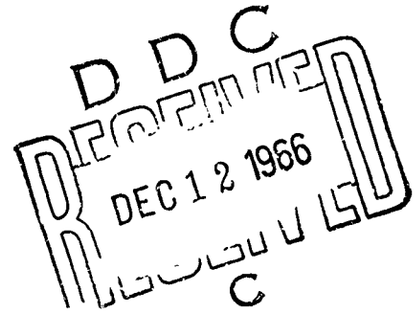

BLANK PAGE

FOREWORD

Cornell Aeronautical Laboratory, Inc. (CAL), Buffalo, New York, performed the research reported herein for Air Programs, Naval Applications Group, Office of Naval Research, Washington, D. C. 20360, under ONR Contract Nonr 3691(00). Dr. P. Crimi of CAL conducted the study, with assistance from Mr. W. G. Brady. Mr. Harvey Selib was responsible for the preparation of the digital machine program. The program was under the supervision of Mr. F. DuWaldt who prepared this summary report.

The work was performed from February 1965 through May 1966 and is a continuation of the work described in CAL Report BB-1665-S-2, "Representation of Propeller Wakes by Systems of Finite Core Vortices", by W. G. Brady and P. Crimi, issued under ONR Contract Nonr 3691(00), February 1965 (DDC No. 612007). As an outgrowth of this research, a companion study on rotor flow fields (in the absence of a ground effect) was performed for the U. S. Army Ballistic Research Laboratories (Contract No. DA 30-069-AMC-645(R)) by Dr. P. Crimi and Mr. A. Sowyrda and published in two volumes:

1. Crimi, P. Theoretical Prediction of the Flow in the Wake of a Helicopter Rotor Part 1 - Development of Theory and Results of Computations CAL Report No. BB-1994-S-1 September 1965

2. Crimi, P. Theoretical Prediction of the Flow in the Wake of a Helicopter Rotor Part 2 - Formulation and Application of the Rotor-Wake Flow Computer Program CAL Report No. BB-1994-S-2 September 1965

The analyses reported herein (in which the effect of ground proximity is included) are similar to those used in the companion study since both stem from the model developed by W. G. Brady, P. Crimi, and A. Sowyrda under ONR Contract Nonr 3691(00).

ABSTRACT

This is a summary report that presents the development of a wake model for a lifting propeller (rotor) in ground effect and the computational procedure used to determine the spacial distribution of wake vorticity and the induced velocity field accompanying that vorticity distribution.

Sample calculations for a two-bladed rotor were carried out on an IBM 7044 computer. Locations of wake vortical elements and the associated induced velocities at selected field points are presented for advance ratios of 0, 0.02, 0.05, and 0.10 for an $\frac{H}{R}$ (ratio of rotor height above ground to rotor radius) of 1.0. Also, a few results for a hovering case with $\frac{H}{R} = 0.5$ are presented. A calculated root-mean-square velocity map is compared with measured hovering data (time averaged) and good agreement is obtained in the outer half of the slipstream. The implications of computed results with respect to the flow field at a horizontal stabilizer or tail rotor are noted as examples of the use of the model.

The wake vortex model used for these calculations is a distorted continuous helix emanating from each blade tip. For purposes of numerical calculation of mutual vortex interference effects, the continuous vortex is approximated by short straight-line filaments. For purposes of numerical calculation of self-induced effects (that is, the effect of an element on itself), the local element curvature and the core diameter are estimated. The Fortran statements of the computer program are presented in the Appendix.

BLANK PAGE

TABLE OF CONTENTS

ILLUSTRATIONS

SYMBOLS

a	ratio of vortex core radius to rotor radius, $\frac{\bar{a}}{R}$
H/R	ratio of height of rotor hub above ground to rotor radius
N_B	number of rotor blades
ρ	air density
P_i	designation for i^{th} wake reference point
R	rotor radius
$\mathcal{R}$	radius of curvature of a vortex tube
$\underline{r}$	position vector of a point in the flow
Δt	incremental time
V_{S_i}	self-induced velocity of a vortex element
(V_x, V_y, V_z)	components of fluid velocity in the directions of x, y and z, respectively, nondimensionalized by $\lambda \Omega R$
$(\overline{V}_{x_i}, \overline{V}_{y_i}, \overline{V}_{z_i})$	time averages of V_x, V_y and V_z respectively
$\underline{V}_f$	free-stream velocity
$\underline{V}$	local fluid velocity
$\overline{V}_r$	time average of the radial velocity
v	induced downwash
$\overline{v}$	time average of v
$\overline{v}_o$	momentum value for the time average of v
W	aircraft weight
(x, y, z)	rectilinear coordinates with origin in the tip-path plane, nondimensionalized by R

α_T	inclination of the free stream to the tip-path plane
Γ	circulation
λ	blade loading parameter; $\lambda = 4W/(\pi^2 N_B \rho \Omega^2 R^4)$
μ	advance ratio; $\mu = V_f/(\Omega R)$
ψ	rotor azimuth angle
Ω	rotor angular speed
$\omega(y)$	magnitude of distributed trailing vorticity in a wing wake

BLANK PAGE

INTRODUCTION

Position and structure of the vortical wake of a propeller (rotor) are important considerations in many practical problems. Among these are (1) calculation of rotor aerodynamics for the purpose of estimating performance, blade dynamic response, and stability and control derivatives; (2) prediction of the flow field in which auxiliary devices operate; (3) estimation of rotor-induced loads on aircraft structures other than the rotor; (4) estimation of the potential for entrainment and transport of ground debris or water droplets; and (5) correction of wind-tunnel data for wall effects. When an actuator is in an axial-flight condition and the free-stream velocity is large compared to the wake-induced velocities, approximate techniques can be used in analyzing the effect of the wake structure relative to the various problem areas indicated above. However, when an actuator is in slow speed flight and/or is highly yawed, the wake structure becomes an important influence. Of particular importance in this latter category are the flow fields associated with VTOL aircraft in the near-hovering condition when the actuator axis is approximately perpendicular to a nearby ground plane. It is to this problem that the current research was directed.

Mathematical description of the flow field for a rotor is made difficult by the interdependence of the solution and the wake position -- that is, the boundary condition is known but the location of the boundary is not known. This situation is characteristic of problems that can be generally classified as "free-boundary problems". The method of solution that can sometimes be used on this class of problems is to guess the position of the boundary, compute the solution, and determine if the computed solution is consistent with the assumed boundary location. This approach is based on the use of space coordinates as independent variables and the computation is cast as some sort of feedback scheme in which the differences between the assumed boundary location and the resulting solution are used to determine a new

estimated boundary position. The technique involved in the current studies is slightly different. Advantage is taken of the azimuthal periodicity of the rotor position and the independent variable is chosen to be time (or azimuthal angle of a reference blade). The point of view, then, is that "new" elements of wake vorticity are generated as the blading rotates and translates. These elements are convected with velocities determined by their self-induced velocities as well as velocities induced by the existing wake structure, the bound vorticity of the blade, and the image vortices introduced to satisfy the ground-plane boundary condition. It is reasonable to assume that, eventually, a stabilized periodic wake array would be obtained since the condition of a fixed periodic blade loading was imposed. This is, however, not always the case -- this situation will be pointed out in the discussion of the sample calculations. It is believed that the lack of perfect periodicity in the solutions is a result of the truncation of the wake extent; but the possibility of a computational -- or even physical -- instability for some cases cannot be completely discounted.

Initial effort in this research task was devoted to the special case of actuators hovering near a ground plane (Reference 1). The wake structure was assumed to be representable by discrete concentric planar vortex rings of finite core diameter. Image rings were used to enforce the ground-plane boundary condition. This model subsequently has been used in the estimation of slipstream envelopes for propellers at zero advance ratio (Reference 2).

Vortex rings were useful devices in analyzing hovering cases because the requirement for axial symmetry gave assurance that the rings would remain planar. In the presence of a free-stream velocity having a component parallel to the actuator plane, however, the axial symmetry disappears and the advantage of the ring representation is lost. Therefore, the continuous distorted helix (recommended in Reference 1) was selected as the model for the current effort. Again, the ground-plane boundary condition was enforced by the influence of an image wake.

A recently completed study (References 3 and 4) has shown that the distorted helix model yields time-averaged velocities that agree well with measurements made in and about a helicopter rotor wake (in the absence of an appreciable ground effect). No check could be made of the ability of the model to represent the time variations of the velocities because measurements are not available.

The digital machine computing program is based on the assumption that the rotor is in steady level flight (or hovering) with specified tip-path-plane angle. Shaft rotational speed, rotor force, initial vortex core diameter, number of blades and the ratio of rotor radius to height above the ground are also inputs. Information relative to the computing program is given in the Appendix.

GENESIS OF THE IDEALIZED MODEL

A detailed analysis of a propeller or rotor flow field in general form would be prohibitively expensive in terms of man-power required and computing costs. It is necessary, therefore, to idealize the physical situation in order to reduce the mathematical complexity. Ultimate justification for the validity of the simplifications introduced rests upon the comparison of the essential quantities with experimental observables or comparison with a more representative analytical model.

The fluid velocities depend primarily upon the effects of the rotor blades, their wake, and the ground boundary proximity. The effects are, of course, interrelated but, for purposes of discussion, will be considered separately.

Rotor or propeller blades may be regarded as high-aspect-ratio wings in a harmonically varying stream. The actuator lift must be approximately equal to the weight of the aircraft. Therefore, the circulation about a given blade must be a harmonic function of azimuth. The radial variation of circulation depends on blade twist, planform, and the influence of the wake. Nonetheless, results of theoretical computations of harmonic air loads and measurements (Reference 5) indicate that the radial variation of circulation is approximately elliptical.

The wake of each blade is a thin sheet of vortical fluid. When the rotor is translating, the vorticity in the sheet has two components (shed vortices initially parallel to the spanwise direction and trailing vortices initially parallel to the chordwise direction). Flow visualization studies indicate that the sheet rolls up within a few chord lengths of the blade to form a single concentrated vortex trailing from near the tip of the blade (see, for example, Reference 6). Theoretically, a similar vortex should arise from the vicinity of the blade root. However, published smoke pictures

as well as an analytical treatment of the wake of a hovering rotor lead to the tentative conclusion (Reference 1) that the root vortex is rapidly convected away from the rotor and/or dissipated.

The effect of the ground can be accounted for by the introduction of an image vortex for every element of the vorticity in the fluid. In this way, the ground boundary condition (the vanishing of the normal velocity component) is satisfied.

The above observations lead to the idealized model used for computational purposes. The fluid is considered to be inviscid and incompressible.

First, the rotor blades are replaced by radial line vortices whose strengths vary once per revolution ($\Gamma \sim 1 - 2\mu \sin\psi$). Blade-induced effects will be reasonably reproduced except in the immediate vicinity of the blades. The neglect of higher harmonic variations of blade circulation is not expected to be important in comparison with the wake effects for field points not too close to the blading. As a consequence of this representation, the blade loading can be regarded as a known quantity.

Second, the wake is idealized as individual free vortices, one trailing from the tip of each blade. The circulation of each tip vortex varies in accordance with the (known) azimuthal variation of the blade circulation. The trailing vortices are assumed to have circular cross sections for purposes of the computation of the self-induced velocity. The effects of shed vortices and trailing root vortices (required by Kelvin's theorem) have been neglected as noted above.

Corresponding to each blade bound vortex and each wake vortex element, there is an image vortex below the ground plane.

Formulation of the digital model for the flow corresponding to the simplified model can be accomplished in a straightforward manner. A coordinate system fixed in the tip path plane is introduced (see Figure 1).

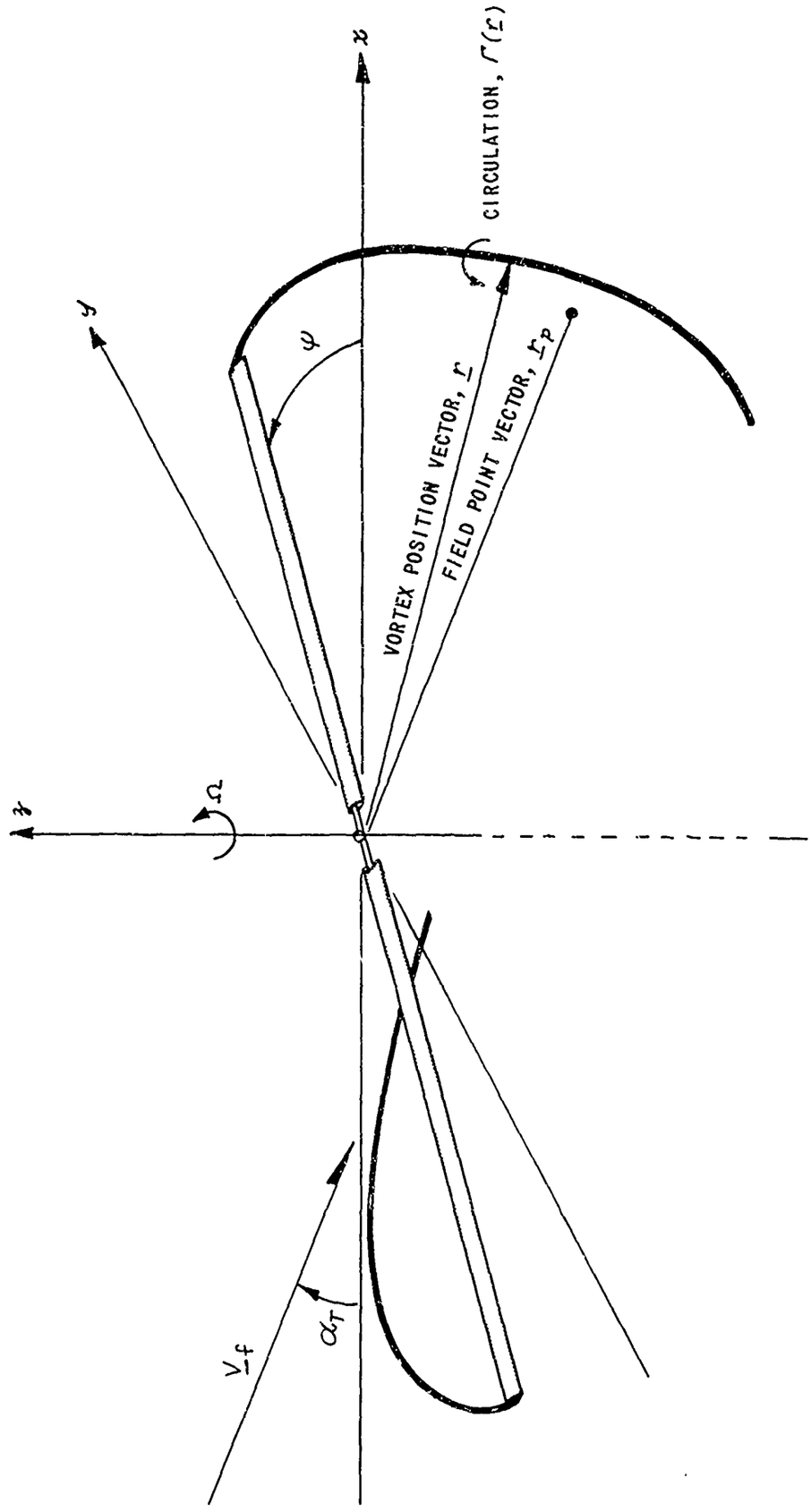

Figure 1 THE COORDINATE SYSTEM

The vector $\underline{V}_f$ in Figure 1 is the free-stream velocity (the negative of the translational velocity of the aircraft), inclined at an angle α_r to the x-axis and parallel to the x-z plane. The angle ψ denotes the azimuth position of the reference blade, and $\underline{r}_p$ is the vector positioning a given point with respect to the origin.

The fluid velocity $\underline{V}$ at a given point located by the vector $\underline{r}_p$ may be expressed in the form

$$\underline{V}(\underline{r}_p) = \frac{-1}{4\pi} \int_{C_V} \frac{\Gamma(\underline{r})\, \underline{r}_1 \times d\underline{r}}{r_1^3} \tag{1}$$

where $\underline{r}_1 = \underline{r}_p - \underline{r}$ and Γ is the circulation about the vortex element at $\underline{r}$. The line integral is to be taken over all vortices in the flow and the image system -- which paths are collectively denoted by C_V. It is necessary to modify this expression when $\underline{r}_p \equiv \underline{r}$ and this point is discussed later. The circulation, Γ, about the blade vortices is estimated directly in terms of flight parameters. The circulation about a wake vortex at a given point is simply that value assigned to the blade vortex when it was generating that segment of wake.

The only information lacking for the complete specification of the flow at a given instant, then, is the location of the wake vortices at that instant. The position of a given point on a wake vortex located by the vector $\underline{r}$ is the time integral of the velocity experienced by that fluid particle

$$\underline{r}(t) = \underline{r}(t_o) + \int_{t_o}^{t} \underline{V}(\underline{r}(\tau))\, d\tau \tag{2}$$

Thus, even after being simplified, the flow can only be obtained as the solution of the nonlinear integral equation formed by the substitution of Equation (1) into Equation (2). A direct analytical solution is not feasible but the problem is amenable to solution by numerical methods using a high-speed digital computer. The manner in which the formulations of Equations (1) and (2) were implemented for digital computation is discussed in the following section.

DESCRIPTION OF THE COMPUTATION MODEL

The idealized continuous model deduced in the previous section is replaced by a sectioned model having locally constant characteristics. Consistent with this replacement is the representation of integrals by sums. This same technique was used in Reference 3 and the following discussion follows closely that given in Reference 3.

Wake Positioning and Displacement

For purposes of numerical analysis, a series of points is marked off on each wake vortex, as shown schematically in Figure 2.

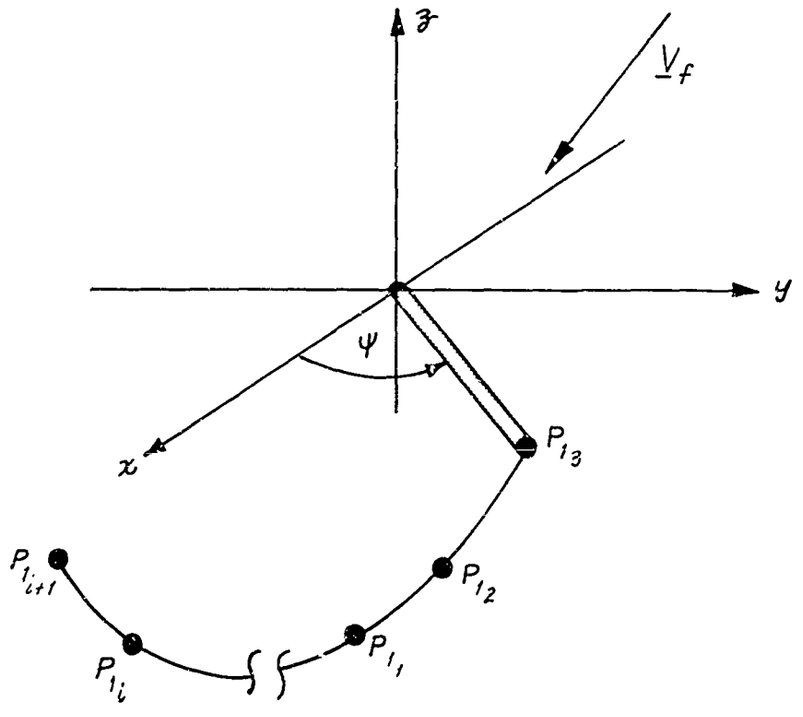

Figure 2 WAKE REFERENCE POINT IDENTIFICATION

Points are placed sufficiently close together so that, for purposes of computation of wake-induced velocities, the segment (i) of wake between points P_i and P_{i+1} may be considered to be a rectilinear vortex having constant circulation along its length. The wake spacial configuration at any instant is then defined by the locations of the end points.

Computations are initiated by specifying that each of the wake vortices lies on a prescribed curve. Generally, the curve is chosen to be a skewed helix with pitch and skew selected from simple momentum considerations. The numerical analogues to Equations (1) and (2) are then performed by first summing the velocity contributions of all vortex elements in the flow at each reference point (Equation (1)), and then convecting each point at the computed velocity for a time interval Δt (Equation (2)). The time interval Δt is chosen to correspond to a small finite change in the azimuth position, $\Delta\psi$, of the blades

$$\Delta t = \frac{\Delta\psi}{\Omega} \tag{3}$$

where Ω is rotor angular speed. Once the new coordinates of each reference point are computed, the azimuth of the blade vortices is increased by $\Delta\psi$ and the velocity computation is performed again. As the blade vortices are repositioned, a wake vortex element is added to the flow at the tip of each blade vortex, the added vortex having a length of approximately $R\Delta\psi$, where R is rotor radius. A corresponding element is dropped from the computations at the downstream end of each wake vortex, so the program is not encumbered by a wake of ever-increasing size. The computations are continued in this manner for a specified time and the results are inspected. If a nearly periodic solution is established in the space volume of interest, the calculation is terminated.

The total number of wake vortices taken into account and the magnitude of $\Delta\psi$ determine the accuracy of the flow representation at a given point. It is judged that, for a two-bladed rotor, a value for $\Delta\psi$ of thirty degrees is sufficiently small to furnish an acceptable estimate of the time variations of the flow consistent with the other approximations introduced. The number of wake elements considered depends on the region of interest and the forward speed. If the flow "near" the rotor plane is desired, then the wake generated by only a few revolutions of the rotor is needed. It has been found, for example, that with an advance ratio, μ, of about 0.25 just two revolutions of wake sufficiently define the flow near the rotor plane in the absence of a ground plane (Reference 3). At lower advance ratios, the free stream does not clear the wake from under the rotor as rapidly so more wake must be retained.

Computation of Velocity Induced by Wake and Blades

The velocity induced at an arbitrary point P by the vortices representing the wake and blades is simply the sum of the effects of an array of rectilinear vortex segments. If V_{w_i} denotes the velocity induced at P by the element between points P_i and P_{i+1}, it is found from Equation (1) that

$$V_{w_i} = \frac{\Gamma_i}{4\pi h}(\cos\theta_i - \cos\theta_{i+1}) \qquad (4)$$

where Γ_i is the strength of the element and θ_i, θ_{i+1} and h are defined in Figure 3. The velocity is directed normal to the plane containing P_i, P_{i+1} and P.

As the field point P is made to approach any point on the line joining P_i and P_{i+1} in Figure 3, the induced velocity increases without

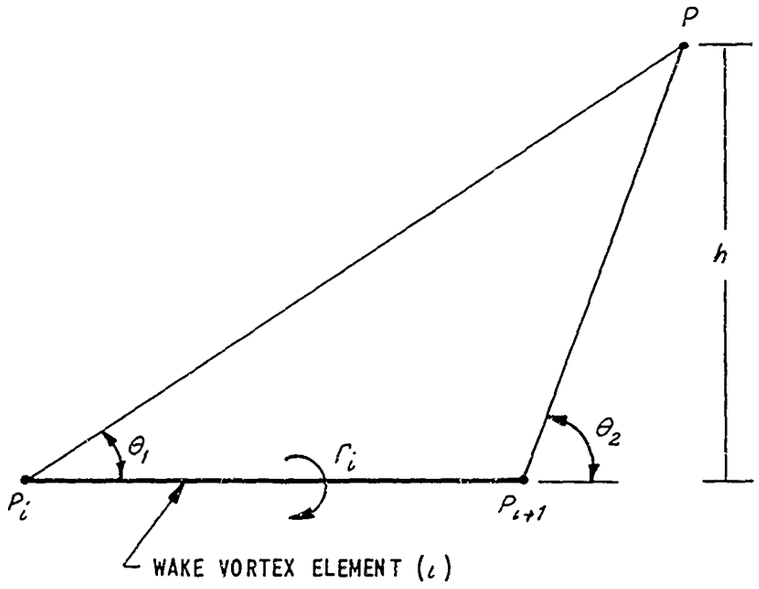

Figure 3 GEOMETRIC RELATIONSHIPS DEFINING THE FLOW INDUCED BY A RECTILINEAR VORTEX ELEMENT

limit because h tends to zero (Equation 4); the velocity becomes indeterminate for $h = 0$. The possibility that this situation will arise at an arbitrarily chosen field point is remote. Conversely, precisely this situation arises in the evaluation of the transport velocities of the ends of each of the wake vorticity elements -- that is, at points P_i and P_{i+1} in Figure 3. Now the singular behavior can be considered to have been introduced as a result of a limiting process in which a vortex element having a finite core diameter retained its strength (circulation) as the core diameter was allowed to approach zero. Evidently, this limiting process is not an admissible operation when the self-induced velocity of a vortex is sought. Therefore, for purposes of computing wake-induced flow at a given wake reference point -- i.e., a vortex joining point -- the effect of the two wake elements adjacent to that

point must be analyzed by taking core size into account (if a point lies outside the core substance of a vortex, the formula for induced velocity is the same as for a vortex with infitesimal core size; i. e., Equation (4)). The self-induced velocities also depend directly on the curvature of (the centerline of) the vortex tube at the point in question. An approximation to the actual curvature is obtained by assuming that the two elements whose effects at point P_i are to be computed lie on the circular arc which passes through points P_{i-1}, P_i and P_{i+1}, as shown in Figure 4. Then it is assumed that the two vortex segments have circular cores of rotational fluid of radii $\bar{a}_{i-1}$ and $\bar{a}_i$, respectively. Further, the approximation is made that the vorticity within the core is tangent to the arc of the tube and of a magnitude which varies linearly with distance from the center of the arc. The assumptions of a linear variation of vorticity and local tangency would seem to be admissible approximations and consistent with the prior assumptions such as the neglect of shed vorticity effects. The self-induced velocity V_{S_i} at point P_i -- i. e., the contributions of the elements adjacent to P_i -- may now be written in integral form by summing the effects of circular-arc vortex filaments of differential corss section. If it is also assumed that the core radii are much less than the radius of curvature $\mathcal{R}$, the integrand may be simplified and the integral evaluated. It is then found that

$$V_{S_i} = \frac{1}{8\pi\mathcal{R}} \left\{ \Gamma_{i-1} \left[\ln\left(\frac{8\mathcal{R}}{\bar{a}_{i-1}} \tan\frac{\phi_{i-1}}{4} \right) + \frac{1}{4} \right] + \Gamma_i \left[\ln\left(\frac{8\mathcal{R}}{\bar{a}_i} \tan\frac{\phi_i}{4} \right) + \frac{1}{4} \right] \right\} \tag{5}$$

where ϕ_{i-1} and ϕ_i are defined in Figure 4. The self-induced velocity is directed normal to the plane of the arc of the tube. The approximate core radius of a given element may be assigned on a rotational basis using energy considerations, as discussed later.

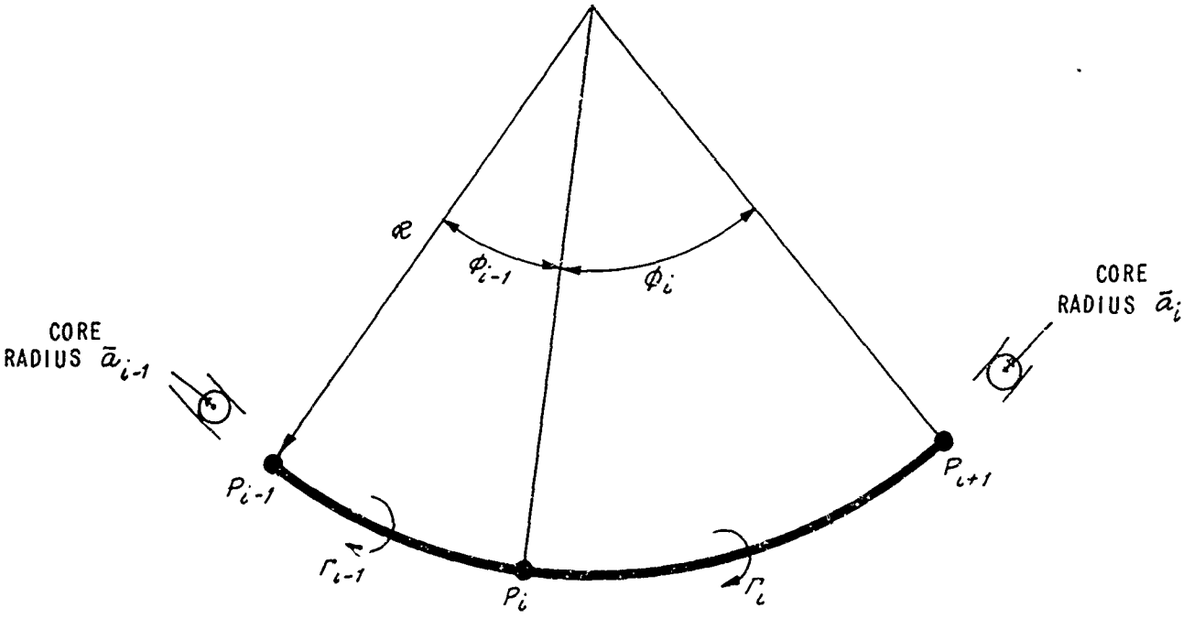

Figure 4 GEOMETRIC RELATIONSHIPS DEFINING THE SELF-INDUCED VELOCITY AT WAKE POINT P_i

Determination of System Parameters

The inputs to the calculation were nondimensionalized for purposes of coding, with lengths made dimensionless by rotor radius, R, and velocities by rotor tip speed, ΩR. The flight conditions of the aircraft being represented relate to the computer program through the following dimensionless parameters: advance ratio $\mu = \frac{V_f}{\Omega R}$, nondimensionalized blade vortex circulation $\frac{\Gamma_B}{\Omega R^2}$, tip-path-plane angle, α_T, and the ratio of wake-vortex core

radius to rotor radius, $\frac{\bar{a}}{R}$. The quantities which determine μ are, of course, generally available. Estimation of the other parameters is accomplished in the manner discussed below.

Radial Maximum of Blade Vortex Strength, $\Gamma_m(\psi)$

The circulation about a translating and rotating rotor blade at a given azimuth position ψ is actually varying in the radial direction (more or less elliptically). It was felt, though, that a sufficient approximation to blade-induced effects would be obtained by making the circulation constant spanwise and of a magnitude equal to the maximum attained on the actual blade. It might be supposed that blade-induced effects would then be somewhat exaggerated but comparisons of computed and measured flows indicate that the error introduced in the root-mean-square velocity estimate is not large enough to be discernable (See Reference 3). The error introduced in the local velocity very near the blade would, however, be expected to be relatively large.

If the circulation is assumed to vary elliptically in the spanwise direction and the advance ratio is in the normal helicopter range, the maximum circulation, Γ_m , about a blade is approximated by (neglecting root effects and making small-angle approximations where appropriate),

$$\Gamma_m \approx \frac{8 L_B(\psi)(1-2\mu \sin\psi)}{\pi \rho \Omega R^2} \tag{6}$$

where L_B is the total lift acting on the blade and ρ is the air density. Then, assuming that the total lift acting on the rotor is constant and equal to the gross weight W of the aircraft, it follows that

$$\frac{\Gamma_m}{\Omega R^2} = 2\pi\lambda(1-2\mu \sin\psi) \tag{7}$$

where λ is a blade loading parameter, defined by

$$\lambda = \frac{4W}{\pi^2 N_B \rho \Omega^2 R^4}$$

with N_B denoting the number of blades on the rotor.

Inclination of the Tip Path Plane, α_T

The tip-path-plane angle is a complicated function of flight conditions, rotor dynamics and blade pitch settings. Various methods are available for computing this angle (see, for example, Reference 7), but their use requires iterative or graphical procedures and the values of parameters which are generally not well defined.

Reasonable values for α_T have been obtained without resorting to elaborate methods by assuming the rotor resultant force to be normal to the tip-path-plane and equating the horizontal component to the fuselage drag.

$$\alpha_T \approx \frac{2C_{D_f}}{\pi N_B} \frac{\mu^2}{\lambda} \qquad (8)$$

where C_{D_f} is the fuselage drag coefficient, defined as the ratio of fuselage drag to $\frac{\pi}{2}\rho V_f^2 R^2$. Equation (8) was obtained by neglecting rotor in-plane drag and fuselage lift. The angle α_T, if assumed to be small, must then be simply the ratio of fuselage drag to rotor thrust (aircraft weight). It was noted in Reference 3 that values for α_T obtained from Equation (8) were found to be within 20 to 30 percent of measured values for a UH-1A helicopter (Reference 8) using a value for C_{D_f} of 0.014 (Reference 9).

Wake-Vortex Core Radius, $\bar{a}$

The nondimensionalized core radius of each vortex element must be specified as it is generated by a blade vortex. This core size should correspond to that of the tip vortex formed in the physical flow when the wake rolls up.

In order to obtain an estimate of the core size, three major simplifying assumptions have been made. First, all vorticity in the flow except that contained in the wake under analysis has been neglected. The justification uses the fact that, some distance from the wake, the flow before and after roll-up is effectively the same. Second, it is assumed that the wake may be considered as though it were generated by a wing of the same geometry as the blade in steady translational flight. That is, the tip and root vortices* of a rotor blade are assumed to have the same core size as the tip vortices generated by a wing of the same aspect ratio in steady translational flight, and having the same loading as the blade had when it generated the segment of wake being analyzed. Third, it is assumed that the roll-up of the wake of a wing in steady translational flight can be treated as an unsteady two-dimensional problem rather than a steady three-dimensional one. The only justification (other than intuitive argument) for the latter two assumptions is that they do yield results which appear to be realistic.

Consider, then, a wing of large aspect ratio in steady translational flight, as shown in Figure 5. If Γ denotes the circulation about the wing, then at some position in the wake upstream of the point where roll-up begins (View A-A, Figure 5), the circulation per unit length $\gamma(y)$ is given by

$$\gamma(y) = \frac{-d\Gamma}{dy} = \omega h \qquad (9)$$

where $\omega(y)$ is the magnitude of the vorticity in the wake and $h(y)$ is the thickness of the wake sheet. Given the loading on the wing -- i.e., on the rotor blade at some azimuth -- $\gamma(y)$ may then be specified through Equation (9).

---

*The net effect of the blade root vortices is neglected in the rotor calculations for reasons given previously on page 4.

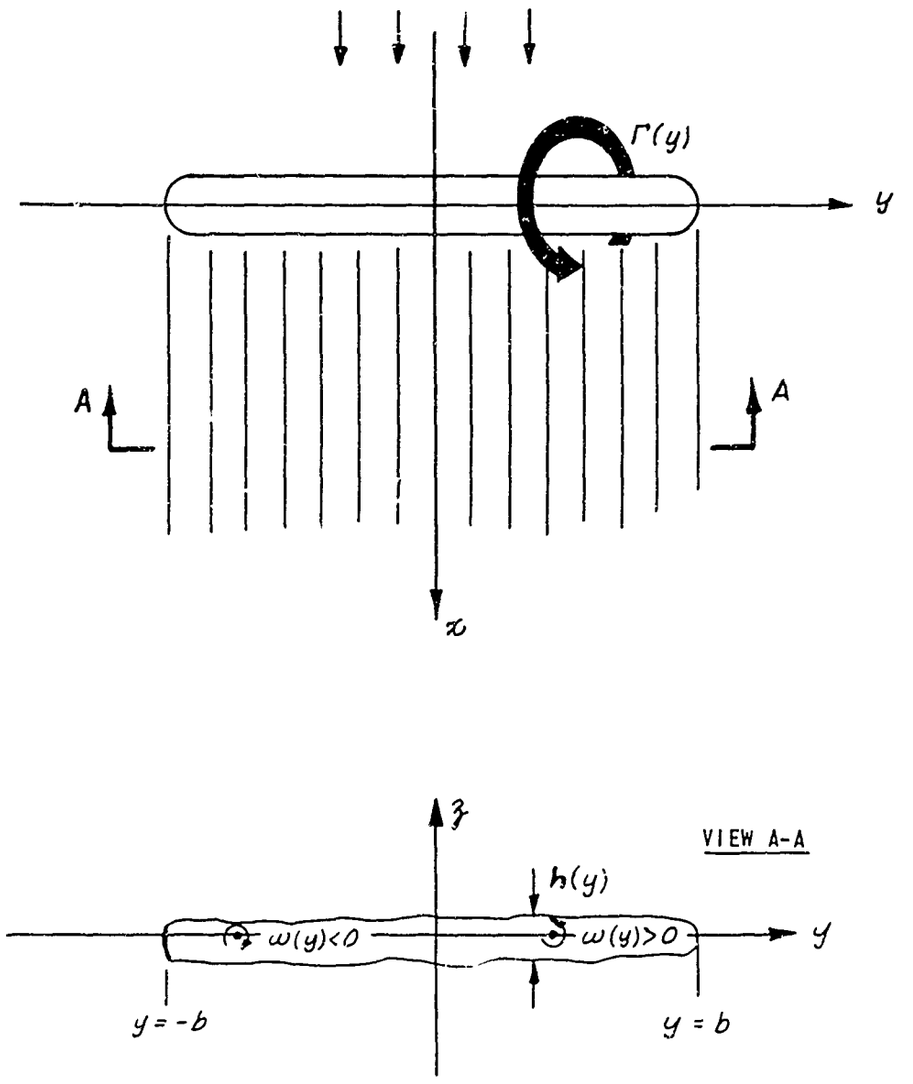

Figure 5 REPRESENTATION OF THE WAKE BEFORE ROLL-UP

Note that $\gamma = 0$ at some point, say y_o, where Γ is a maximum. Also, since $\Gamma(-b) = \Gamma(b) = 0$, $-b$ corresponding to blade root and b to blade tip, it follows that

$$-\int_{-b}^{y_o} \gamma(y)\,dy = \int_{y_o}^{b} \gamma(y)\,dy = \Gamma_m$$

where Γ_m denotes the maximum value of $\Gamma(y)$. Replacing variation in x in the wake by variation in time in a plane parallel to the y-z plane and fixed in the wake, the sheet of vorticity would be observed to roll up into a pair of vortices whose cores consist of the rotational fluid which was contained in the sheet.

This process will be assumed, in what follows, to be two dimensional. That is, the flow in the wake-fixed plane is taken to be the same as though the wake were extended to positive and negative infinity in the x-direction, and that in each plane parallel to that plane the flows are identical; or taken still another way, it is assumed that derivatives with respect to x are small in comparison to changes in y or z insofar as roll-up is concerned.

If the cores of the vortices formed by the roll-up are assumed to be of circular section and of approximately uniform vorticity, and if it is further assumed that ω is constant in the sheet before roll-up (except at y_o, where it changes sign), it follows that the core radii of the two vortices will be equal. Further, because the moment of impulse of the flow is conserved, the vortices locate on the y-axis with their respective position $y = y_2$ and $y = y_R$ given by

$$y_L = \frac{1}{(-\Gamma_m)} \int_{-b}^{y_o} y\,\gamma(y)\,dy$$

$$y_R = \frac{1}{\Gamma_m} \int_{y_o}^{b} y\,\gamma(y)\,dy \qquad (10)$$

The situation after roll-up is as shown in Figure 6.

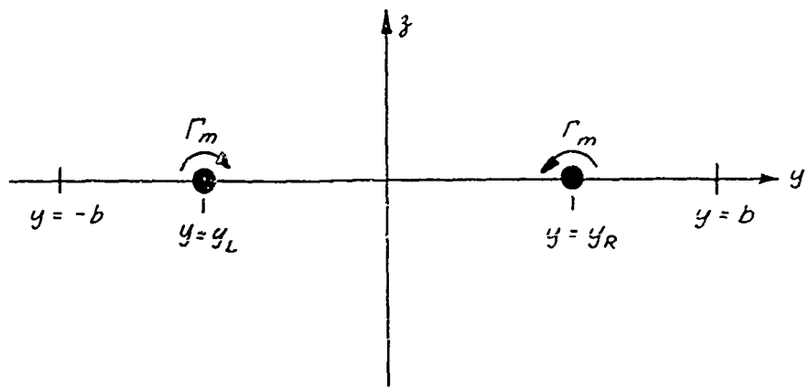

Figure 6 REPRESENTATION OF THE WAKE AFTER ROLL-UP

If viscous effects are neglected, the kinetic energy of the flow per unit depth, T, must be conserved. By deriving expressions for T for before and after roll-up and equating them, a relationship for core radius a may be obtained.

From Reference 10, T is given, in general, by

$$T = -\frac{\rho}{2}\iint \omega \Psi \, dy\,dz \tag{11}$$

where

$$\Psi(y,z) = \frac{1}{2\pi}\iint \omega \ln\left[\frac{(y-\eta)^2+(z-\zeta)^2}{b^2}\right]^{1/2} d\eta\,d\zeta$$

The integrals are taken over the entire area where ω is not zero. If $\frac{\gamma}{h}$ is substituted for ω in Equation (11) and h is assumed to be much less than b, the integrands can be simplified and the integrals evaluated. It is then

found that, in the limit of vanishing sheet thickness, Γ before roll-up is given by

$$T = -\frac{\rho}{4\pi}\int_{-b}^{b}\int_{-b}^{b}\gamma(y)\gamma(\eta)\ln\left|\frac{y-\eta}{b}\right|dy\,d\eta - \tag{12}$$

Similarly, it is found that after roll-up,

$$T = \frac{\rho\Gamma_m^2}{2\pi}\left[\ln\frac{(y_R-y_L)}{\bar{a}} + \frac{1}{4}\right] \tag{13}$$

so that the core radius is determined from

$$\ln\left(\frac{y_R-y_L}{\bar{a}}\right) = -\frac{1}{2}\int_{-b}^{b}\int_{-b}^{b}\frac{\gamma(y)\gamma(\eta)}{\Gamma_m^2}\ln\left|\frac{y-\eta}{b}\right|dy\,d\eta - \frac{1}{8} \tag{14}$$

The result of Equation (14) may be put in a form more directly related to blade circulation as follows. Let Γ be expanded in a Fourier series according to

$$\frac{\Gamma(\theta)}{\Gamma_m} = \frac{2}{\pi}\sum_{k=1}^{\infty} a_k \sin k\theta \tag{15}$$

where $\cos\theta = \frac{y}{b}$. Then

$$\gamma(\theta) = \frac{1}{b\sin\theta}\frac{d\Gamma}{d\theta}$$

$$= \frac{2\Gamma_m}{\pi b\sin\theta}\sum_{k=1}^{\infty} k a_k \cos k\theta$$

Also, it is found from Equations (10) and (15) that

$$\frac{y_R-y_L}{b} = \frac{1}{b\Gamma_m}\int_{-b}^{b} y\gamma(y)\,dy = a_1$$

If γ and $y_R - y_L$ are then substituted in Equation (14) and the integrations performed, it is found that

$$a = \frac{\bar{a}}{R} = \frac{a_1}{2}\left(1 - \frac{r_o}{R}\right) e^{-\left[\sum_{k=1}^{\infty} k a_k^2 - \frac{1}{4}\right]} \tag{16}$$

where r_o is the radial distance from the axis of revolution to the blade root.

An indication of the order of magnitude of core radius predicted by Equation (16) can be obtained by considering the case of an elliptic distribution for Γ (i.e., minimum wing induced drag, and hence maximum core radius). Supposing r_o to be zero, and substituting coefficients appropriate to the elliptic distribution ($a_1 = \frac{\pi}{2}, a_2 = \cdots a_n = 0$), find a value for a of 0.0862. This value agrees with that given in Reference 11.

Some numerical computations were performed (Reference 3), utilizing Equation (16), to determine the order of magnitude of core size predicted by this method and to provide an indication of the amount by which the core size varies with azimuth and forward speed. Data for the computations were generated by a blade-loads program that CAL developed for the U. S. Army Aviation Materiel Laboratories (these results are generally in good agreement with experimentally obtained loadings). Three flight conditions were considered: (1) a UH-1A rotor at 105 knots forward speed, (2) a UH-1A rotor at 30 knots forward speed, and (3) a 5-foot-diameter experimental rotor in hovering flight. The ratio of rotor radius to vortex core radius was calculated for four azimuth positions of the blades in each case, using a 12-point harmonic analysis of circulation distribution. The results of the computations are tabulated below.

Flight Condition	Ratio of Rotor Radius to Core Radius			
	$\psi = 0^{\circ}$	$\psi = 90^{\circ}$	$\psi = 180^{\circ}$	$\psi = 270^{\circ}$
105 knots - UH-1A	24.0	13.3	17.5	21.0
30 knots - UH-1A	18.7	15.0	14.4	24.1
Hover - 5-Foot Rotor	21.9	21.9	21.9	21.9

This method of predicting vortex core radius appears to provide a reasonable order of magnitude for that quantity -- from about 4.0 to 7.5 percent of rotor radius. Most notable is the lack of any substantial variation in core radius either with forward speed or azimuth position. The variations obtained may be considered small since a change of 20 or 30 percent in core radius produces a much smaller change in self-induced velocity, with the latter varying as the logarithm of the former. For example, with a changed from 0.05 to 0.065, the change of the self-induced velocities would be approximately 5%.

It was, therefore, possible to incorporate a major simplification in the digital computer program by assigning a representative value of 0.05 to the ratio of core radius to rotor radius, independent of azimuth position or flight conditions. It was verified (Reference 3) that this simplification does not cause an appreciable error.

RESULTS OF SAMPLE COMPUTATIONS

A few exploratory calculations were made. All were done for a two-bladed rotor. The table of conditions covered is given below.

Case No.	Advance Ratio μ	Height-to-Rotor Radius Ratio H/R	Tip-Path-Plane Tilt, α_T degrees	Loading Parameter λ	Number of Blades N_B	Tip Vortex Core Radius-to-Rotor-Radius Ratio a
1	0	0.5	0	0.00506	2	5×10^{-5}
2	0	1.0	0	0.00478	2	0.05
3	0.02	1.0	0	0.00478	2	0.05
4	0.02	1.0	0.6	0.00203	2	0.05
5	0.05	1.0	1.25	0.00203	2	0.05
6	0.10	1.0	2.50	0.00203	2	0.05

Preliminary Remarks

The computing program used in this study allowed the choice of 100 field points at which velocities could be computed. In addition, of course, the velocities at the end points of the vortex elements representing the rolled-up wake vorticity were always calculated. The program is set up in such a manner that the solution (vortex end points), after a certain running time, can be stored on punched cards so that additional calculations can be initiated without going through the whole starting process. For example, in the interest of economy, it has been the practice to run the program for a time period that corresponds to the replacement of all the initialized wake by elements which have been free to convect in the developed velocity field. That is, if the wake has been specified to consist of m revolutions per blade, the problem is run for the time equivalent of m revolutions.

At this point, the computation is stopped, the selected field-point coordinates are inserted, and the problem is restarted and run for, say, one additional rotor revolution. In this way, the computations at the field points are made only after an iterated wake position has been obtained. The problem can then be restarted again with new designators for the field points so that the velocity field appropriate for a given problem can be expanded to the extent necessary. One might, for example, be interested in computing the velocity distribution in the space volume to be occupied by the wing, fuselage, tail, and tail rotor.

The particular problem being attacked also determines the amount of computation required in the sense that the wake shape should be stabilized relative to the space volume of interest. In practice, this means that calculations along the ground plane, for example, generally require a larger wake array than the calculation of the velocity field very near the rotor plane.

The purposes of the various calculations given in Table 1 are the following:

Case 1 - Comparison of the distorted helix model results with those obtained from the vortex ring model for hovering flight (Reference 1).

Case 2 - Provides a comparison of calculated results with experimental data (time-averaged velocities).

Case 3, Case 4 - Provide an illustration of the effects of a change in actuator loading.

Case 4, Case 5, Case 6 - Show the effects of advance ratio (including the effect of the estimated trim tip-path-plane angle).

Most of the results are presented in terms of nondimensional space coordinates and velocities. In those cases where the interpretation is most easily made in dimensional quantities, a tip speed of 690 ft/sec. was used in converting to the dimensional velocities.

Comparison of Distorted-Helix Solution with Vortex-Ring Solution, H/R = 0.5

Results obtained with the distorted-helix model are compared with results obtained from the vortex-ring model (Reference 1) for hovering. Averaged (in the root-mean-square sense) axial velocities halfway between the rotor and the ground plane are shown in Figure 7 and the time-averaged radial velocities at the ground plane are shown in Figure 8. It can be seen that there is reasonably good agreement between the results of the two models in terms of the averaged quantities. In Figure 9, the time variation (in terms of the azimuthal position of the reference blade) of the radial velocity along the ground at various radial positions is shown. Here, differences in detail can be noted although again it is evident that the mean velocities are approximately the same (note the broken scales for $x = 0.6$ and 1.0). The differences in form of the velocity time histories are to be expected. As the helix moves past a fixed point on the ground, and the blade bound vortex rotates in the rotor plane, a relatively smooth velocity variation is obtained. The ring-vortex solution, on the other hand, shows a discontinuous velocity distribution at points in time corresponding to the impulsive addition of a ring to the flow. The characteristic dominant frequency for both the helix and the rings is the blade passage frequency. Radial ground velocities at $x = 0.2$, 0.6, and 1.0 are in phase for the ring solution because the vorticity vectors are always contained in planes normal to the shaft axis. The distorted-helix solution, on the other hand, contains the effects of a swirl velocity component induced by the axial component of vorticity. The relative phasing between the velocities obtained from the ring and helix solutions has no significance because the impulsive ring has no absolute time reference. The ring solution in Figure 9 was phased so that new rings were arbitrarily introduced when $\psi = \frac{N_B \pi}{2}$ in the helix solution.

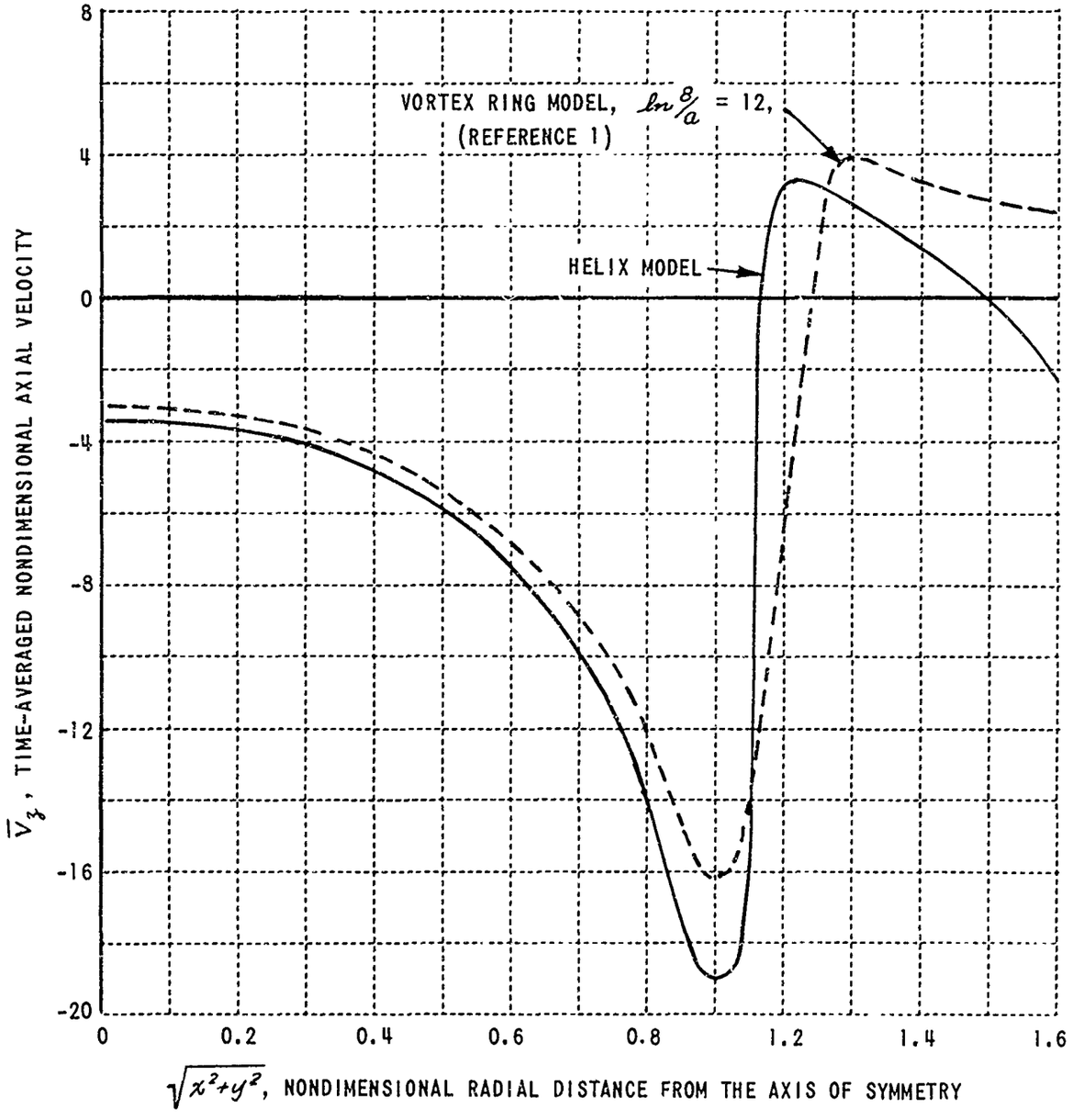

Figure 7 COMPARISON OF RING AND HELIX SOLUTIONS FOR THE RADIAL DISTRIBUTION OF THE TIME-AVERAGED AXIAL VELOCITIES AT $z = -0.25$. CONDITIONS: $\mu = 0$, $H/R = 0.5$.

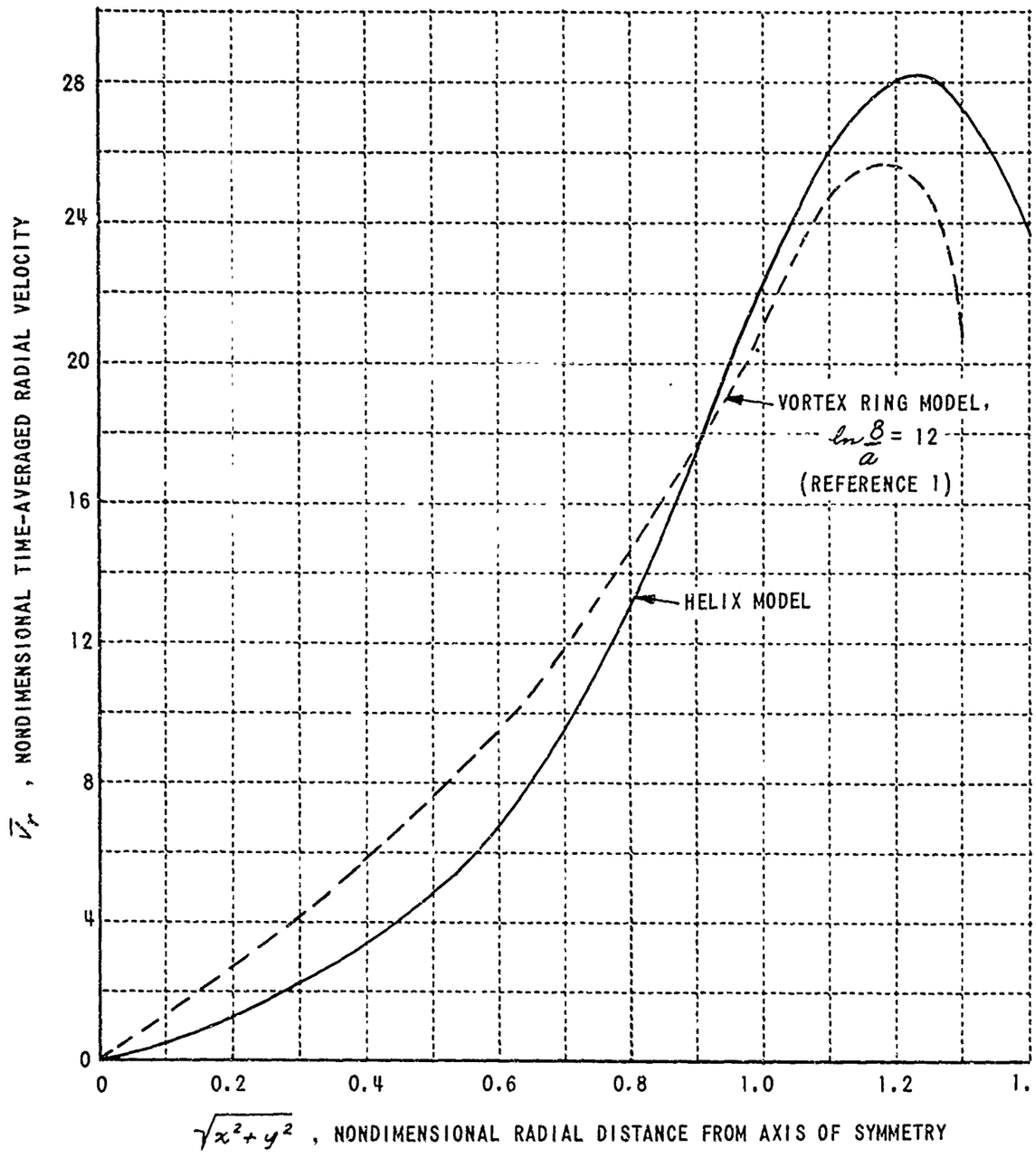

Figure 8 COMPARISON OF RING AND HELIX SOLUTIONS FOR THE TIME-AVERAGED GROUND VELOCITIES AT $z = -0.5$. CONDITIONS: $\mu = 0$, $\frac{H}{R} = 0.5$.

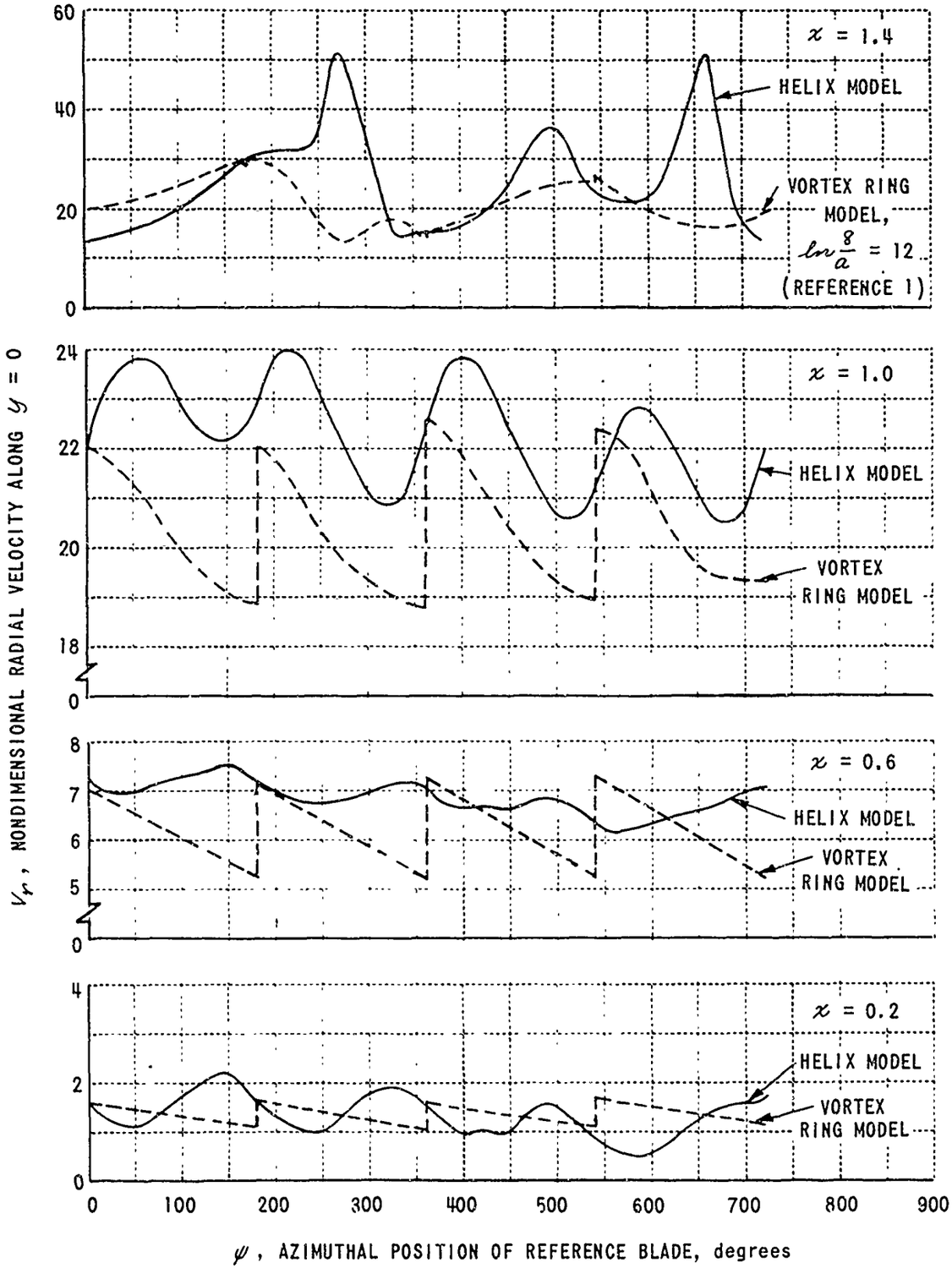

Figure 9 COMPARISON OF HELIX AND RING MODEL TIME HISTORIES OF GROUND-PLANE RADIAL VELOCITIES. CONDITIONS: $\mu = 0$, $\frac{H}{R} = 0.5$.

At a fixed point "near" the actuator, of course, the velocity solution corresponding to Figure 9 is very nearly periodic. The lack of periodicity with a fundamental of one-per-revolution seen in Figure 9 probably reflects the finite extent of the wake used in the calculations and the tendency of the vortex elements to coil at the wake termination. Inclusion of diffusion and dissipation effects -- which should have become significant because the vorticity has existed for a time period corresponding to roughly 60 chord lengths of blade travel per revolution -- would probably alleviate this situation.

Comparison of Calculated Hovering Results with Experimental Data (Time-Averaged Velocities)

It was shown in Reference 3 that the time-averaged velocity distribution alculated on the basis of the distorted-wake-helix model agreed well with measurements made in the wake of a helicopter rotor in a tunnel at an advance ratio of 0.14. Measurements of wake velocity distributions for rotors at low advance ratios in ground effect are sparse. In Figure 10, measurements (Reference 6) for a hovering model rotor one radius above the ground are compared with computed results. Since the measurements were confined to the three horizontal planes and one vertical plane, indicated by the dash lines in Figure 10, the experimental velocity contours indicated are not necessarily accurate. The corresponding computed root-mean-square velocity ratios show the same general character as the measurements over approximately the outer half of the flow field. The differences between the calculated and measured results incrase toward the centerline of the rotor. It is speculated that this difference might be due to the neglect of the blade inboard vorticity in these calculations. Similarly, the measurements in this region should be treated with some caution because the velocities were deduced from pressure readings and some question arises with respect to the assignment of a meaning to a "static pressure" reading in a confused velocity field.

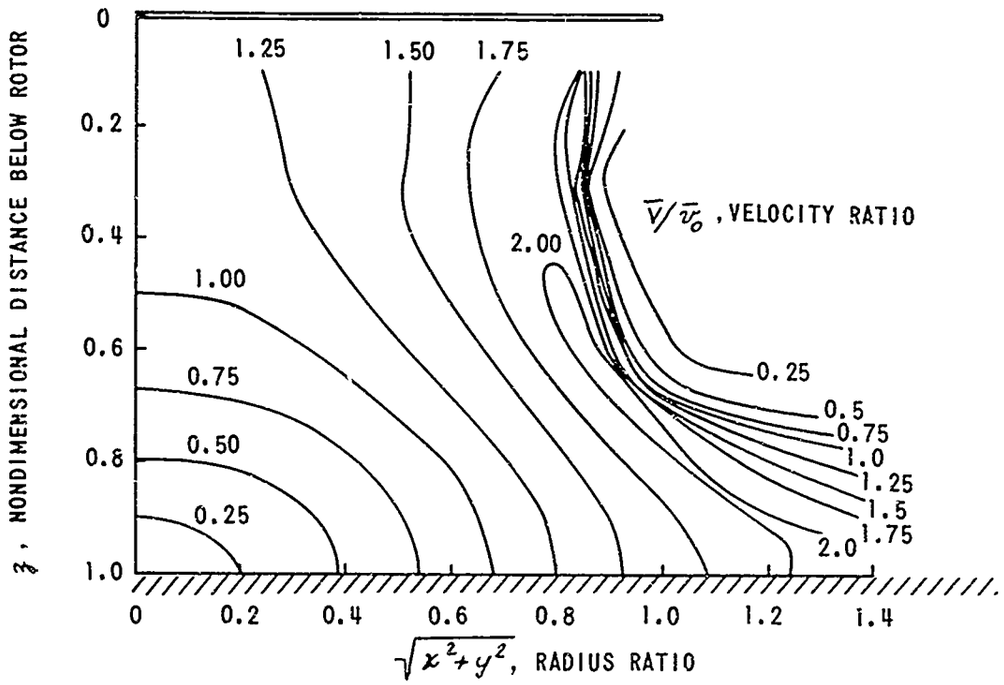

(a) CALCULATED VELOCITY CONTOUR MAP FOR A ROTOR 1.0 RADIUS ABOVE GROUND

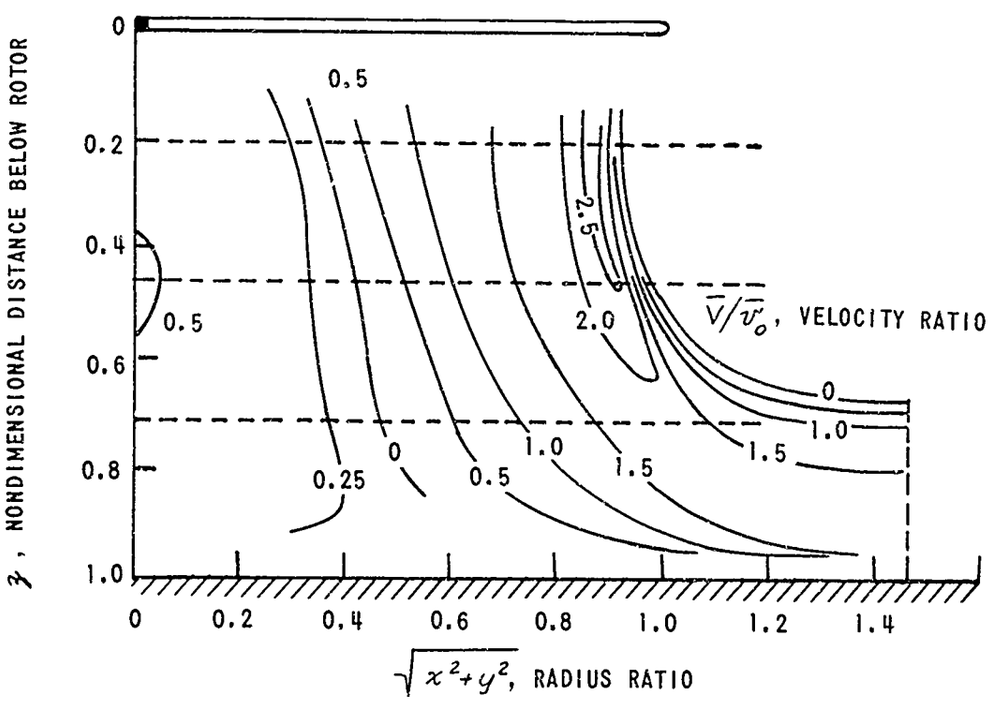

(b) MEASURED VELOCITY CONTOUR MAP FOR A ROTOR 1.0 RADIUS ABOVE GROUND (REFERENCE 6)

Figure 10 CALCULATED AND MEASURED TIME-AVERAGED VELOCITY RATIOS. $\mu = 0, \frac{H}{R} = 1.0$

In Figure 11, the measured and calculated root-mean-square velocity ratio profiles along a line normal to the ground at a distance one and one-half radii from the shaft centerline are compared. Qualitative agreement is noted except very close to the ground plane where boundary layer effects (neglected in the calculation) could be expected to be important.

The method of measurement employed in the test (Reference 6) precluded the possibility of determining the time variations of the velocities under the hovering model. The calculated velocities vary with time (azimuthal position of reference blade) and some idea of the variations can be obtained from Figures 12 and 13. Values of the velocity components at points on a line parallel to the x-axis and halfway between the rotor and the ground (Figure 12) and along the ground (Figure 13) are compared. In particular, the time-averaged values are shown compared with the values computed when the reference blade is at $\psi = 0$ degrees and when the reference blade is at $\psi = 90$ degrees (see Figure 1 for coordinate system). It is evident from the figures that the computations indicate sizable time variations.

Effects of Actuator Loading; $\mu = 0.02$, H/R = 1

The calculated effect of a change in actuator loading on the geometry of the wake vorticity can be seen in Figure 14 where the traces of the tip trailing vortex cores in the x-z plane are shown at the time when the reference blade vortex (Blade No. 1) is at $\psi = 0$. The cores for the more highly loaded case ($\lambda = 0.00478$) exhibit a wider separation along a trajectory than do those for the lightly loaded case ($\lambda = 0.00203$). Further, the estimated trajectory is less inclined relative to the rotor for the more highly loaded case. These differences* arise, of course, from the greater induced velocity (and the greater energy) associated with the vorticity of the more highly loaded blades.

* The small difference in tip-path-plane angles (0.6°) for the two cases is believed to have a negligible effect.

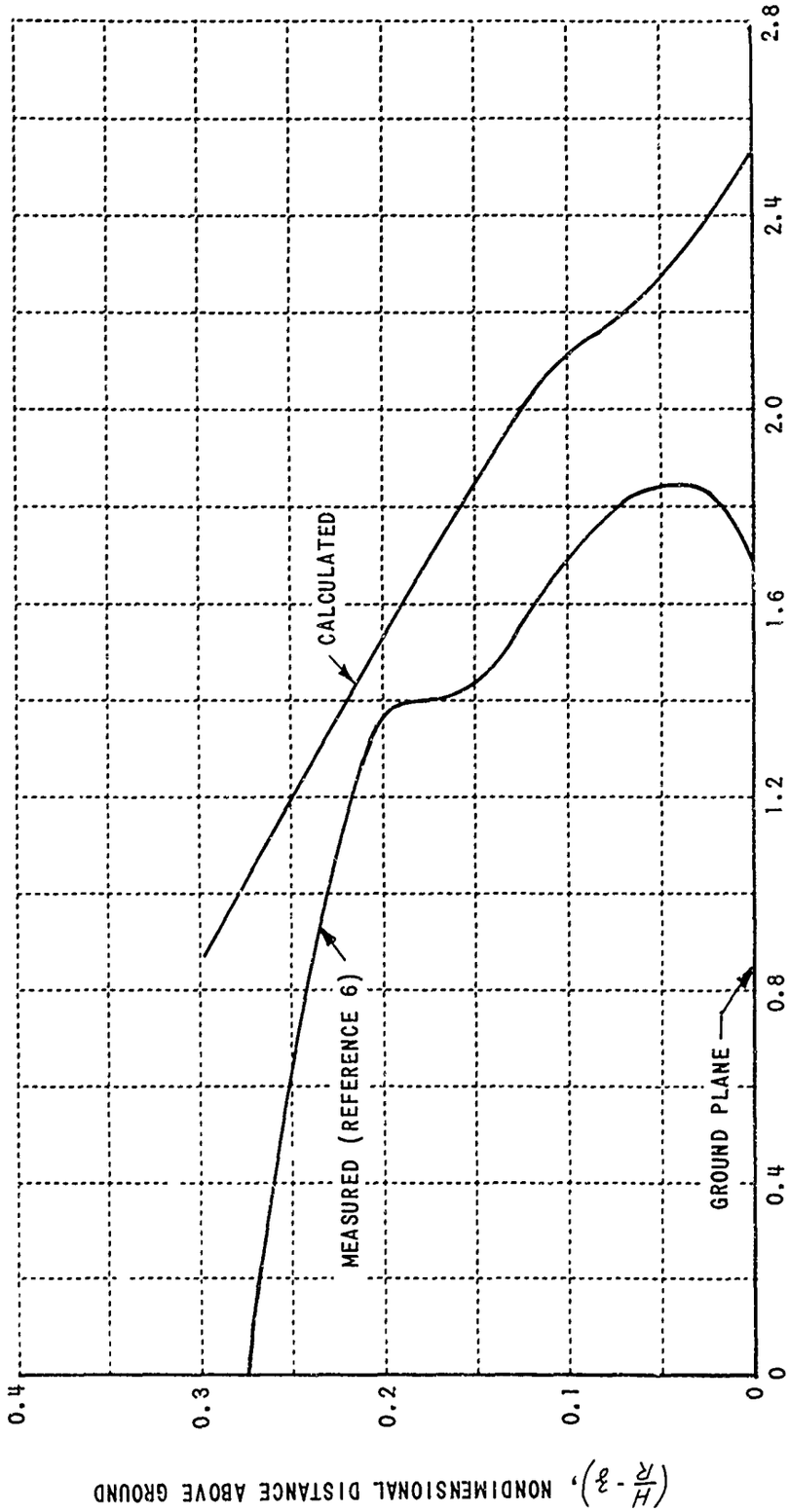

Figure 11 COMPARISON OF MEASURED AND CALCULATED TIME-AVERAGED TOTAL VELOCITY PROFILES NORMAL TO THE GROUND PLANE (ζ = -1.0)
CONDITIONS: μ = 0, H/R = 1.0, $\sqrt{x^2+y^2}$ = 1.5

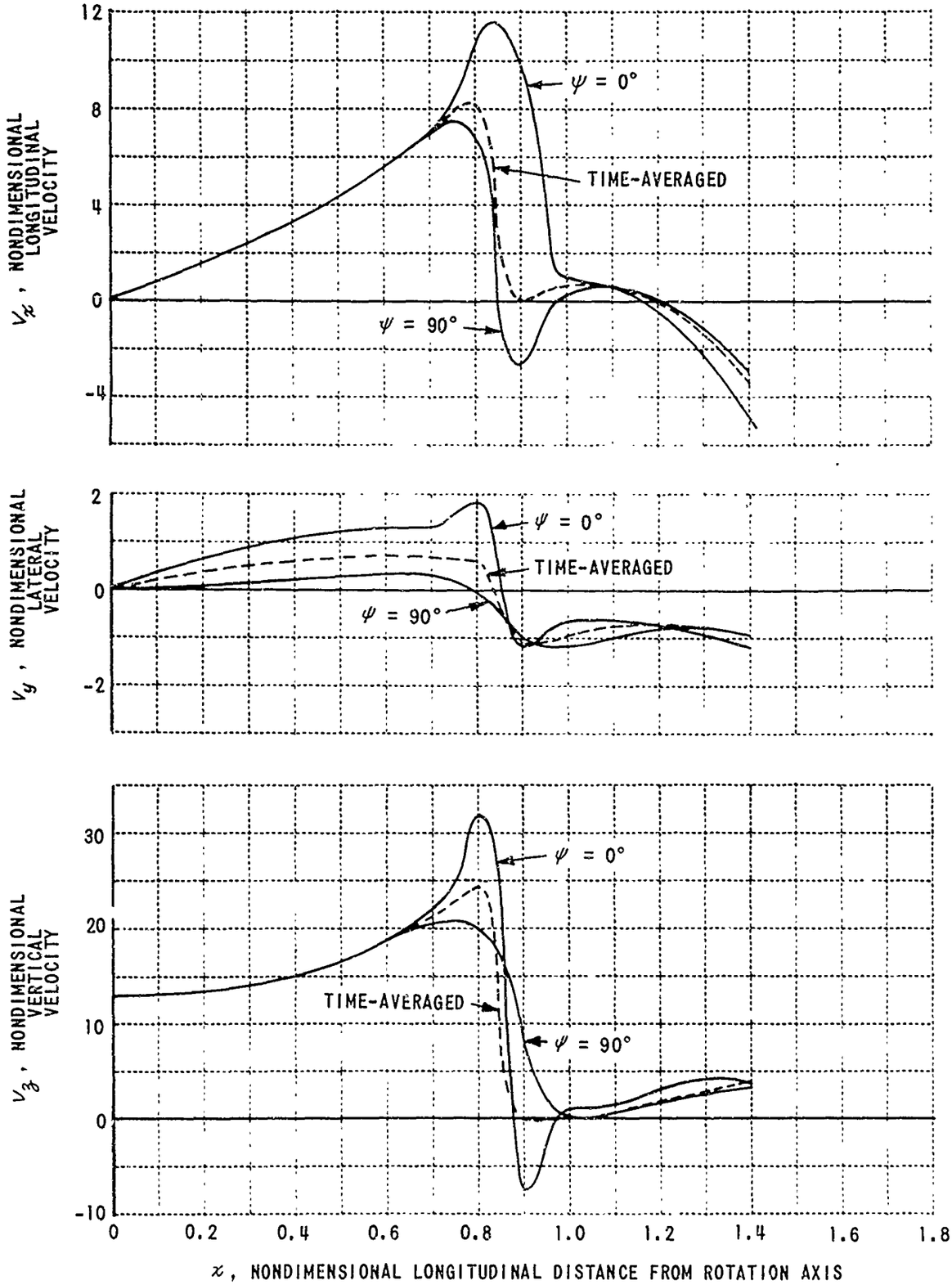

Figure 12 COMPARISON OF CALCULATED TIME-AVERAGED VELOCITY COMPONENTS WITH VELOCITY COMPONENTS CALCULATED WHEN THE REFERENCE BLADE IS AT ψ = 0 OR ψ = 90°. (HELIX MODEL). CONDITIONS: μ = 0, $\frac{H}{R}$ = 1.0; z = -0.5, y = 0.

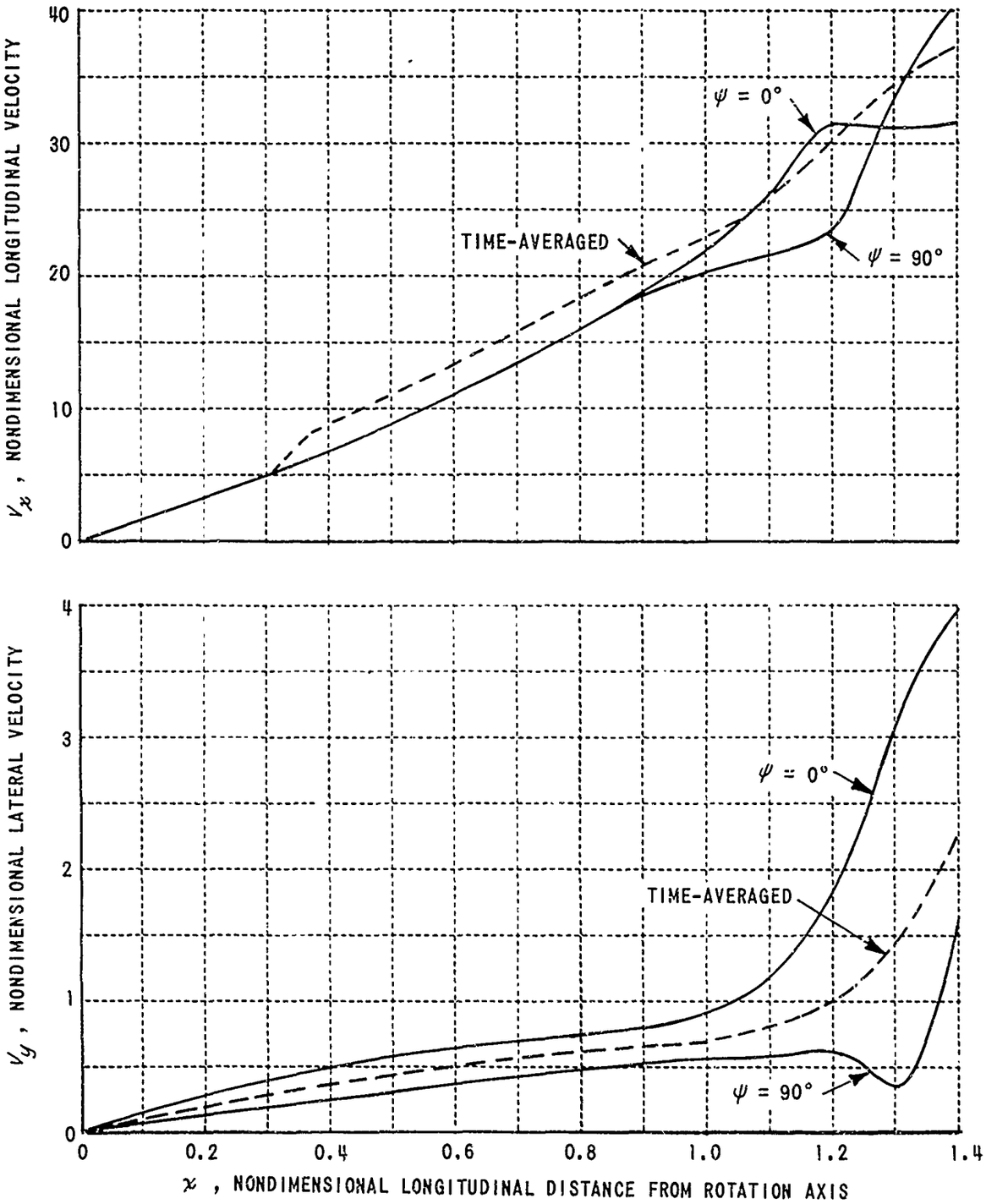

Figure 13 COMPARISON OF CALCULATED TIME-AVERAGED VELOCITY COMPONENTS WITH VELOCITY COMPONENTS CALCULATED WHEN THE REFERENCE BLADE IS AT $\psi = 0$ AND $\psi = 90°$. (HELIX MODEL). CONDITIONS: $\mu = 0$, $\frac{H}{R} = 1.0$; $z = -1.0$, $y = 0$.

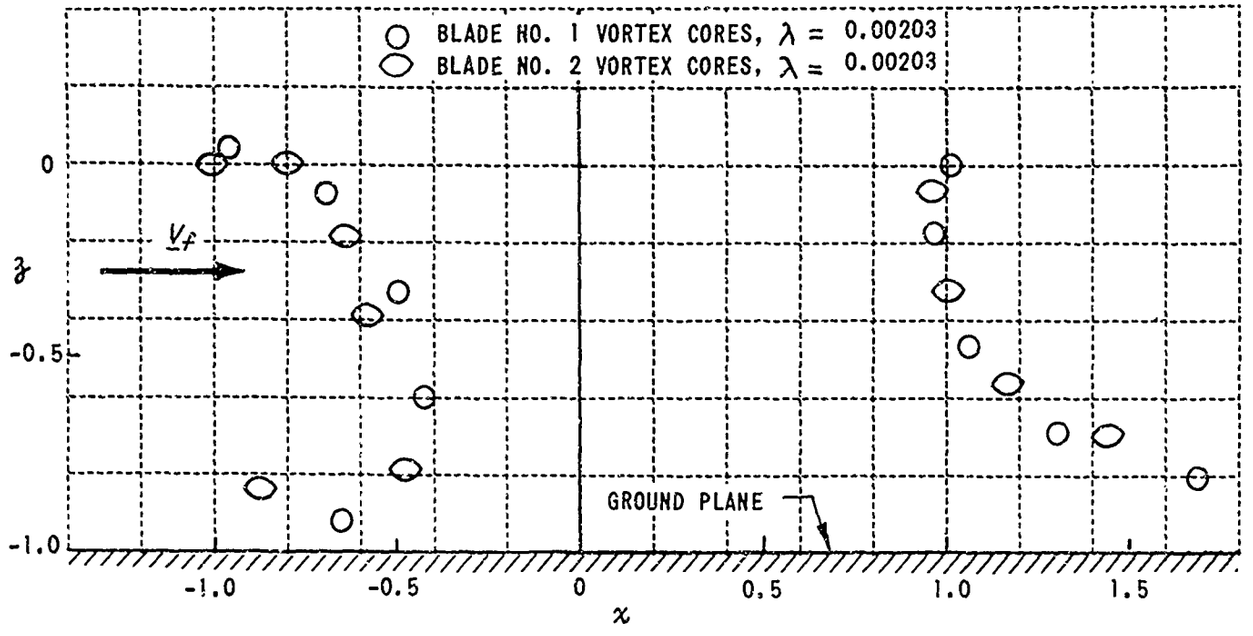

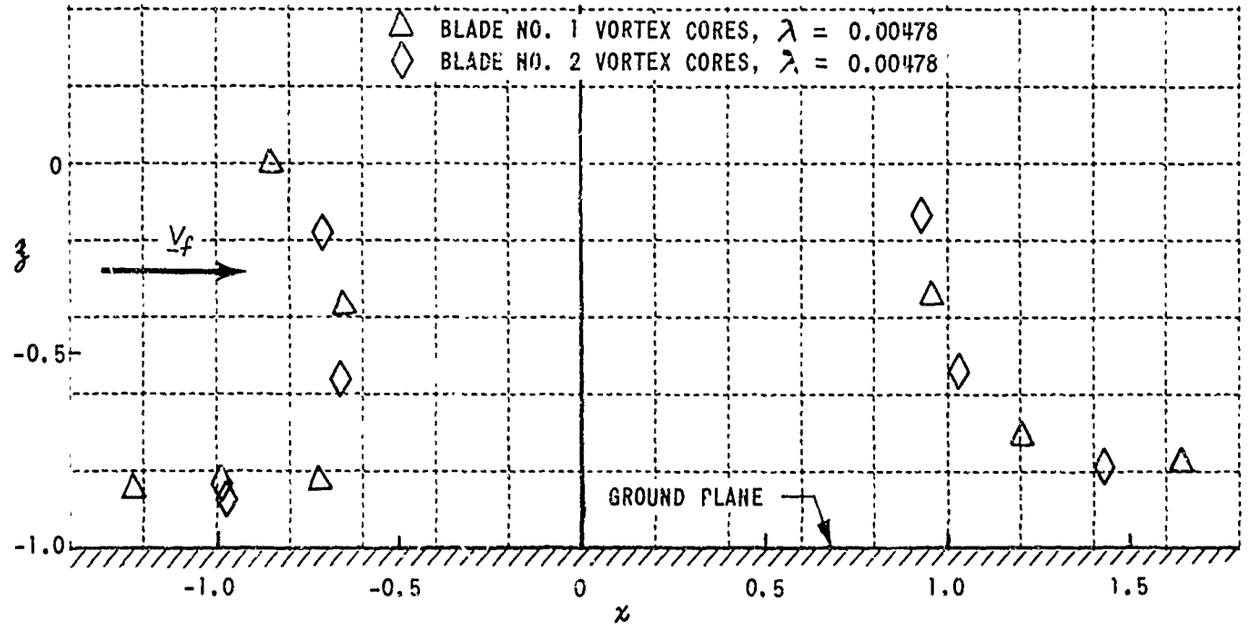

Figure 14 CALCULATED WAKE CORE LOCATIONS IN THE LONGITUDINAL PLANE FOR TWO LOADING CONDITIONS; $\mu = 0.02$, $\frac{H}{R} = 1.0$, $\psi_{\text{REF. BLADE}} = 0.$

The reference blade bound vortex is located at $\psi = 0^{\circ}$ at the instant shown in Figure 14. It can be seen that the last vortex generated by Blade No. 1 is above the tip path at $\psi = 180^{\circ}$ -- that is, the vortex tube is passing above Blade No. 2 which is at $\psi = 180^{\circ}$. It might be concluded that at some time during the next half revolution, Blade No. 2 would cut through the vortex tube generated by Blade No. 1. This does not, however, appear to be the case. The tip vortex from Blade No. 1 slides outboard relative to Blade No. 2 as Blade No. 2 rotates. At the time at which the core is in the tip-path-plane, it is also outboard of the blade tip and no intersection occurs. The miss-distance is small and, therefore, no definite conclusion can be drawn with respect to the behavior expected of the physical system -- the position errors introduced by the idealizations introduced are probably of the same order as the miss-distance.

In Figures 15 and 16, the velocity time histories at two points in the plane of symmetry and near the location that might be occupied by a horizontal stabilizer and/or a tail rotor are compared for the two loading cases. One of the field points ($x = 1.0$, $y = 0.0$, $z = -0.25$) is outside the slipstream envelope (see Figure 14) and the velocities do not differ greatly for the two loadings (Figure 15). Apparently the differences in spacings and vortex strengths for the two cases introduce compensating effects. Another interesting feature of Figure 15 is that both the x and z velocity components experience reversals at blade-passage frequency. One could anticipate, therefore, that a tail plane or tail rotor would experience shaking forces and these would be transmitted to the fuselage.

Velocity component time histories at a field point inside the slipstream are shown in Figure 16. This location ($x = 0.8$, $y = 0.0$, $z = -0.25$) might also be a candidate location for a stabilizing surface and/or a tail rotor. The calculations indicate that the relative amplitudes of the velocity fluctuations at this location are nearly proportional to the loading parameter, λ. The velocity component normal to the reference rotor plane, V_z, is, of

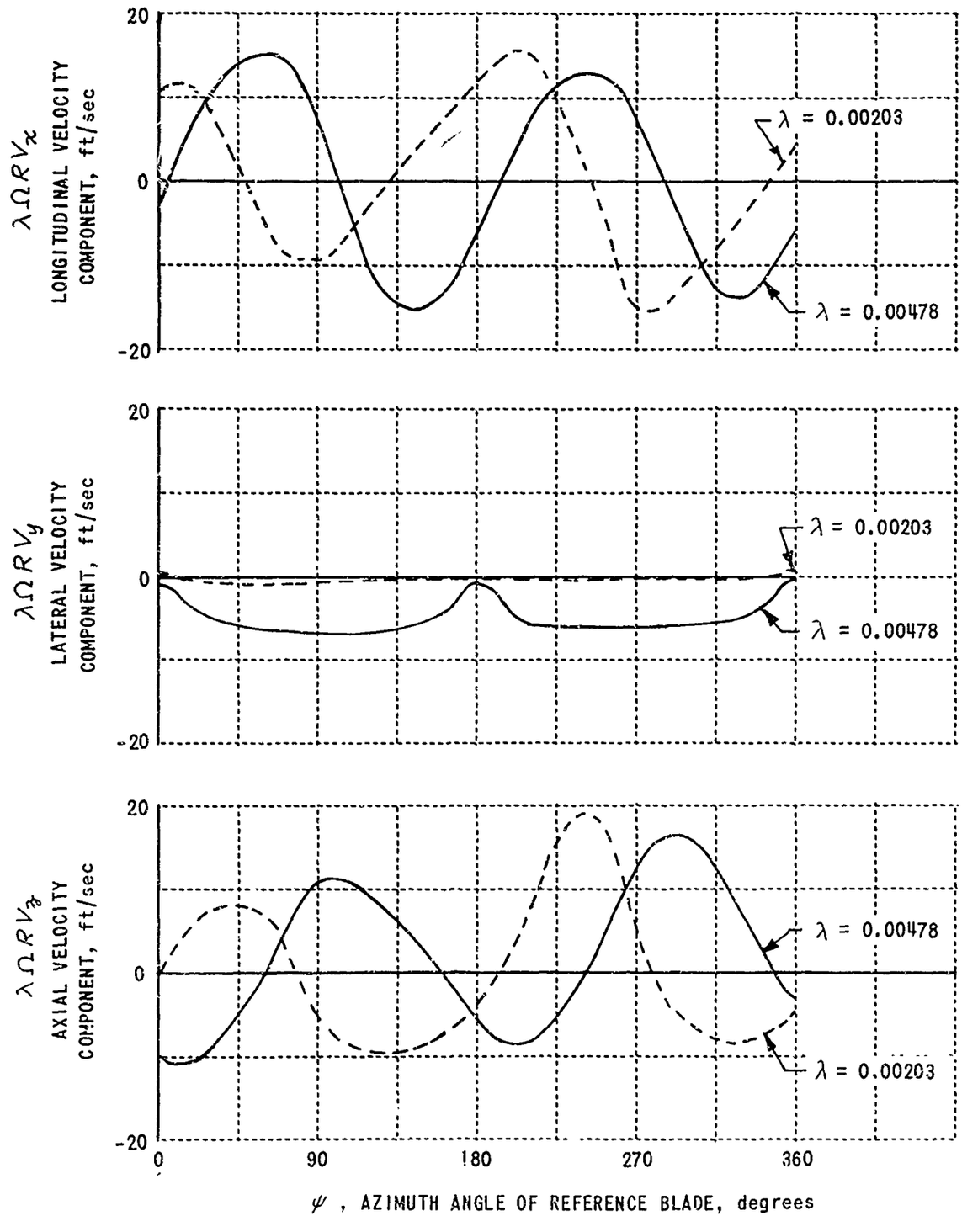

Figure 15 VELOCITY TIME HISTORIES AT A FIELD POINT (x = 1.0, y = 0.0, z = -0.25) FOR TWO VALUES OF THE LOADING PARAMETER, λ, AT μ = 0.02, $\frac{H}{R}$ = 1.0.

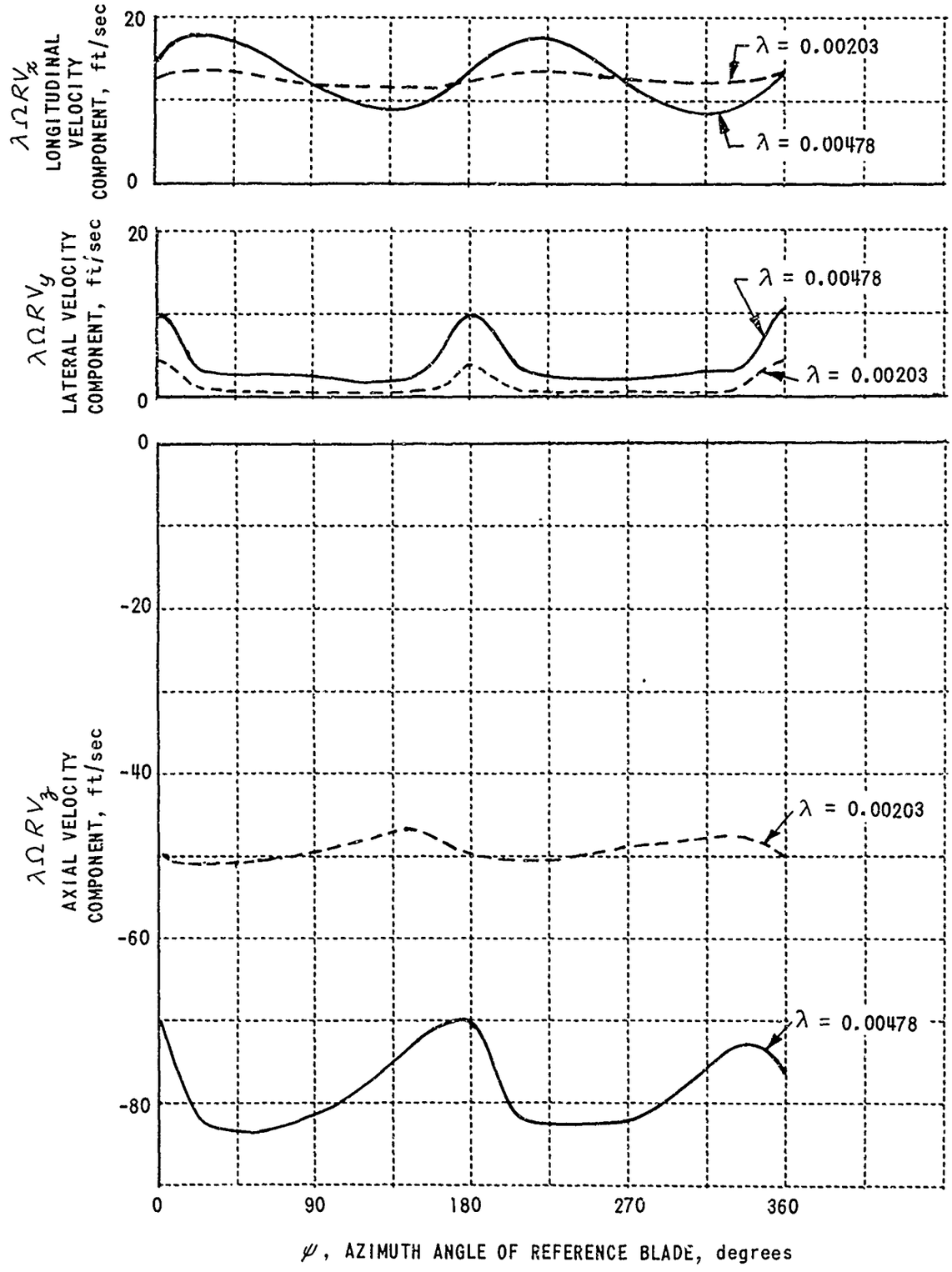

Figure 16 VELOCITY TIME HISTORIES AT A FIELD POINT (x = 0.8, y = 0.0, z = -0.25) FOR TWO VALUES OF THE LOADING PARAMETER, λ, AT μ = 0.02, $\frac{H}{R}$ = 1.0.

course, higher for the higher loading parameter and this velocity component dominates in the slipstream. Again, sizable velocity fluctuations with respect to time are indicated.

Another characteristic of the slipstream velocity is shown in Figure 17 for the highly loaded case ($\lambda = 0.00478$). Figure 17 shows the difference in the resultant velocities ($\lambda \Omega R \sqrt{V_x^2 + V_z^2}$) that might be experienced at the two tips of a stabilizing surface ($x = 0.8$, $y = \pm 0.15$, $z = -0.25$). The velocity fluctuations correspond to differential aerodynamic angles of attack of approximately 7°. Therefore, the oscillating forces would excite fuselage bending and the oscillatory couple would tend to shake the fuselage in torsion.

Effects of Advance Ratio

Effects of advance ratio on the slipstream shape and the velocity components were calculated for a fixed value of 0.00203 for the loading parameter, λ. The estimated tip-path-plane trim angle, α_T, was changed as a function of advance ratio, μ. The pairs (μ, α_T) are (0.02, 0.6°) in Figure 18, (0.05, 1.25°) in Figure 19, and (0.10, 2.5°) in Figure 20. These plots will not be discussed in any detail -- they are only intended to indicate major features of the flow fields.

Slipstream Location. Comparison of Figures 19a and 20a -- the traces in the plane of symmetry of the vortex cores when Blade No. 1 is at $\psi = 0^\circ$ -- displays a slipstream "tuck-under" between $\mu = 0.05$ and 0.10. Below some critical advance ratio in this range the ground effect forces the wake vorticity to translate upstream near the wall (Figures 18a and 19a); above this advance ratio, the free-stream velocity overpowers the ground effect and the vorticity is swept downstream. Extrapolation of wind-tunnel data to free flight conditions (out-of-ground effect) could be compromised severely by differences introduced by this effect -- in particular,

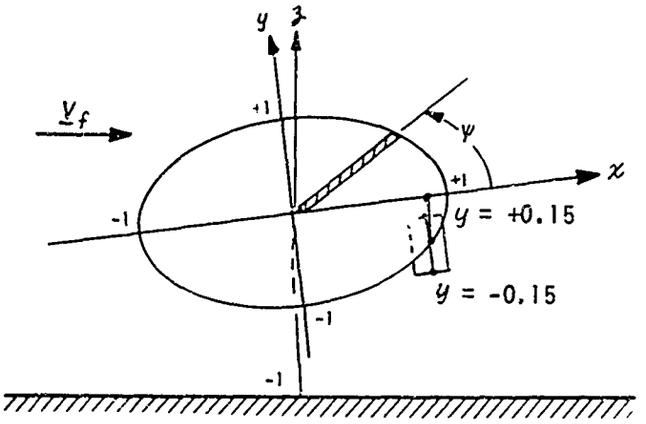

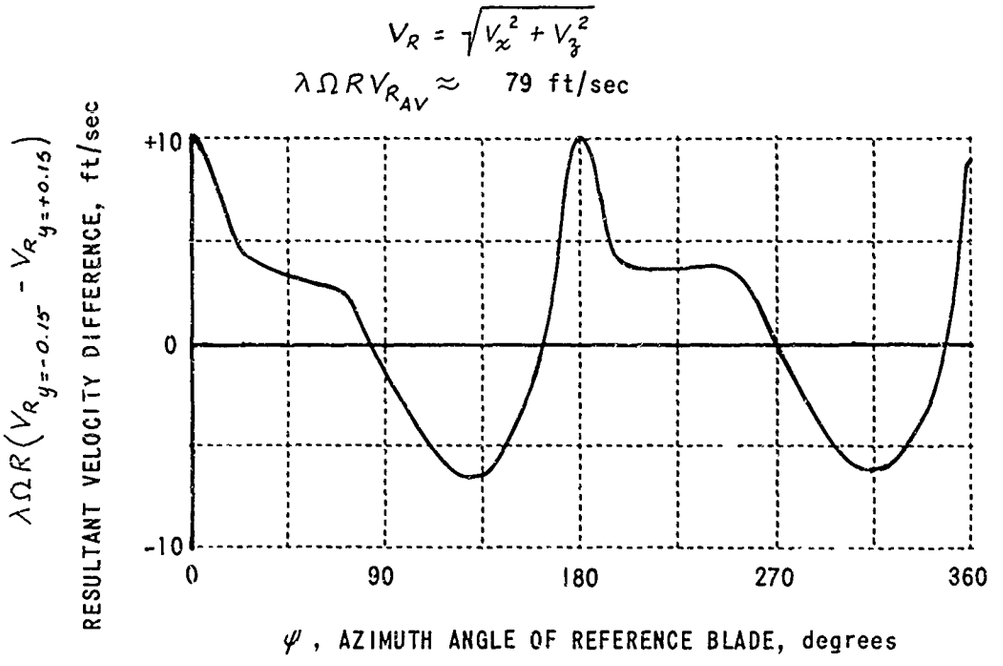

Figure 17 TIME HISTORY OF RESULTANT VELOCITY DIFFERENCE BETWEEN TWO FIELD POINTS, (0.8, -0.15, -0.25) AND (0.8, +0.15, -0.25) FOR μ = 0.02, ω/Ω = 1.0, λ = 0.00478.

at low advance ratios, the forces and moments measured in a wind tunnel could differ significantly from those that would be experienced in the absence of a tunnel floor.

Velocities Just Below the Tip Path Plane. Figures 18b, 19b and 19c, 20b and 20c show the calculated time histories of the nondimensional velocities immediately below the tip path plane ($z = -0.01$) along the longitudinal axis ($y = 0.0$) for advance ratios of 0.02, 0.05, and 0.10 respectively. The sharp peaks* in the V_y component for $|x|<|$ indicate the passage of the blade bound vortex; and the peaks are of nearly equal magnitude because of the assumption that the blade bound vortex strength does not vary in the radial direction. Therefore, the V_y values indicated should be reduced by the ratio of the local Γ to the constant (maximum) value used in the calculations to obtain a more representative V_y radial variation. The x-components of the velocity, V_x, show sizable time variations in the vicinity of the slipstream boundary -- a reversal in sign occurring at blade passage frequency near $|x| = 1$ at $\mu = 0.02$ and 0.05. Interior to the slipstream ($|x|< 0.8$, say), V_x changes with time at fixed points are indicated to be relatively small. The V_z components show the characteristic rise and fall, at blade passage frequency, expected near the rotor plane in the interior of the slipstream. Near the boundary of the slipstream, this axial component is strongly influenced by the tip vortex as well as the bound vortex and large time variations can occur. The sign of the mean value changes as the slipstream boundary is crossed.

Figures 19d and 19e, 20d and 20e show the velocity time histories just below the rotor ($z = -0.10$) along the lateral axis ($x = 0.0$). General characteristics are similar to those indicated above with the V_x and V_z velocity components interchanged with respect to the effect of the blade bound vortex effect.

*The peaks should be somewhat rounded -- the sharpness indicated is the result of using straight lines in the plotting routine to join calculated points.

Velocities Near Fuselage. Velocity time histories along a line representative of a fuselage location are shown in Figures 19f and 19g and 20f and 20g for $\mu = 0.05$ and 0.10. The lateral velocity component, V_y, is seen to be relatively small. The longitudinal, V_x, and axial, V_z, nondimensional components are large and oscillatory. It would be expected that these components would give rise to oscillatory fuselage forces.

Figures 19g and 20g show the change in environment experienced by a tail rotor ($0.6 < x < 1.3$, $y = 0.0$, $z = -0.25$). It is apparent that the velocity field in the vicinity of a tail rotor is nonuniform and, consequently, oscillatory tail rotor loads would exist.

Flow Near a Stabilizing Surface. Figures 19h, and 20h illustrate the velocity variations in the regions of the tips of possible stabilizer positions ($0.6 < x < 0.9$, $y = +0.15$, $z = -0.25$). Figure 20h ($\mu = 0.10$) indicates time variations of V_x and V_z at these locations that are significant while Figure 19h ($\mu = 0.05$) exhibits a much smaller nonuniformity. Sidewash velocities, V_y, are small.

Velocities Along the Ground Plane. Figures 19i and 19j, and 20i and 20j show the velocity components along the ground at the plane of symmetry ($y = 0$). The oscillatory component of V_x and the change of V_x with x decrease with increasing advance ratio in the region inspected. The V_y component is small along the line on which the calculations were made and $V_z = 0$ by imposition of the boundary condition.

CONCLUDING REMARKS

The model developed provides estimates of the velocity field in the vicinity of a rotor (propeller) operating in ground effect. In particular, the time variations predicted appear to be reasonable -- at least over the outer half of the slipstream and at field points outside the slipstream. Since there are no known suitable surveys that show the time variation of velocities in the vicinity of a rotor, it was not possible to verify this most important aspect of the present effort nor to test the validity of the many assumptions. Briefly, these assumptions were the following:

1. Incompressible fluid.
2. Inviscid fluid.
3. Negligible effect from root vortex.
4. Negligible effect from shed vorticity at small advance ratios ($\mu < 0.10$).
5. Self-induced velocity determined by local vortex curvature.
6. Blade bound vortex constant along span.
7. Constant initial vortex core diameter.
8. Vortex core diameter estimated from wing theory.

It is believed that the theory developed is applicable to a variety of problems that arise from the interaction of propeller (rotor) flow fields with other aerodynamic surfaces. It should be recognized, however, that only the zeroth-order effect -- the velocity field in the absence of aerodynamic surfaces -- has been obtained. Questions related to the interaction of, say, a wing surface or a tail rotor blade with a free vortex have not been investigated.

The calculated results indicate that, at low advance ratios, the ground effect forces the wake to translate upstream. Consequently, wind-tunnel measurements of forces and moments acting on rotors (and fuselages, stabilizing surfaces and tail rotors) may not be representative of out-of-ground-effect behavior.

RECOMMENDATIONS

1. Direct measurement of time-dependent flow quantities in and near the wake of a propeller (rotor) in ground effect is recommended. In particular, velocities in the flow field and wind-tunnel wall (or ground) pressure distributions would be desirable. Comparison of these measurements with the theoretical results would furnish a measure of the validity of the theory.

2. Vorticity diffusion and dissipation effects should be incorporated in the theory.

3. An effort should be made to investigate the effects of shed vorticity components and the inboard trailing vorticity components.

4. The utility of the theory for engineering purposes should be established. In particular, measurements of the time-dependent pressure distribution on a wing or fuselage in a rotor wake (compound configuration) could be compared with estimates based on the calculated rotor flow field.

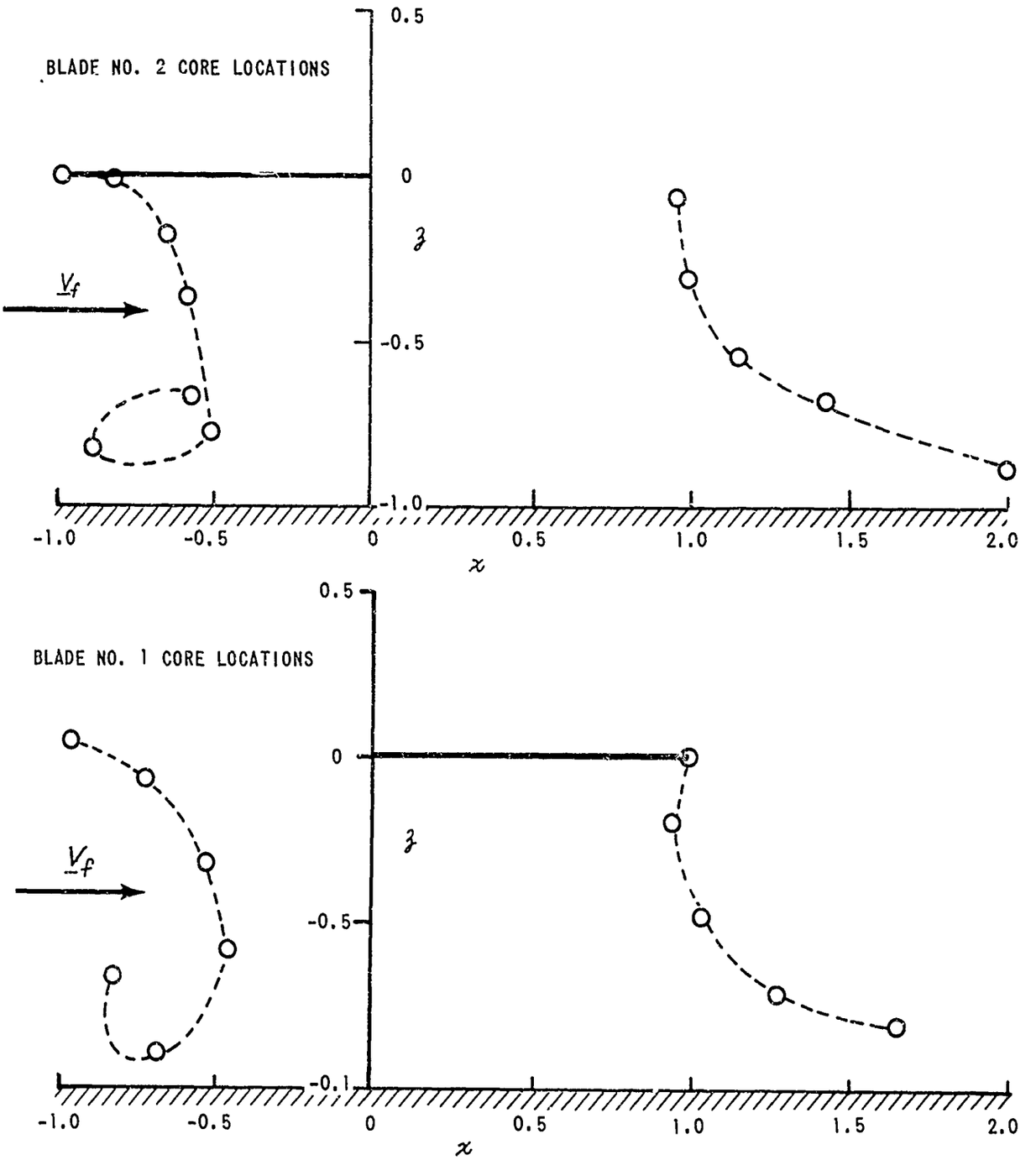

Figure 18a POSITIONS OF WAKE VORTICITY (CORES) IN LONGITUDINAL PLANE OF SYMMETRY WHEN BLADE NUMBER 1 IS AT ψ = 0°. CONDITIONS: μ = 0.02, λ = 0.00203, α_T = 0.6°.

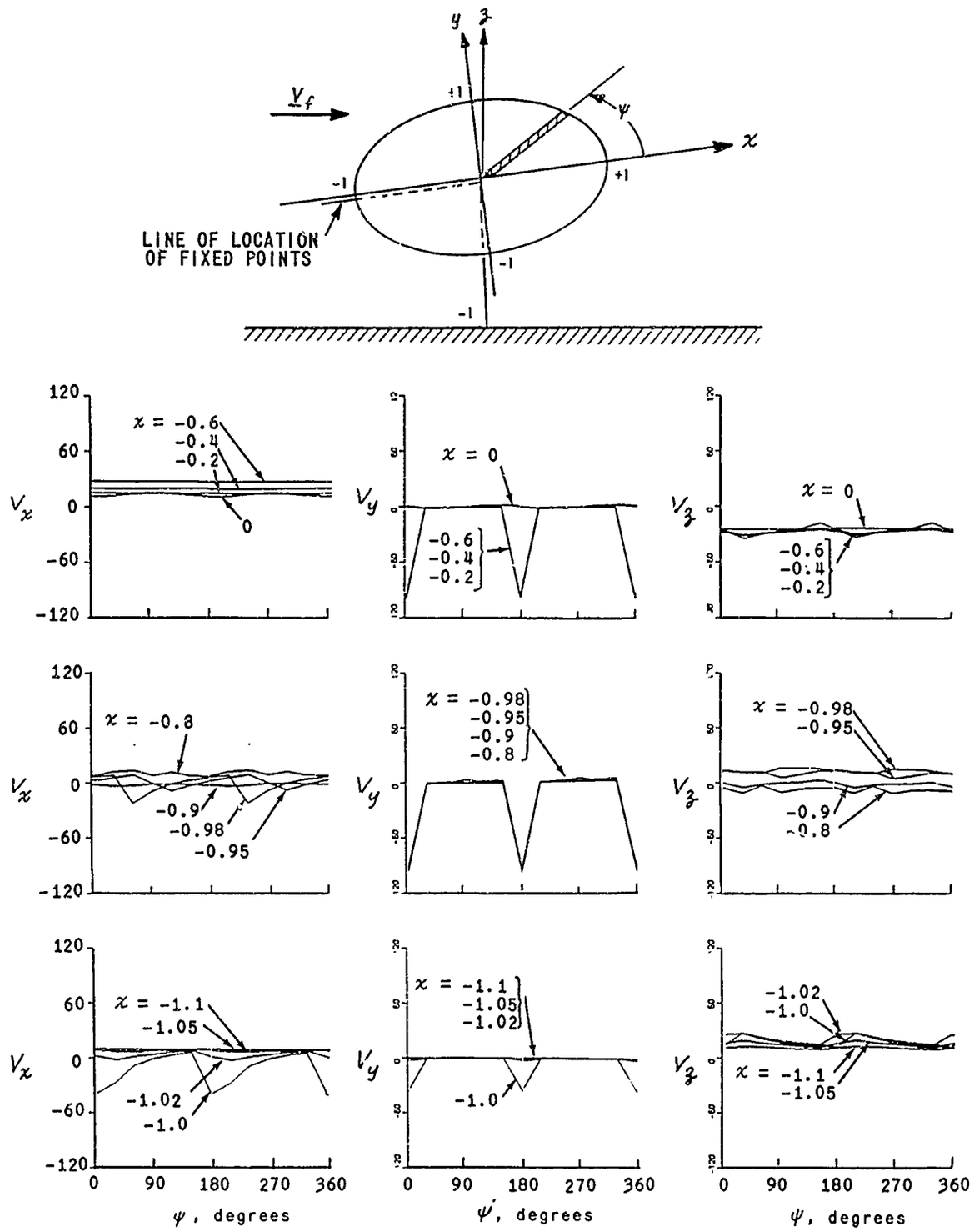

Figure 18b NONDIMENSIONAL VELOCITIES AT FIXED FIELD POINTS NEAR THE TIP PATH PLANE VS REFERENCE BLADE POSITION, ψ. CONDITIONS: μ = 0.02, λ = 0.00203, α_r = 0.6°; y = 0.00, z = -0.010, x VARIABLE.

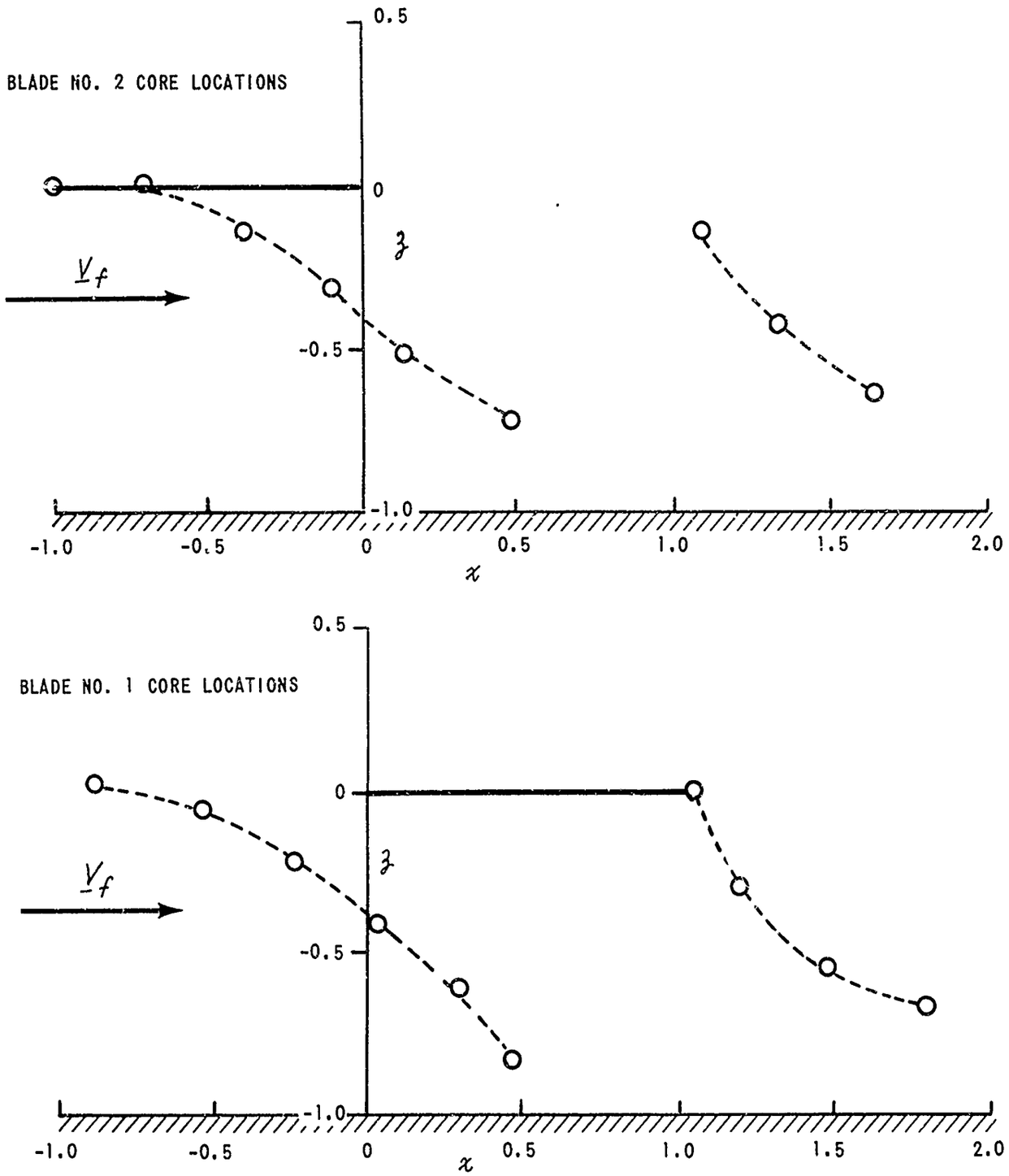

Figure 19a POSITIONS OF WAKE VORTICITY (CORES) IN LONGITUDINAL PLANE OF SYMMETRY WHEN BLADE NUMBER 1 IS AT $\psi = 0°$. CONDITIONS: $\mu = 0.05$, $\lambda = 0.00203$, $\alpha_T = 1.25°$.

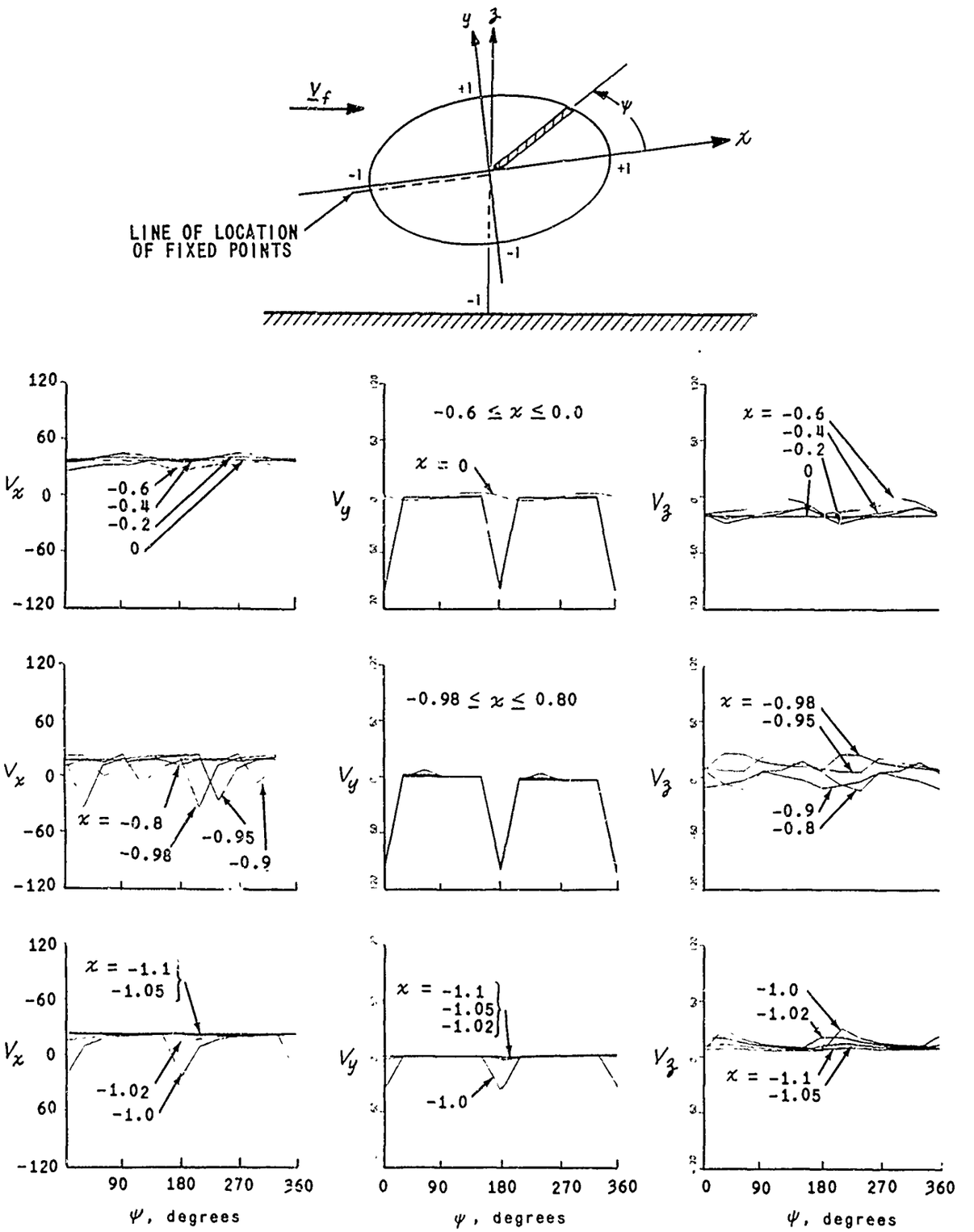

Figure 19b NONDIMENSIONAL VELOCITIES AT FIXED FIELD POINTS NEAR THE TIP PATH PLANE VS REFERENCE BLADE POSITION, ψ.
CONDITIONS: $\mu = 0.05$, $\lambda = 0.00203$, $\alpha_T = 1.25°$;
$y = 0.00$, $z = -0.010$, x VARIABLE.

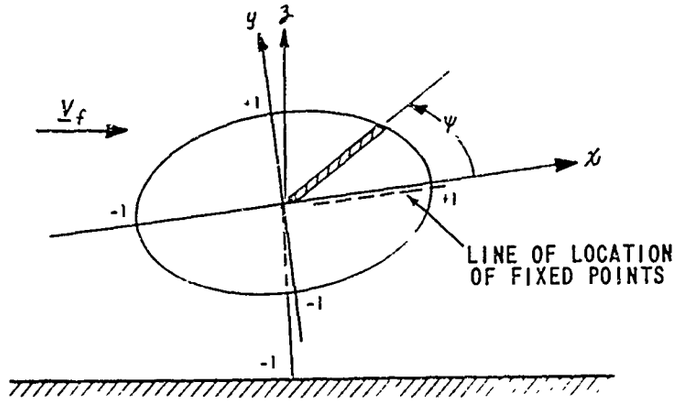

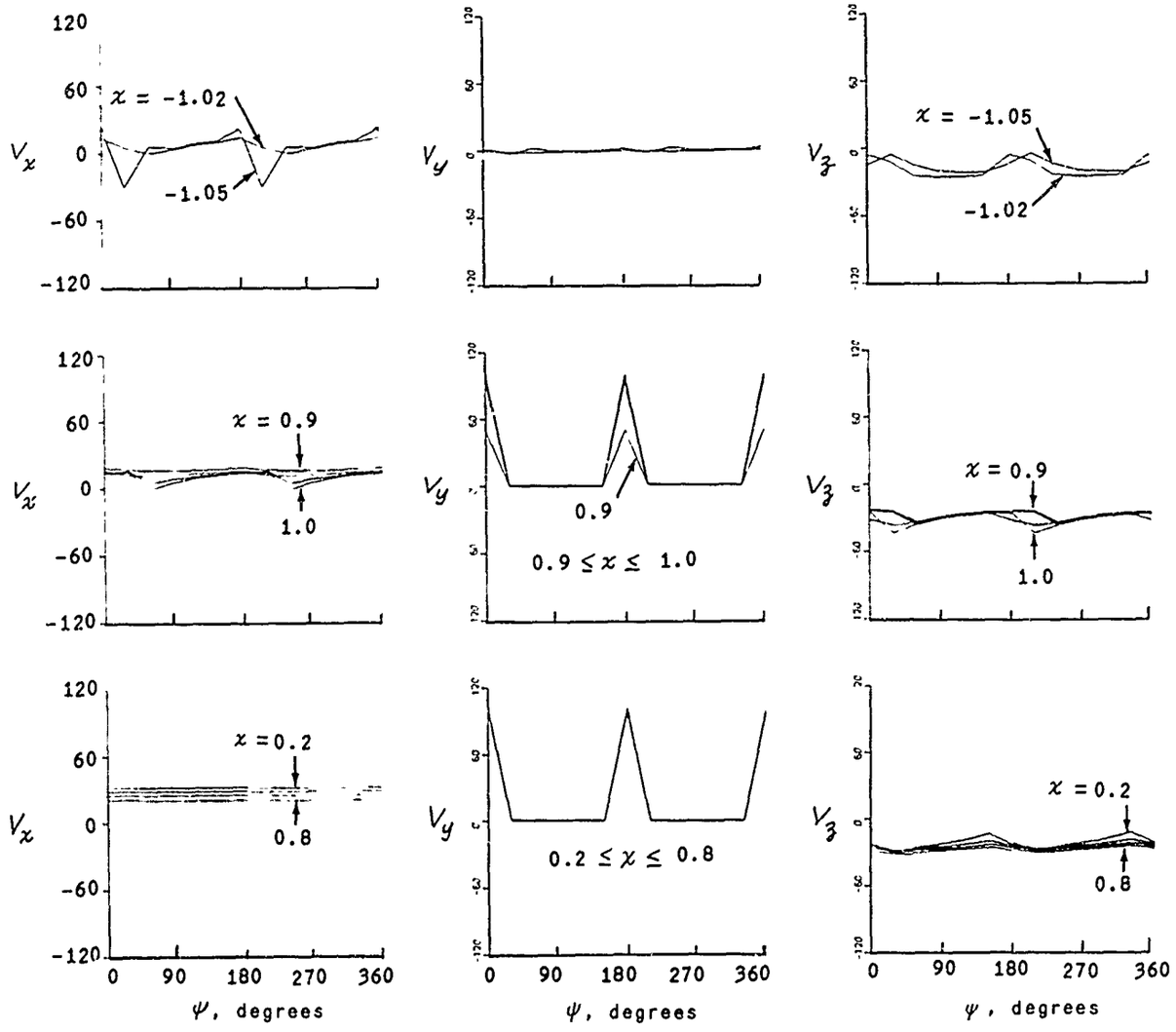

Figure 19c NONDIMENSIONAL VELOCITIES AT FIXED FIELD POINTS NEAR THE TIP PATH PLANE VS REFERENCE BLADE POSITION, ψ. CONDITIONS: $\mu = 0.05$, $\lambda = 0.00203$, $\alpha_T = 1.25°$, $y = 0.00$, $z = -0.010$, x VARIABLE.

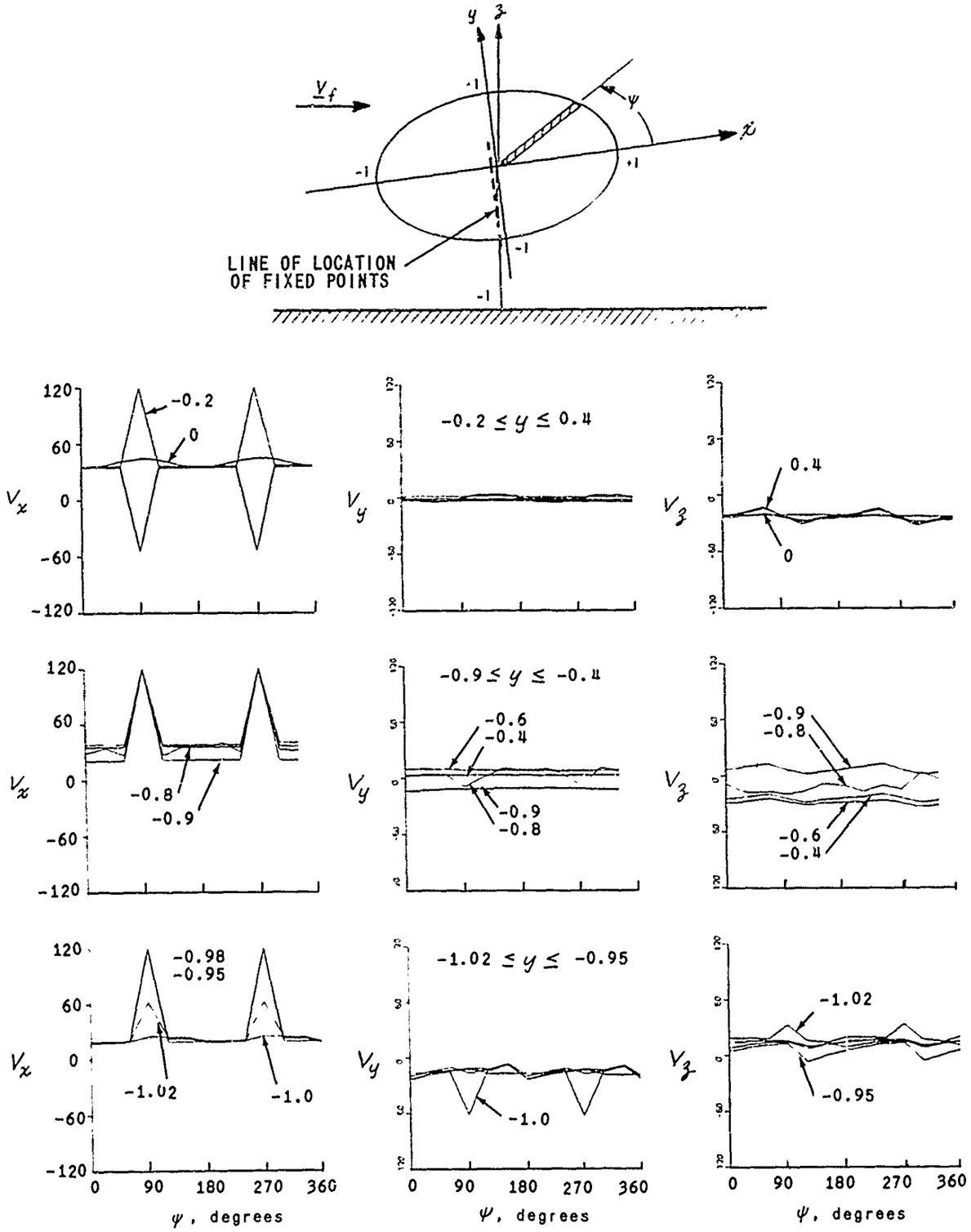

Figure 19d NONDIMENSIONAL VELOCITIES AT FIXED FIELD POINTS NEAR THE TIP PATH PLANE VS REFERENCE BLADE POSITIONS, ψ. CONDITIONS: $\mu = 0.05$, $\lambda = 0.00203$, $\alpha_T = 1.25°$; $x = 0.00$, $z = -0.010$, y VARIABLE.

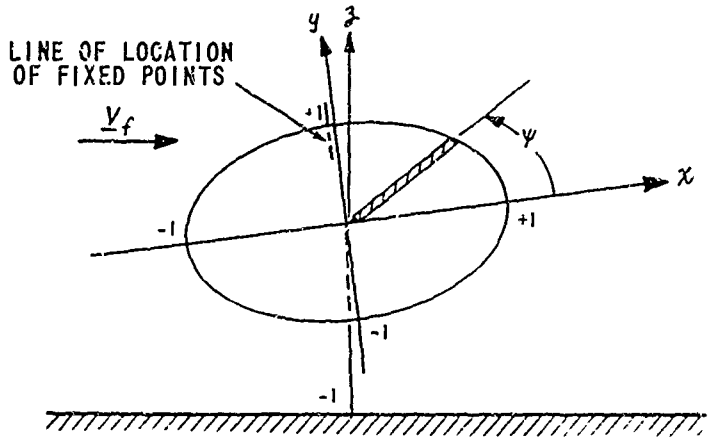

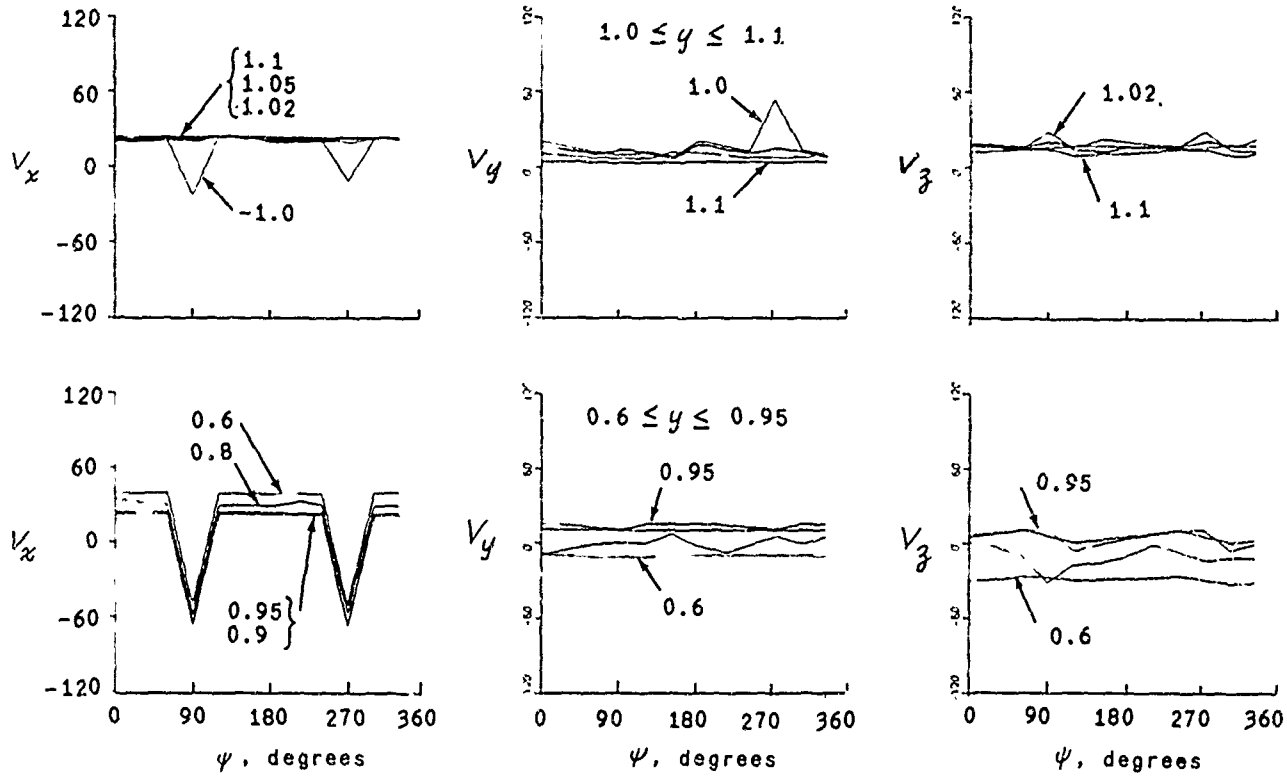

Figure 19e NONDIMENSIONAL VELOCITIES AT FIXED FIELD POINTS NEAR THE TIP PATH PLANE VS REFERENCE BLADE POSITION, ψ. CONDITIONS: $\mu = 0.05$, $\lambda = 0.00203$, $\alpha_r = 1.25°$; $x = 0.00$, $z = -0.010$, y VARIABLE.

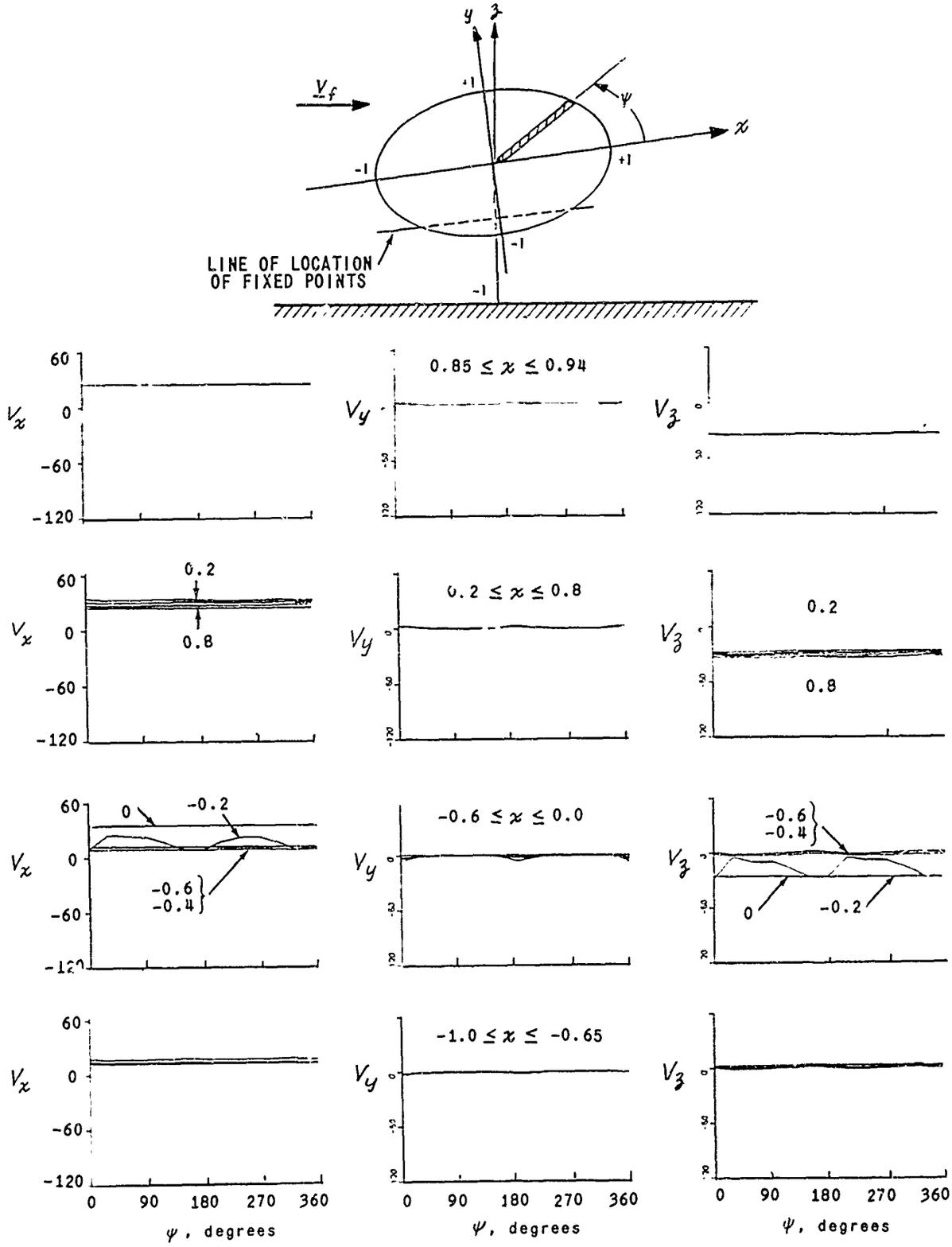

Figure 19f NONDIMENSIONAL VELOCITIES AT FIXED FIELD POINTS NEAR FUSELAGE LOCATION VS REFERENCE BLADE POSITION, ψ. CONDITIONS; μ = 0.05, λ = 0.00203, α_T = 1.25°; y = 0.00, z = -0.25, x VARIABLE.

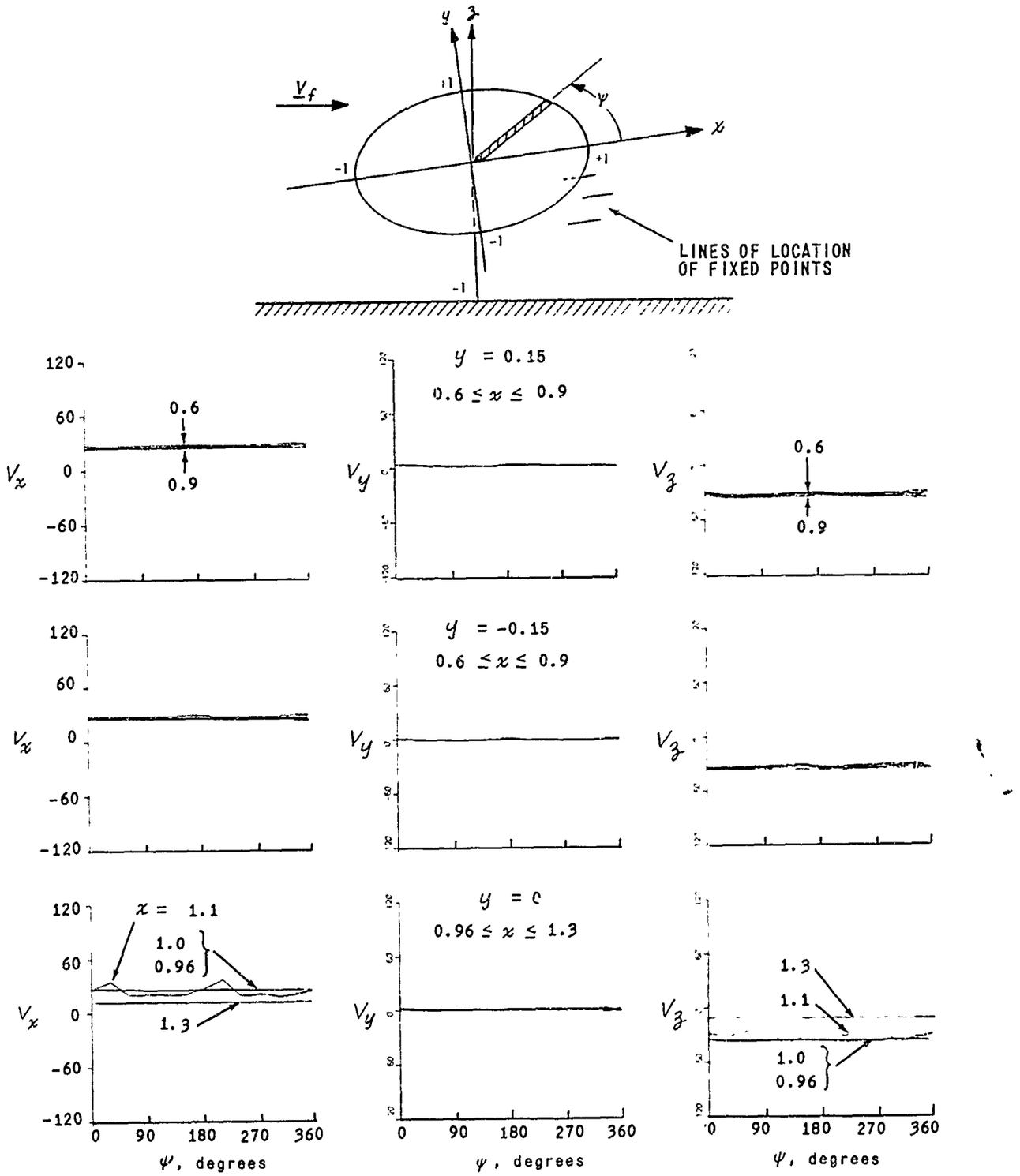

Figure 19g NONDIMENSIONAL VELOCITIES AT FIXED FIELD POINTS NEAR STABILIZER AND/OR TAIL ROTOR LOCATIONS VS REFERENCE BLADE POSITION, ψ. CONDITIONS: $\mu = 0.05$, $\lambda = 0.00203$, $\alpha_T = 1.25°$; $z = -0.25$, x AND y VARIABLE.

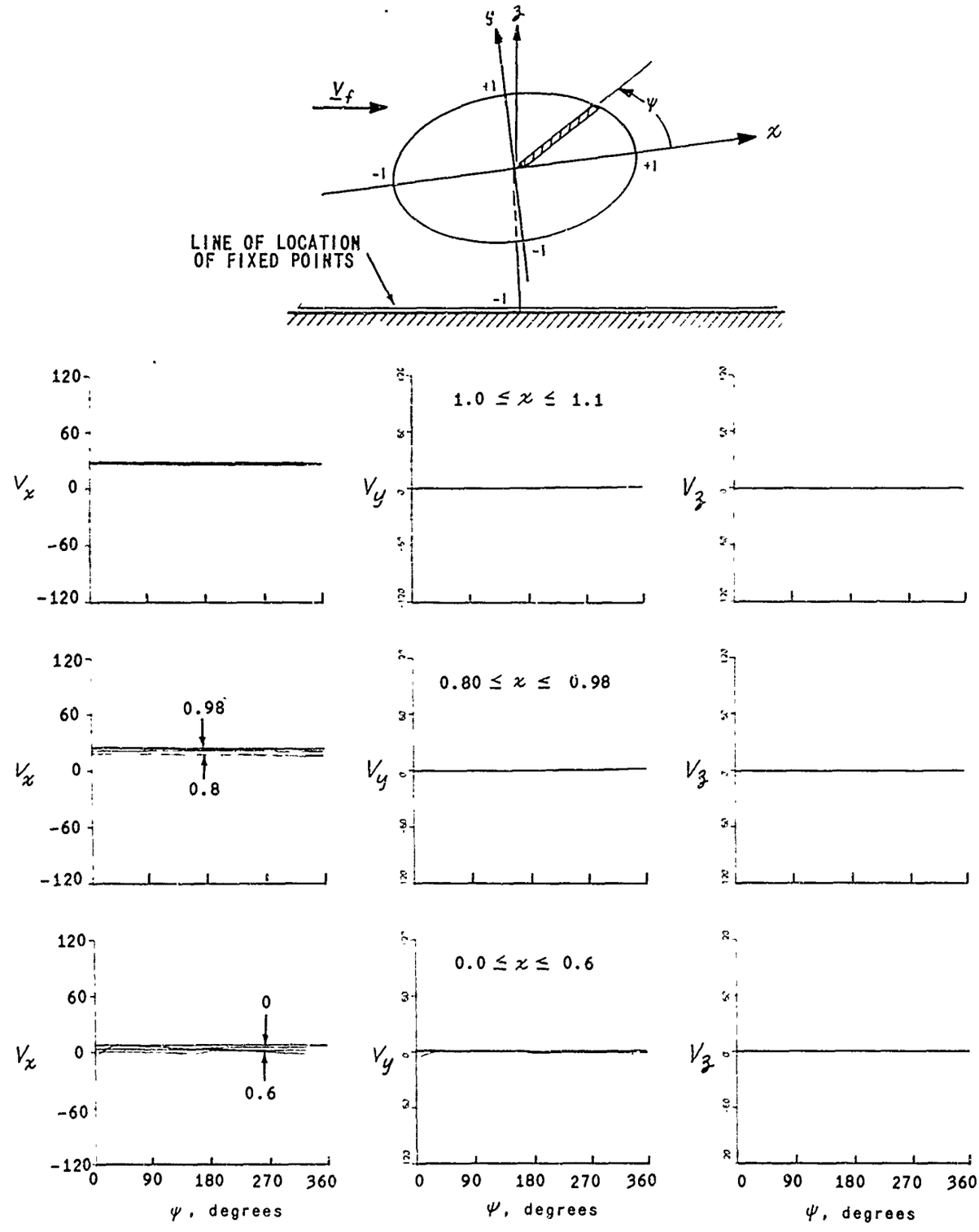

Figure 19h NONDIMENSIONAL VELOCITIES ALONG GROUND
CONDITIONS: μ = 0.05, λ = 0.00203, α_T = 1.25°;
y = 0.00, z = z_{GROUND}, x VARIABLE.

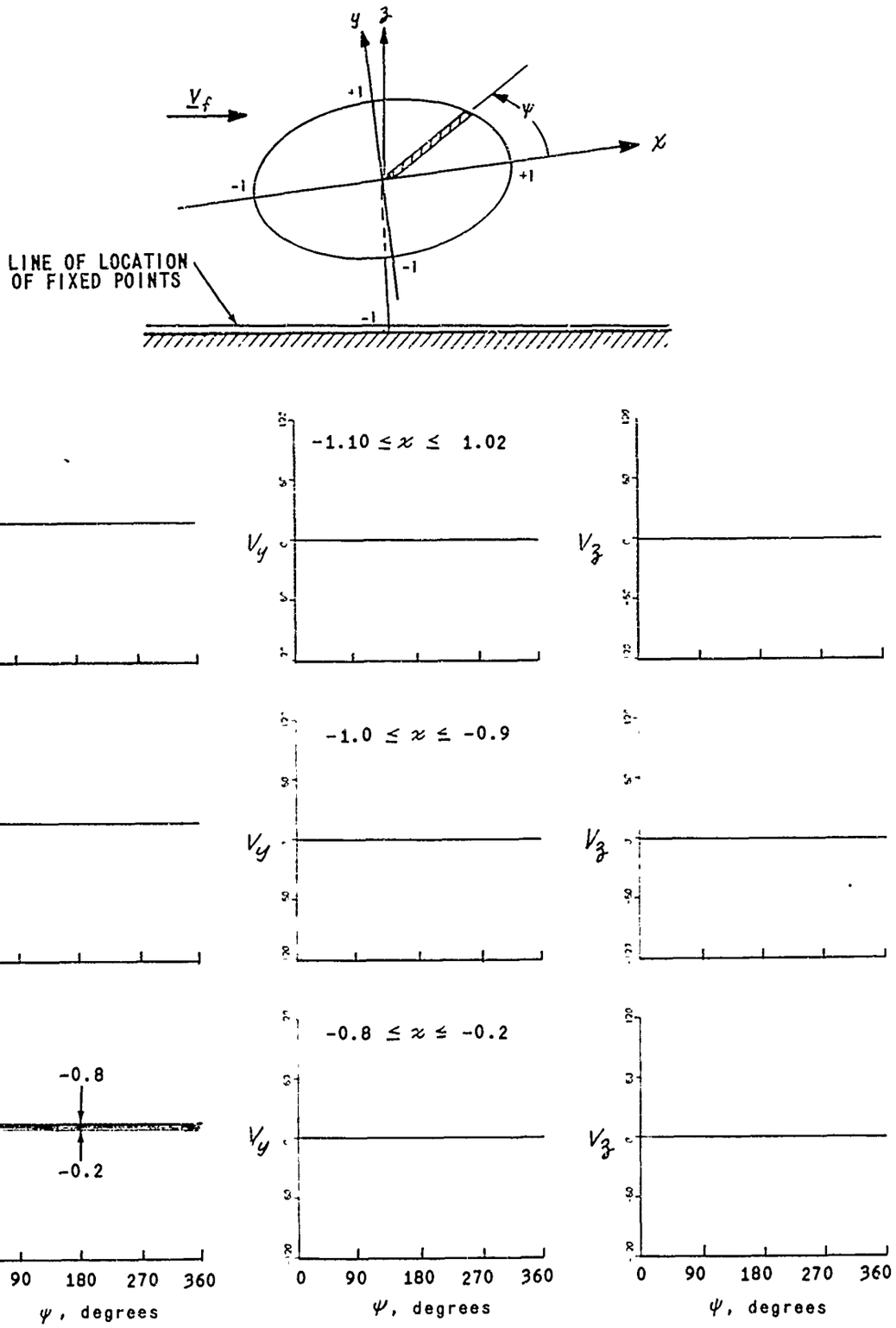

Figure 19i NONDIMENSIONAL VELOCITIES ALONG GROUND.
CONDITIONS: μ = 0.05, λ = 0.00203, α_T = 1.25°;
y = 0.00, z = z_{GROUND}, x VARIABLE.

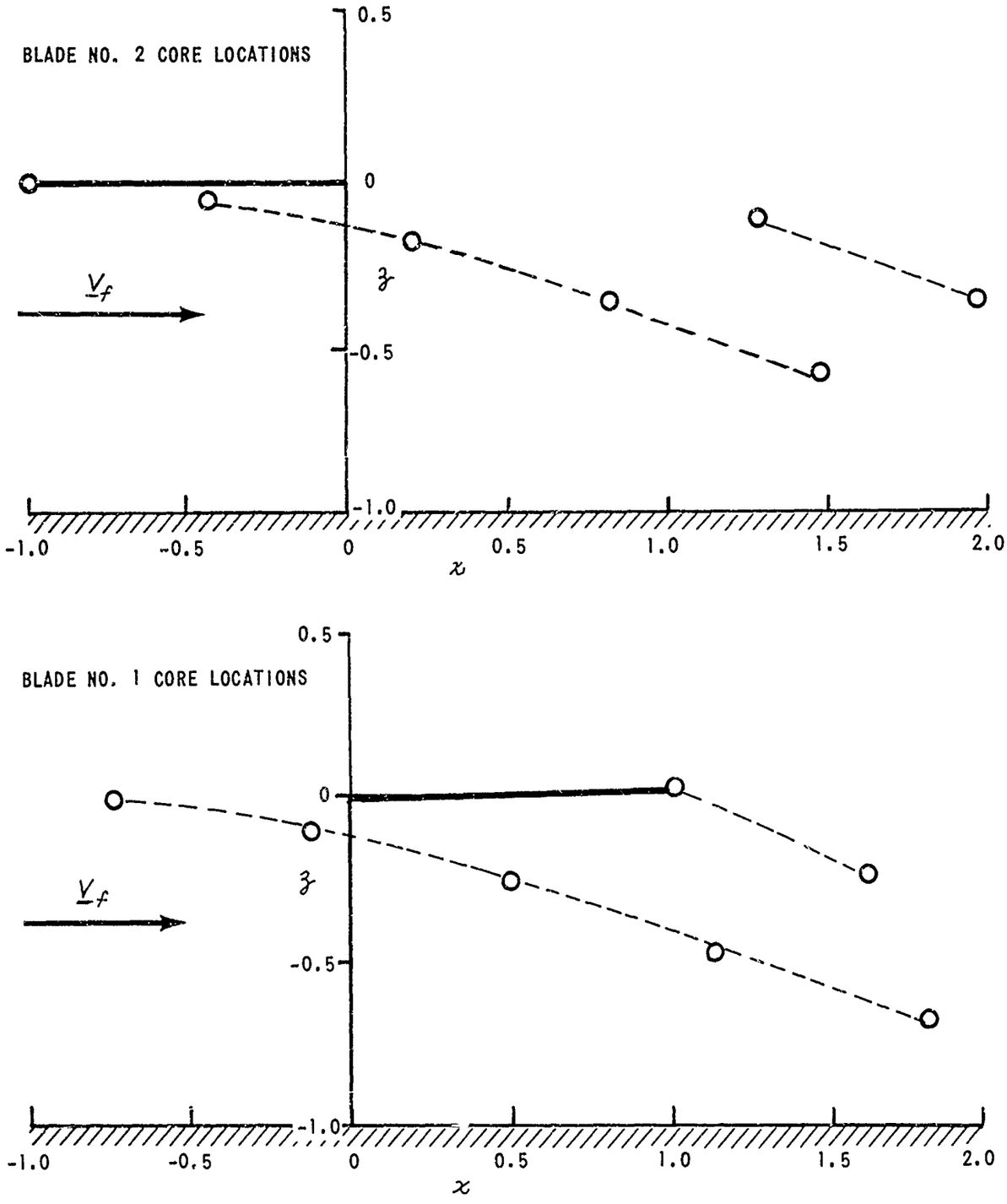

Figure 20a POSITIONS OF WAKE VORTICITY (CORES) IN LONGITUDINAL PLANE OF SYMMETRY WHEN BLADE NUMBER 1 IS AT $\psi = 0°$. CONDITIONS: $\mu = 0.10$, $\lambda = 0.00203$, $\alpha_T = 2.5°$.

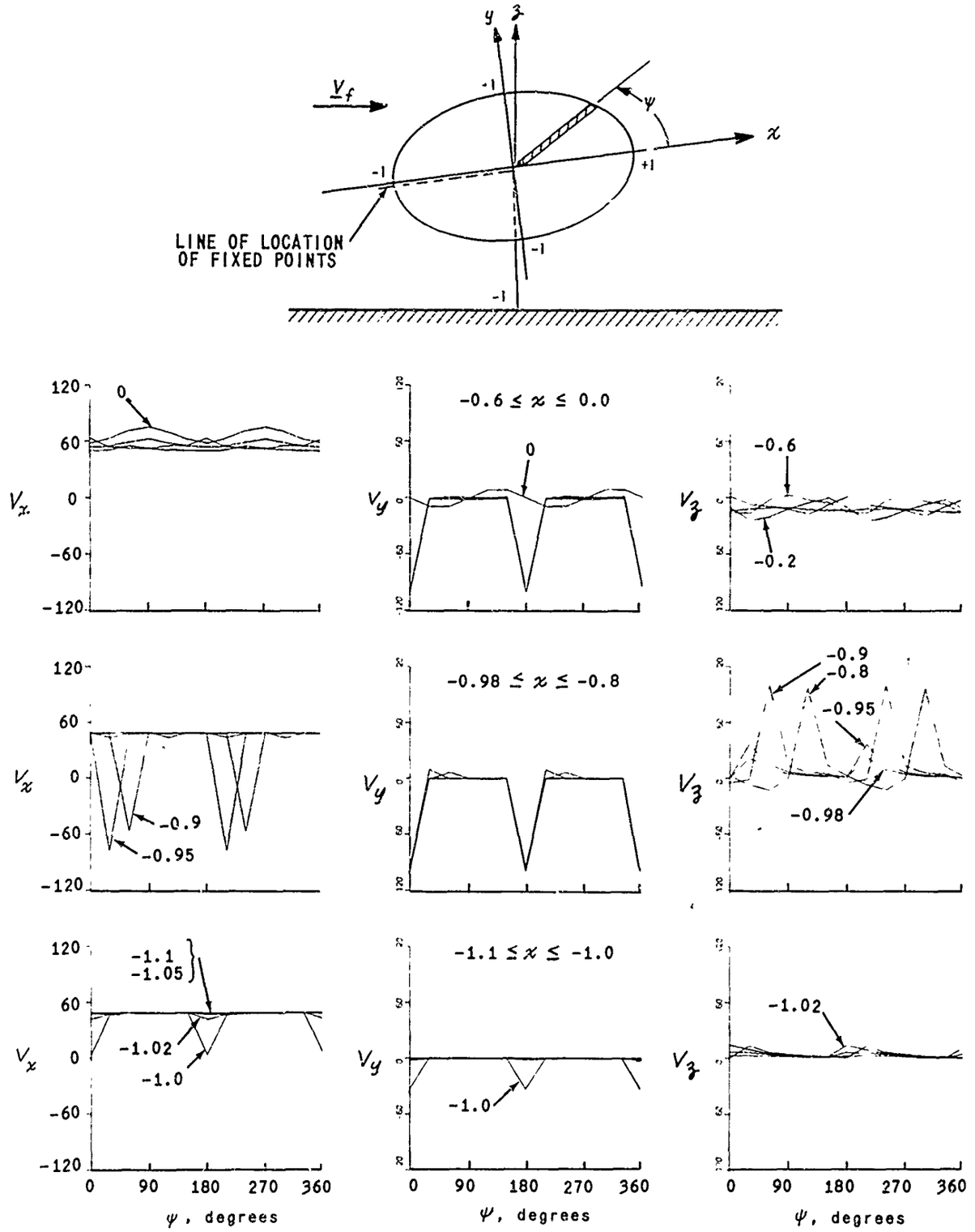

Figure 20b NONDIMENSIONAL VELOCITIES AT FIXED FIELD POINTS NEAR THE TIP PATH PLANE VS REFERENCE BLADE POSITION, ψ .
CONDITIONS: μ = 0.10, λ = 0.00203, α_T = 2.5°;
y = 0.00, z = -0.010, x VARIABLE.

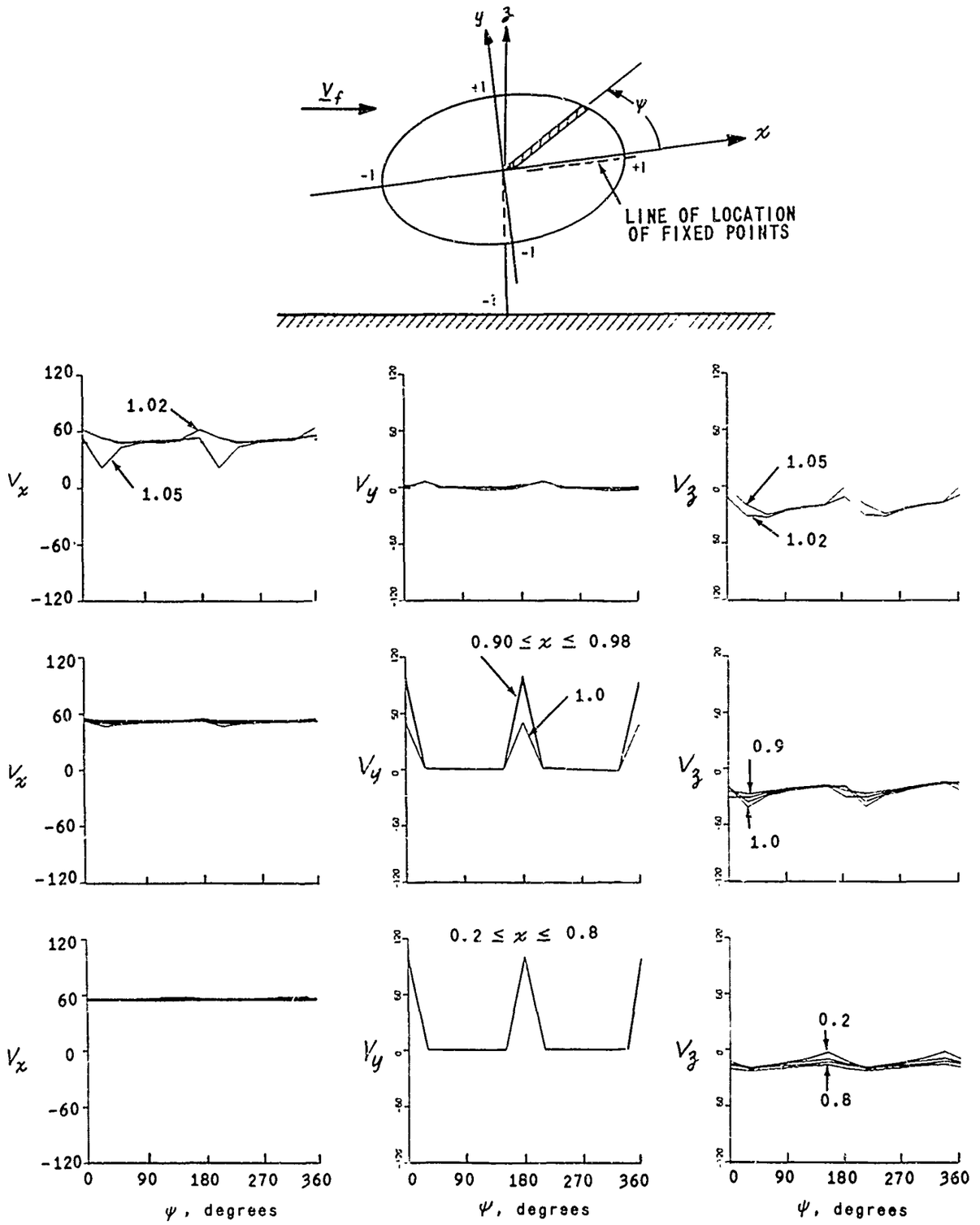

Figure 20c NONDIMENSIONAL VELOCITIES AT FIXED FIELD POINTS NEAR THE TIP PATH PLANE VS REFERENCE BLADE POSITION, ψ . CONDITIONS: μ = 0.10, λ = 0.00203, α_T = 2.5°; x = 0.00, z = -0.010, y VARIABLE.

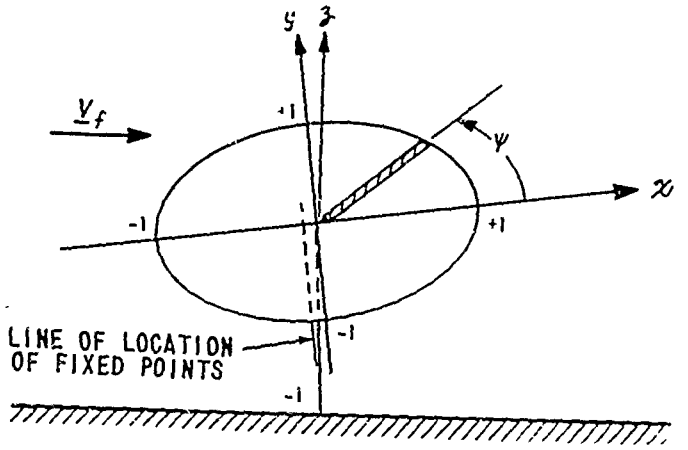

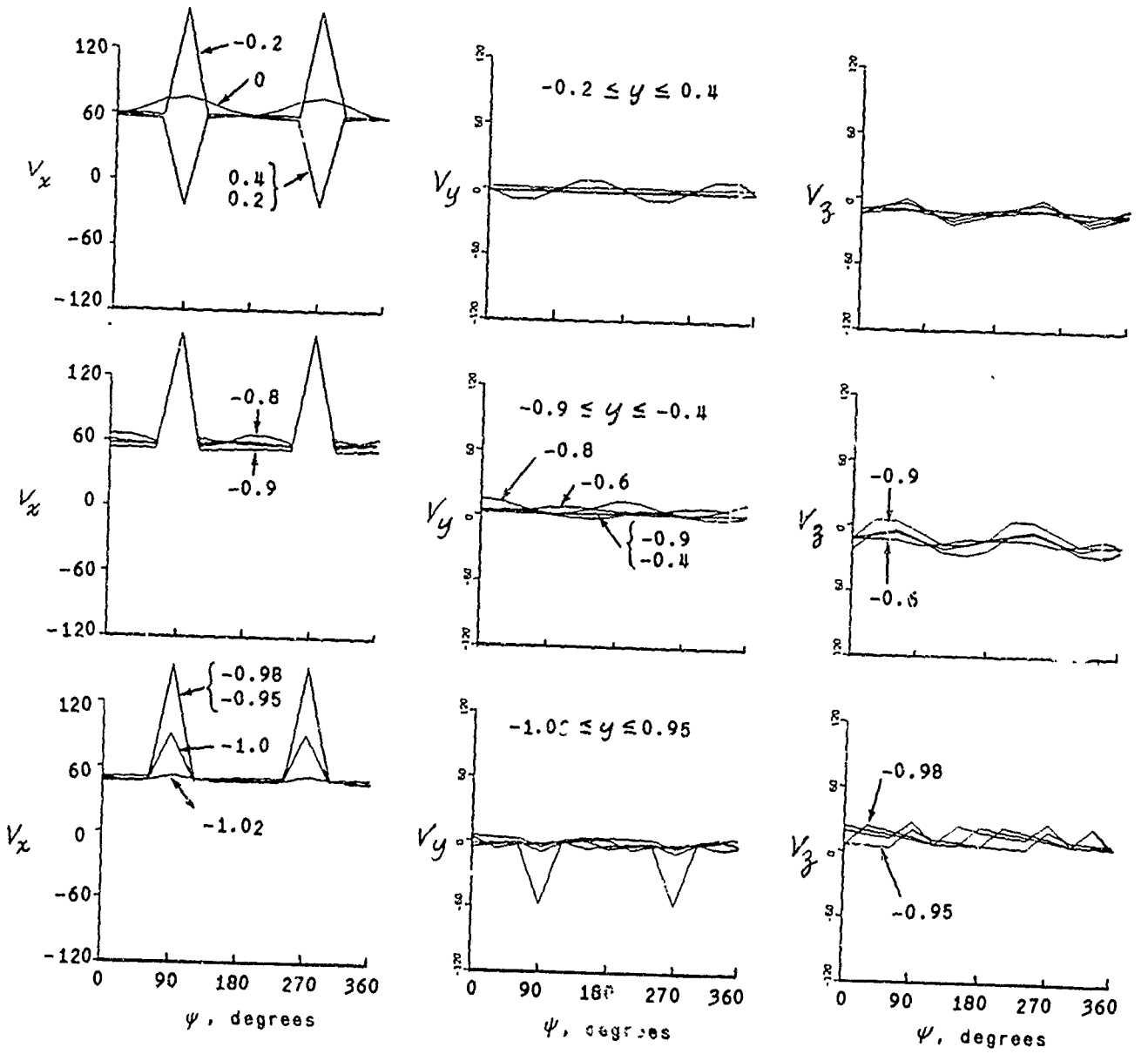

Figure 20d NONDIMENSIONAL VELOCITIES AT FIXED FIELD POINTS NEAR THE TIP PATH PLANE VS REFERENCE BLADE POSITIONS, ψ. CONDITIONS: $\mu = 0.10$, $\lambda = 0.00203$, $\alpha_T = 2.5°$; $y = 0.00$, $z = -0.10$, x VARIABLE.

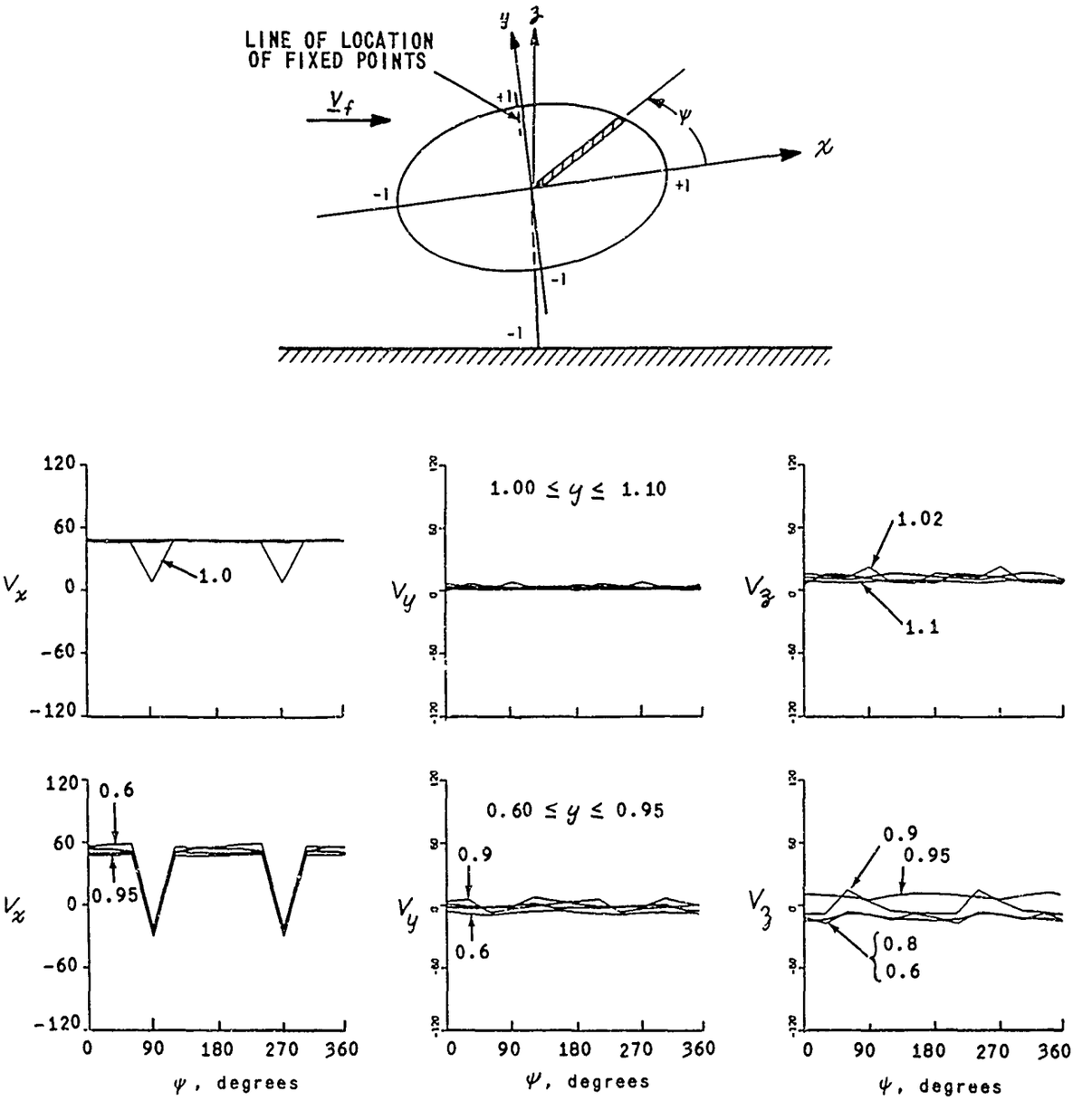

Figure 20e NONDIMENSIONAL VELOCITIES AT FIXED FIELD POINTS NEAR THE TIP PATH PLANE VS REFERENCE BLADE POSITION, ψ . CONDITIONS: μ = 0.10, λ = 0.00203, α_r = 2.5°; x = 0.00, z = -0.10, y VARIABLE.

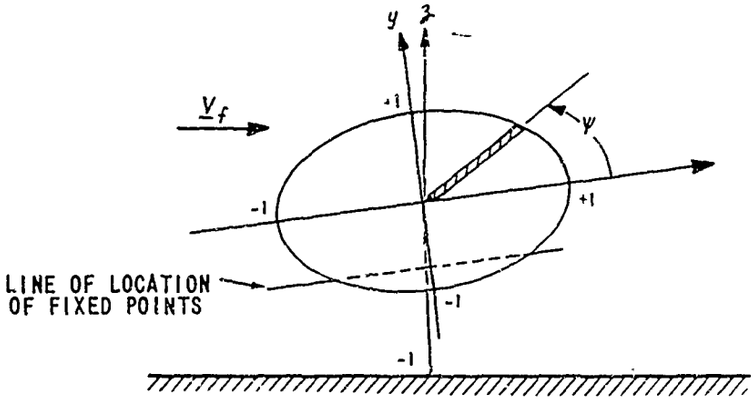

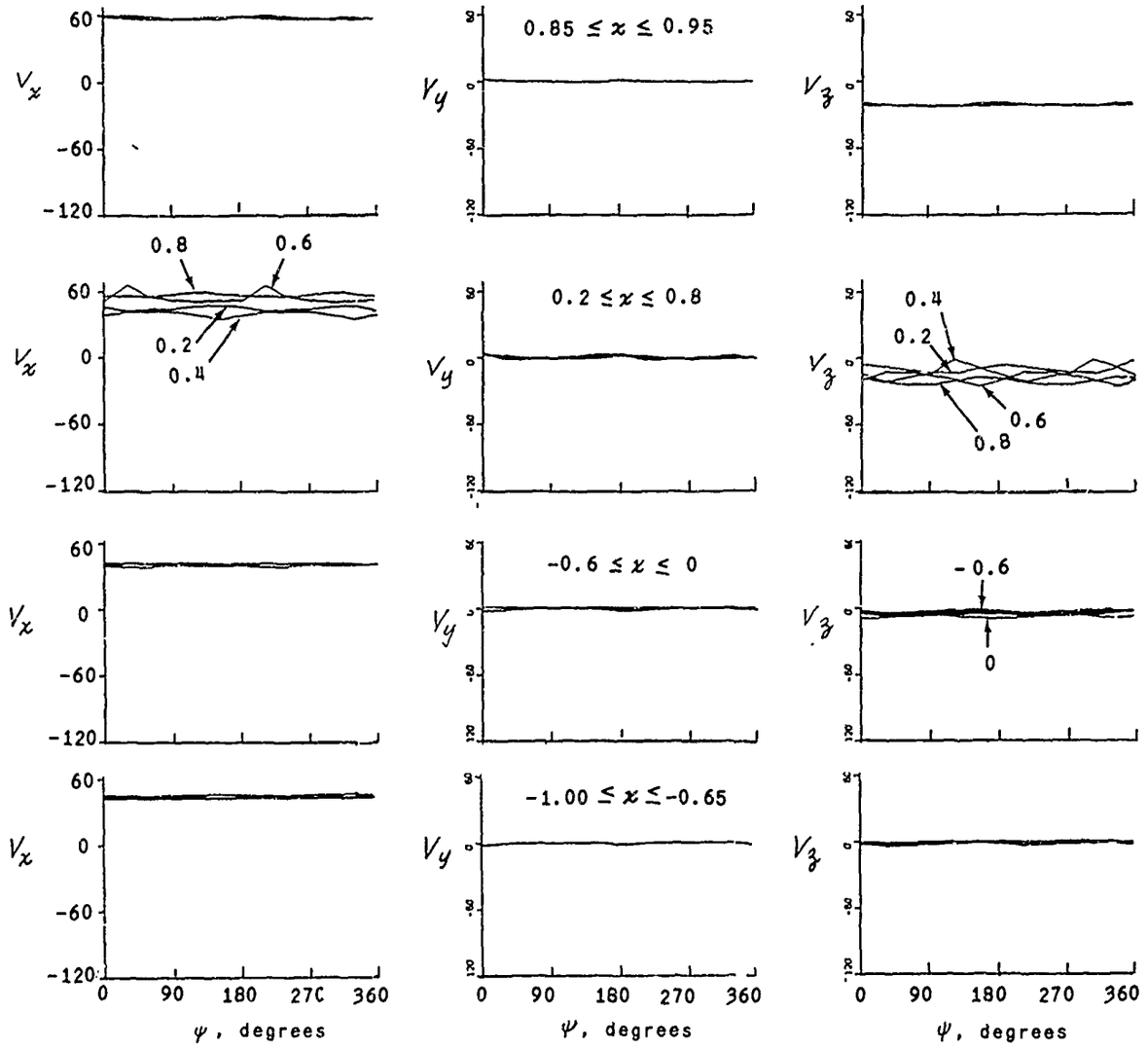

Figure 20f NONDIMENSIONAL VELOCITIES AT FIXED FIELD POINTS NEAR FUSELAGE LOCATION VS REFERENCE BLADE POSITION, ψ.
CONDITIONS: μ = 0.10, λ = 0.00203, α_T = 2.5°;
y = 0.00, z = -0.25, x VARIABLE.

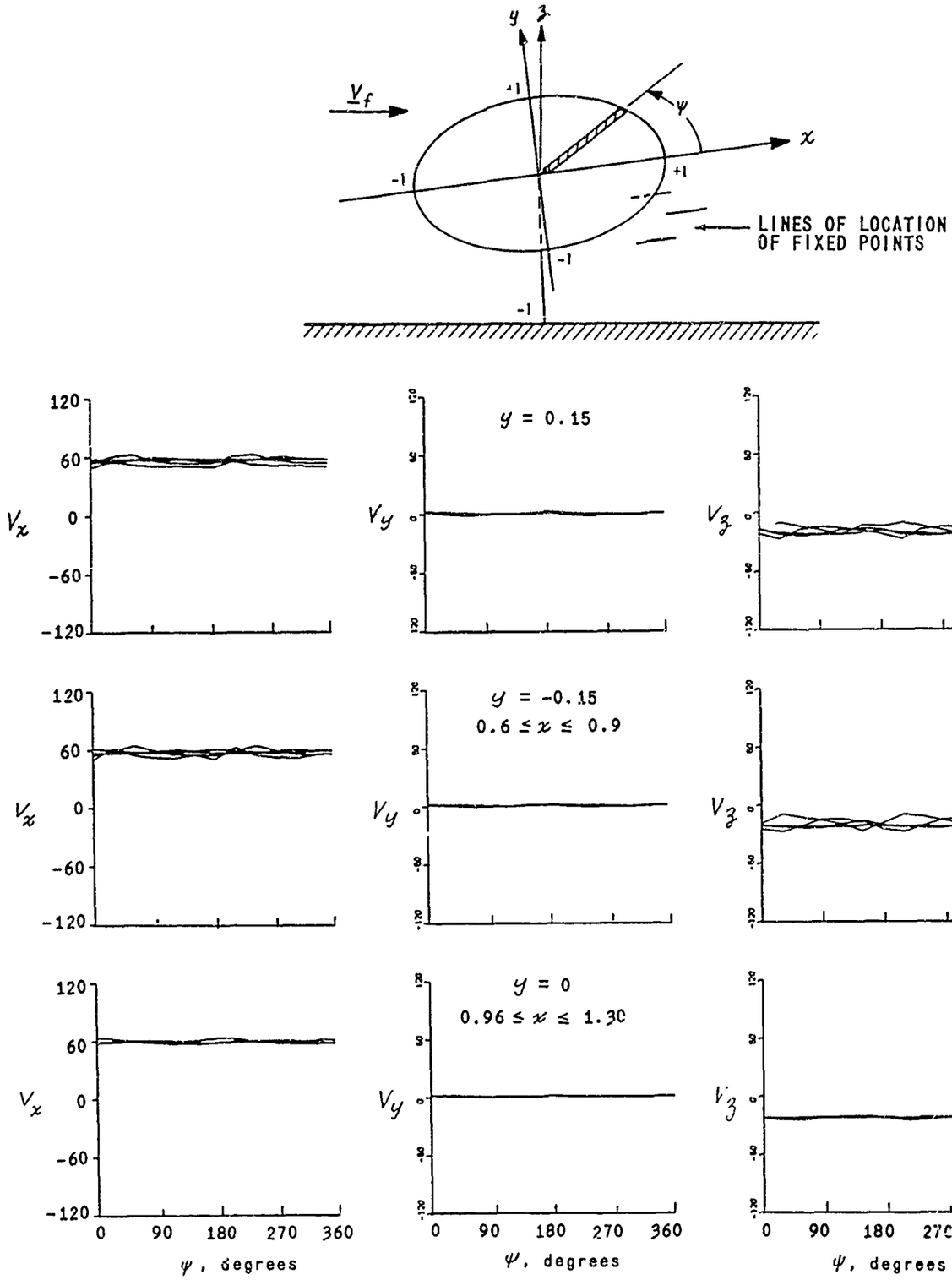

Figure 20g NONDIMENSIONAL VELOCITIES AT FIXED FIELD POINTS NEAR STABILIZER AND/OR TAIL ROTOR LOCATIONS VS REFERENCE BLADE POSITION, ψ. CONDITIONS: $\mu = 0.10$, $\lambda = 0.00203$, $\alpha_T = 2.5°$; $z = -0.25$, x AND y VARIABLE.

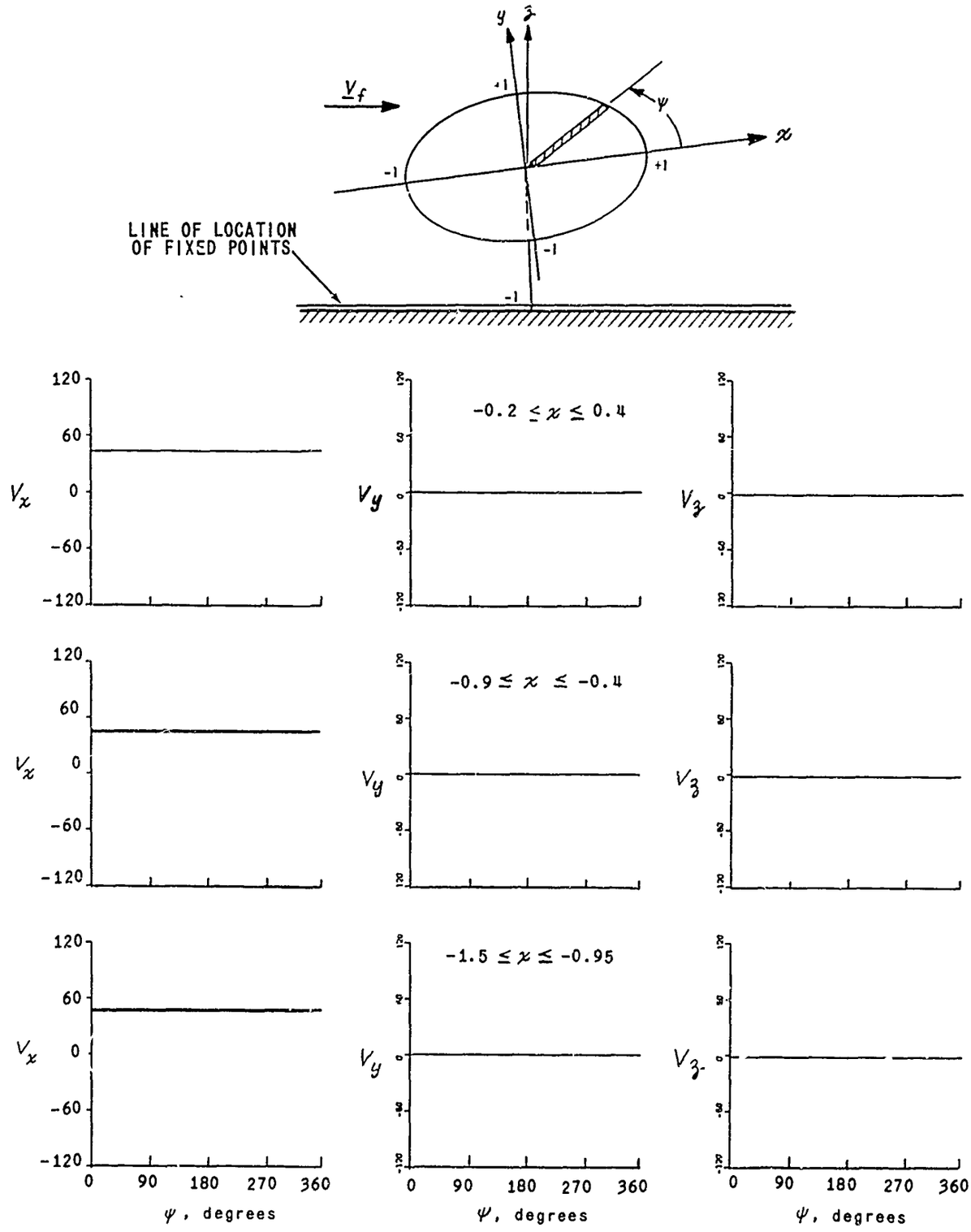

Figure 20h NONDIMENSIONAL VELOCITIES ALONG GROUND.
CONDITIONS: $\mu = 0.10$, $\lambda = 0.00203$, $\alpha_T = 2.5°$;
$y = 0.00$, $z = z_{GROUND}$, x VARIABLE.

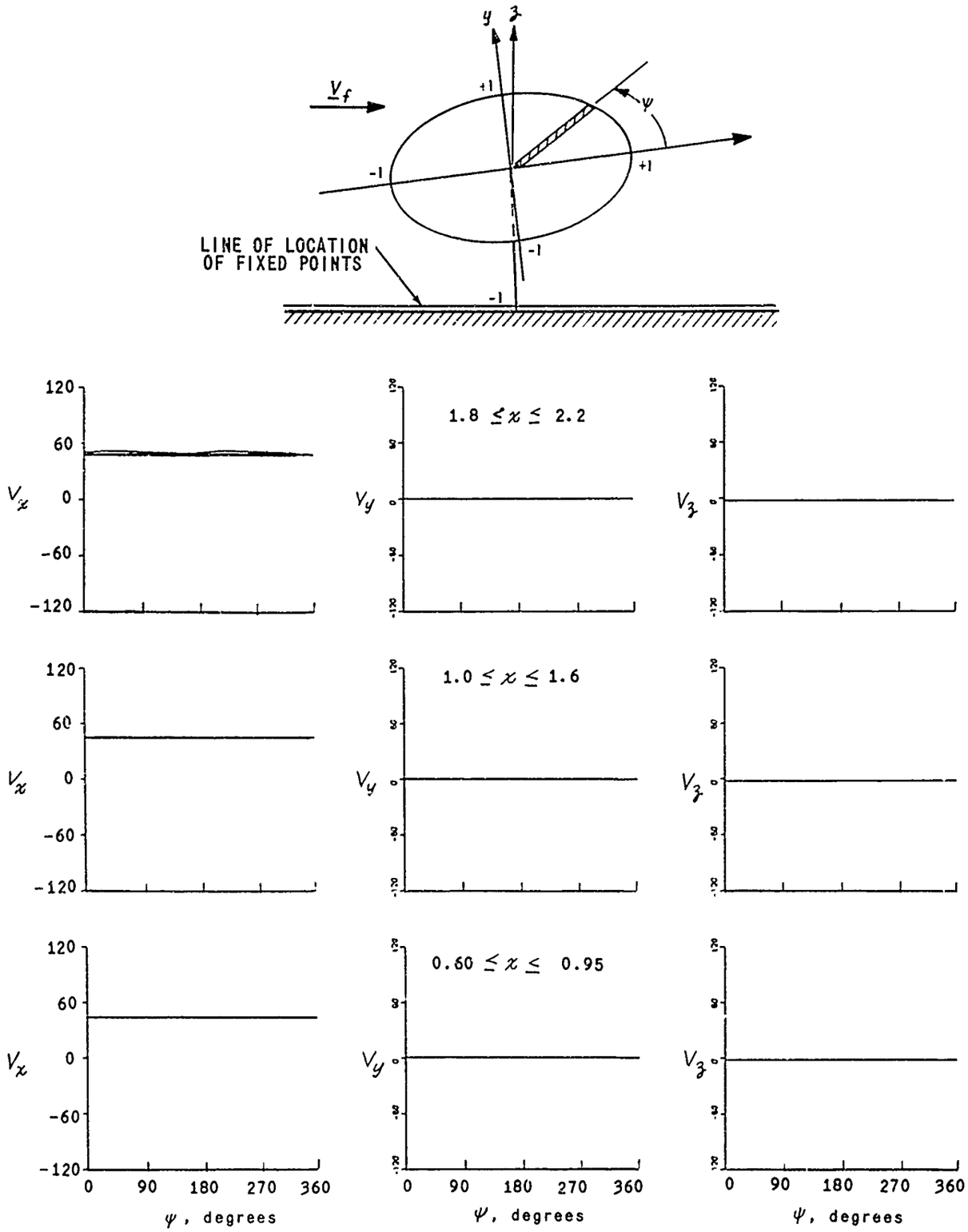

Figure 20i NONDIMENSIONAL VELOCITIES ALONG GROUND.
CONDITIONS: μ = 0.10, λ = 0.00203, α_T = 2.5°;
y = 0.00, $z = z_{GROUND}$, x VARIABLE.

APPENDIX

OPERATIONAL INFORMATION FOR THE COMPUTING PROGRAM

This program is written in FORTRAN IV, with the exception of subroutine CLEAR, which is written in MAP. This routine is used to initialize storages to be zero.

INPUTS

CARD 1	NB:	Number of blades, N_B
	NRW:	Number of revolutions of wake per blade, N_R
	NA:	Number of azimuth stations, N_A
	NPNCH:	Punch option. If zero, no cards are punched at the end of a run. If not zero, all wake point coordinates and core sizes at the final azimuth position are punched on cards.
	NOPT:	If zero, the initial wake configuration is computed. If not zero, initial wake configuration is read in.
	NTAPE:	If not zero, wake point coordinates and velocities are saved on utility Tape 4.
	NPRINT:	If NPRINT = 1, coordinates and velocities for each wake point are printed; if NPRINT = 2, those for every other point are printed; if 3, every third; etc.
	LNCT:	Number of lines desired per page of output.
	NFPT:	(Not used in the study reported here)
	NXPT:	Number of points off the wake for which velocities are to be calculated.
	NPINT:	Output is produced at intervals of NPINT steps; i. e., if NPINT = 1, the data for each azimuth position is printed.

CARD 2	PSI0:	Initial position of Blade 1, ψ_{init}, degrees.
	REV:	Number of revolutions of rotor for which calculations are to be performed, N_{RV}
	XLAM:	λ
	XMU:	μ
	ALPHAT:	α_T (degrees)
	RB:	R/C = ratio of blade radius to blade chord.
	H:	H/R
CARD 3, 4	GAMB:	Normalized strengths of Blade 1;* NA of them.
	A1:	Core sizes at Blade 1; (NA of them).
	A:	Initial core sizes; (NRW)(NA)(NB) of them.

Coordinates of points off the wake at which velocities are to be computed NXPT points in all (up to three sets of coordinates per card):

XIPT	YIPT	ZIPT
x	y	z

Initial Wake Configuration - Read in only if NOPT is not zero.

X:	(NRW)(NB)(NA) of them.
Y:	(NRW)(NB)(NA) of them.
Z:	(NRW)(NB)(NA) of them.

A listing of the program is given on the pages which follow.

*Estimated as $\Gamma_{B_1}(\psi) = 1 - 2\,\mu \sin\psi$ in the absence of data.

```
$IBFTC ?ZHWVG  LIST,REF
C      HELICOPTER WAKE VORTICITY WITH GROUND EFFECTS - MAIN PROGRAM
       COMMON X(340,5),Y(340,5),Z(340,5),U(340,5),V(340,5),W(340,5),
      1       GAMA(340,5),SE(340,5),GAMB(100),AI(100),A(340,5),PI,RAD,
      2        VMU,XMCL,XMSL,NB,NBW,NA,NW,NOPT,NTAPE,NPRINT,NOVCH,PSIO,
      3        XMU,XLAM,ALPHAT,PINT,PSIF,XNA,DPSI,NB1,NW1,XNW,XNB,TPNB,
      4        SAT,CAT,C1,C2,PSI,TPI,XI,T1,T2,XJ,NPS,JPS,IPS,IPS1,XXX,YYY,
      5        ZZZ,IST,IND,IFLG,SIG1,SIG2,SIG3,GGG,DEN,XMU1,XMU2,XMU3,IR1,
      6        XMX,XMY,XMZ,SIG4,SIG5,RR,SQI1,SE,SQI,SG,BE,LPS,SEG1,SEG2,
      7        SUM,LNCT,XIPT(100),YIPT(100),ZIPT(100),VX(100),VY(100),
      8        VZ(100),NXPT,NAB,FACTR,R3,H,WCRAB,SAT2,CAT2,SA2T,CA2T,THCAT
      9        ,THSAT
       DIMENSION GAMB(100)
       EQUIVALENCE(GAMB(1),GAMA)
     1 CALL CLEAR(X,NAB)
       PI = 3.14159265358
       RAD = .01745329252
       TPI = 2.0*PI
       READ 1000,NB,NBW,NA,NPNCH,NOPT,NTAPE,NPRINT,LNCT,NEPT,NXPT,NPINT,
      1           NOVCH
 1000 FORMAT(12I6)
       CALL OVDCHK(NOVCH)
       IF(NTAPE.LT.0) REWIND 4
       READ 1001,PSIO,DEN,XI/R,XMU,ALPHAT,RP,H
 1001 FORMAT(8F10.5)
       READ 1001,(GAMB(I),I=1,NA)
       READ 1001,(AI(I),I=1,NA)
       NB1 = NB
       NW = NBW*NA
       NW1 = NW+1
       NAB = NB*NA
       XNA = NA
       DPSI = 2.0*PI/XNA
       XNW = NW
       XNB = NB
       SAT = SIN(ALPHAT*RAD)
       CAT = COS(ALPHAT*RAD)
       SAT2 = SAT**2
       CAT2 = CAT**2
       SA2T = SIN(2.0*ALPHAT*RAD)
       CA2T = COS(2.0*ALPHAT*RAD)
       THSAT = 2.0*H*SAT
       THCAT = 2.0*H*CAT
       WCRAB = SQRT(.5*(SQRT((PI*XMU**2*XLAM*.25)**2+XMU**4)-XMU**2))
       XMWSC = (XMU+WCRAB*SAT)*CAT
       XMWSS = (XMU+WCRAB*SAT)*SAT
       WCCAT = WCRAB*CAT
       WCCATH = WCCAT/H
       C1 = XMU*CAT
       C2 = (XMU*SAT+XLAM)
       C3 = XMU*SAT+SQRT(XLAM**XMU/2.0)
       XMCL = C1/XLAM
       XMSL = XMU*SAT/XLAM
       TMP = PI*DPSI
```

```
      TMP1 = SQRT(TMP*(TMP+2.0))
      ERR = (TMP-TMP1+ALOG(1.0+TMP+TMP1))/DPSI
      READ 1001,((A(I,J),I=1,NW),J=1,NB1)
  101 IF(NXPT.EQ.0) GO TO 103
      READ 1001,(XIPT(I),YIPT(I),ZIPT(I),I=1,NXPT)
  103 PSIF = PSIF+360.0*DEV
      CALL IDOUT
      NCT = 0
      TPNB = 2.0*PI/XNB
      PSI = PSI0*RAD
      PSI0 = PSI
      PSIF = PSIF*RAD+0.05
      IF(NOPT.EQ.0) GO TO 2
    2 READ 1003,((X(I,J),I=1,NW1),J=1,NB)
 1003 FORMAT(5E12.5)
      READ 1003,((Y(I,J),I=1,NW1),J=1,NB)
      READ 1003,((Z(I,J),I=1,NW1),J=1,NB)
      GO TO 7
    3 DO 6  I=1,NW1
      XI = FLOAT(I-1)*DPSI
      EXPI = EXP(WOCATH*XI)
    4 DO 5  J=1,NB
      PSI0J = PSI0+FLOAT(J-1)*TPNB
      SPS0J = SIN(PSI0J)
      CPS0J = COS(PSI0J)
      THT0J = ATAN2(SPS0J,CPS0J*CAT)
      GIJ = (H+SAT*CPS0J)/EXPI-H
      RIJ = SQRT(1.0-SAT**2*CPS0J**2)+XLAM*(H**2*(EXPI-1.0)/(WOCAT*(H+SAT*
     1      CPS0J))-XI)/(2.0*H)
      X(I,J) = RIJ*CAT*COS(XI-THT0J)+XI*XMUSC+GIJ*SAT
      Y(I,J) = -RIJ*SIN(XI-THT0J)
      Z(I,J) = -RIJ*SAT*COS(XI-THT0J)-XI*XMUSS+GIJ*CAT
    5 CONTINUE
    6 CONTINUE
    7 NPS = AMOD(PSI0,2.0*PI)/DPSI+1.5
      IF (NPS.GT.NA) NPS = 1
      DO 9  J=1,NB
      JPS = MOD(NPS+(NA*(J-1)))/NB+NAB,NA)
      IF (JPS.EQ.0) JPS = NA
      IPS1 = JPS
      DO 8  I=1,NW
      IPS = IPS1
      IPS1 = IPS-1
      IF(IPS1.EQ.0) IPS1 = NA
      GAMA(I,J) = (GAMP(IPS)+GAMP(IPS1))/2.0
    8 CONTINUE
    9 CONTINUE
      IF(NTAPE.EQ.0)GO TO 10
      WRITE(4)NB,NBW,NA,NBNCH,NOPT,NTAPE,NPRINT,LNCT,NFPT,NXPT,NPINT,
     1        NOVCH,PSI0, DEV,XLAM,XMU,ALPHAT,BB,H
      WRITE(4)XIPT,YIPT,ZIPT
      CALL REWD(4)
   10 DO 12  J=1,NB1
      DO 11  I=1,NW
```

```
      SEG(I,J) = SQRT((X(I,J)-X(I+1,J))**2+(Y(I,J)-Y(I+1,J))**2+(Z(I,J)-
     1           Z(I+1,J))**2)
   11 CONTINUE
   12 CONTINUE
   13 DO 29  I=1,NW
      DO 28 J=1,NB1
      XXX = X(I,J)
      YYY = Y(I,J)
      ZZZ = Z(I,J)
      U(I,J) = 0.0
      V(I,J) = 0.0
      W(I,J) = 0.0
  130 DO 135  LL=1,NB
      XXBR = X(1,LL)*CA2T-Z(1,LL)*SA2T-THSAT
      YYBR = Y(1,LL)
      ZZBR = -(Z(1,LL)*CA2T+X(1,LL)*SA2T+THCAT)
      XXBR1 = X(2,LL)*CA2T-Z(2,LL)*SA2T-THSAT
      YYBR1 = Y(2,LL)
      ZZBR1 = -(Z(2,LL)*CA2T+X(2,LL)*SA2T+THCAT)
      SGBR1 = SQRT((XXX-XXBR)**2+(YYY-YYBR)**2+(ZZZ-ZZBR)**2)
  131 DO 134  IRR=1,NW
      SGBR2 = SQRT((XXX-XXBR1)**2+(YYY-YYBR1)**2+(ZZZ-ZZBR1)**2)
      SEGSQ = SEG(IRR,LL)**2
      HM1 = SGBR1**2+SGBR2**2
      IF (HM1.GT.SEGSQ) GO TO 132
      HM2 = .25*((SGBR1+SGBR2)**2-SEGSQ)*(SEGSQ-(SGBR1-SGBR2)**2)/SEGSQ
      IF (HM2.GT.A(IRR,LL)**2)GO TO 132
      GGG = -GAMA(IRR,LL)/SEG(IRR,LL)
      GO TO 133
  132 GGG = -GAMA(IRR,LL)*(SGBR1+SGBR2)/(SGBR1*SGBR2*((SGBR1+SGBR2)**2
     1       -SEGSQ))
  133 XNU1 = (YYY-YYBR1)*(ZZBR-ZZBR1)-(ZZZ-ZZBR1)*(YYBR-YYBR1)
      XNU2 = (ZZZ-ZZBR1)*(XXBR-XXBR1)-(XXX-XXBR1)*(ZZBR-ZZBR1)
      XNU3 = (XXX-XXBR1)*(YYBR-YYBR1)-(YYY-YYBR1)*(XXBR-XXBR1)
      U(I,J) = U(I,J)+XNU1*GGG
      V(I,J) = V(I,J)+XNU2*GGG
      W(I,J) = W(I,J)+XNU3*GGG
      SGBR1 = SGBR2
      XXBR = XXBR1
      YYBR = YYBR1
      ZZBR = ZZBR1
      XXBR1 = X(IRR+2,LL)*CA2T-Z(IRR+2,LL)*SA2T-THSAT
      YYBR1 = Y(IRR+2,LL)
      ZZBR1 = -(Z(IRR+2,LL)*CA2T+X(IRR+2,LL)*SA2T+THCAT)
  134 CONTINUE
  135 CONTINUE
   14 DO 25  L=1,NB1
      IST = 1
      IND = NB
      IFLG = 1
      IF (L.NE.J) GO TO 16
      IND = I-2
      IFLG = 2
      IF (IND.GT.0) GO TO 16
```

```
   15 IST = I+1
      IND = NW
      IFLG = 1
      IF (IST.GT.NW) GO TO 18
   16 SIG2 = SQRT((XXX-X(IST,L))**2+(YYY-Y(IST,L))**2+(ZZZ-Z(IST,L))**2)
      DO 17 IR=IST,IND
      SIG1 = SIG2
      SIG2 = SQRT((XXX-X(IR+1,L))**2+(YYY-Y(IR+1,L))**2+(ZZZ-Z(IR+1,L))
     1       **2)
      SEGSQ = SEG(IR,L)**2
      HM1 = SIG1**2+SIG2**2
      IF(HM1.GT.SEGSQ)GO TO 160
      HM2 = .25*((SIG1+SIG2)**2-SEGSQ)*(SEGSQ-(SIG1-SIG2)**2)/SEGSQ
      IF(HM2.GT.A(IR,L)**2)GO TO 160
      GGG = GAMA(IR,L)/SEG(IR,L)
      GO TO 161
  160 GGG = GAMA(IR,L)*(SIG1+SIG2)/(SIG1*SIG2*((SIG1+SIG2)**2-SEGSQ))
  161 XNU1 = (YYY-Y(IR+1,L))*(Z(IR,L)-Z(IR+1,L))-(ZZZ-Z(IR+1,L))*
     1       (Y(IR,L)-Y(IR+1,L))
      XNU2 = (ZZZ-Z(IR+1,L))*(X(IR,L)-X(IR+1,L))-(XXX-X(IR+1,L))*
     1       (Z(IR,L)-Z(IR+1,L))
      XNU3 = (XXX-X(IR+1,L))*(Y(IR,L)-Y(IR+1,L))-(YYY-Y(IR+1,L))*
     1       (X(IR,L)-X(IR+1,L))
      U(I,J) = U(I,J)+XNU1*GGG
      V(I,J) = V(I,J)+XNU2*GGG
      W(I,J) = W(I,J)+XNU3*GGG
   17 CONTINUE
      GO TO (18,15),IFLG
   18 IF (L.NE.J) GO TO 25
      IR1 = I-1
      IF (I.EQ.1) IR1 = 1
      XMX = (Y(IR1,L)-Y(IR1+1,L))*(Z(IR1+1,L)-Z(IR1+2,L))-(Y(IR1+1,L)-
     1       Y(IR1+2,L))*(Z(IR1,L)-Z(IR1+1,L))
      XMY = (Z(IR1,L)-Z(IR1+1,L))*(X(IR1+1,L)-X(IR1+2,L))-(Z(IR1+1,L)-
     1       Z(IR1+2,L))*(Y(IR1,L)-X(IR1+1,L))
      XMZ = (X(IR1,L)-X(IR1+1,L))*(Y(IR1+1,L)-Y(IR1+2,L))-(X(IR1+1,L)-
     1       X(IR1+2,L))*(Y(IR1,L)-Y(IR1+1,L))
      SIG4 = SEG(IR1+1,L)
      SIG3 = SEG(IR1,L)
      SIG5 = SQRT((X(IR1+2,L)-X(IR1,L))**2+(Y(IR1+2,L)-Y(IR1,L))**2+
     1       (Z(IR1+2,L)-Z(IR1,L))**2)
      DEN = (SIG3+SIG4-SIG5)*(SIG3+SIG4+SIG5)*(SIG4+SIG5-SIG3)*(SIG3+
     1       SIG5-SIG4)
      IF (DEN.EQ.0.0) GO TO 25
      IF(DEN.LT.0.0)WRITE(6,1002)I,J,SIG3,SIG4,SIG5
 1002 FORMAT(2X43HDENOMINATOR NEGATIVE FOR R COMPUTATION  I =I3,3X3HJ =
     1       I3,3X6HSIG3 =F16.8,3X6HSIG4 =F16.8,3X6HSIG5 =F16.8 )
      RR = SIG3*SIG4*SIG5/SQRT(ABS(DEN))
      SQI1 = SQRT((2.0*RR-SIG3)*(2.0*RR+SIG3))
      IF (SIG3**2.LE.SIG4**2+SIG5**2) GO TO 19
      SF = (2.0*RR+SQI1)/SIG3
      GO TO 20
   19 SF = (2.0*RR-SQI1)/SIG3
      IF(SF.EQ.0.0) SF = 1.0E-20
```

```
   20 SQT = SQRT((2.0*RR-SIG4)*(2.0*RR+SIG4))
      IF (SIG4**2.LE.SIG4**2+SIG**2) GO TO 21
      SG = (2.0*RR+SQT)/SIG4
      GO TO 22
   21 SG = (2.0*RR-SQT)/SIG4
      IF(SG.EQ.0.0) SG = 1.0E-20
   22 IF (I.EQ.1) GO TO 23
      BF = (GAMA(IM1,J)*(ALOG(8.0*SF/A(IM1,J))+.25)+GAMA(I,J)*(ALOG(8.0*
     1       SG/A(I,J))+.25))/(4.0*RR*SQRT(XMX**2+XMY**2+XMZ**2))
      GO TO 24
   23 BF = (GAMA(I,J)*(ALOG(8.0*SF/A(I,J))+.25))/(4.0*RR*SQRT(XMX**2+
     1      XMY**2+XMZ**2))
   24 U(I,J) = U(I,J)+XMX*BF
      V(I,J) = V(I,J)+XMY*BF
      W(I,J) = W(I,J)+XMZ*BF
   25 CONTINUE
      SIG1 = SQRT(XXX**2+YYY**2+ZZZ**2)
      XXRR = -THSAT
      YYRR = 0.0
      ZZRR = -THCAT
      SGRR1 = SQRT((XXX-XXRR)**2+(YYY-YYRR)**2+(ZZZ-ZZRR)**2)
   26 DO 27  I=1,MR
      LPS = MOD(APS+(MA*(L-1))/MR+MAR,MA)
      IF(LPS.EQ.0) LPS = MA
      XXRR1 = X(1,L)*CA2T-THSAT
      YYRR1 = Y(1,L)
      ZZRR1 = -X(1,L)*SA2T-THCAT
      XNU11 = (YYY2-YYY)*(ZZRR1-ZZRR)+(ZZZ-ZZRR)*(YYRR1-YYRR)
      XNU21 = (ZZZ2-ZZZ)*(XXRR1-XXRR)+(XXX-XXRR)*(ZZRR1-ZZRR)
      XNU31 = (XXX2-XXX)*(YYRR1-YYRR)+(YYY-YYRR)*(XXRR1-XXRR)
      SGRR2 = SQRT((XXX-XXRR1)**2+(YYY-YYRR1)**2+(ZZZ-ZZRR1)**2)
      GGG1 =GAMA(LPS)*(SGRR1+SGRR2)/(SGRR1*SGRR2*((SGRR1+SGRR2)**2-1.0))
      U(I,J) = U(I,J)-GGG1*XNU11
      V(I,J) = V(I,J)-GGG1*XNU21
      W(I,J) = W(I,J)-GGG1*XNU31
      IF((I.EQ.1.AN).L.EQ.J)GO TO 260
      PSIRK = FLOAT(LPS-1)*DPSI
      SINPSI = SIN(PSIRK)
      COSPSI = COS(PSIRK)
      RMH2 = (YYY-COSPSI)**2+(YYY-SINPSI)**2+ZZZ**2
      IF (RMH2+SIG1**2.GT.1.0) GO TO 258
      RMH = SQRT(RMH2)
      H2 = .25*((SIG1+RMH)**2-1.0)*(1.0-(SIG1-RMH)**2)
      IF (H2*RR**2.GT.1.0) GO TO 258
      HH = SQRT(H2)
      XHT = XXX*(COSPSI**2+SINPSI**2/(HH*RR))-YYY*SINPSI*COSPSI*(1.0/
     1       (HH*RR)-1.0)
      YHT = YYY*(SINPSI**2+COSPSI**2/(HH*RR))-XXX*SINPSI*COSPSI*(1.0/
     1       (HH*RR)-1.0)
      ZHT = ZZZ/(HH*RR)
      XNU11 = -YHT*Z(1,L)+ZHT*Y(1,L)
      XNU12 = -ZHT*Y(1,L)+XHT*Z(1,L)
      XNU13 =-YHT*Y(1,L)+YHT*X(1,L)
      SIG2 = SQRT((XHT-X(1,L))**2+(YHT-Y(1,L))**2+(ZHT-Z(1,L))**2)
```

```
      GO TO 259
  258 XNU1 = -YYY*Z(I,L)+ZZZ*Y(I,L)
      XNU2 = -ZZZ*X(I,L)+XXX*Z(I,L)
      XNU3 = -XXX*Y(I,L)+YYY*X(I,L)
      SIG2 = SQRT((XXX-X(I,L))**2+(YYY-Y(I,L))**2+(ZZZ-Z(I,L))**2)
  259 GGG = GAMA(LPS)*(SIG1*SIG2)/(SIG1*SIG2*((SIG1+SIG2)**2-1.0))
      U(I,J) = U(I,J)+XNU1*GGG
      V(I,J) = V(I,J)+XNU2*GGG
      W(I,J) = W(I,J)+XNU3*GGG
      GO TO 27
  260 W(I,J) = W(I,J)-GAMA(LPS)*EPR
   27 CONTINUE
      U(I,J) = U(I,J)+XMCL
      W(I,J) = W(I,J)-XMSL
   28 CONTINUE
   29 CONTINUE
   30 IF(NCT.NE.0)GO TO 31
      IF(NXPT.NE.0)CALL VLCTY
      CALL OUTPUT
   31 NCT = NCT+1
      IF(NCT.GE.NPRINT)NCT = 0
      IF(NTAPE.EQ.0) GO TO 310
      WRITE(4)PSI,XMU,XLAM,ALPHAT,NR,NRM,NA,NW
      WRITE(4) ((X(I,J),Y(I,J),Z(I,J),U(I,J),V(I,J),W(I,J),GAMA(I,J),
     1          A(I,J),I=1,NW1),J=1,NR1)
      WRITE(4)VX,VY,VZ
  310 PSI = PSI+DPSI
      NPS = NPS+1
      IF (NPS.GT.NA) NPS = 1
      IF(PSI.LE.PSIE) GO TO 32
      IF(NTAPE.NE.0) END FILE 4
      IF(NPUNCH.EQ.0) GO TO 1
      PUNCH 1004
 1004 FORMAT(74H77    REINCORTED VAKE VORTICITY CALCULATIONS - HARVEY
     1SELIR              77 )
      PUNCH 1001,((A(I,J),I=1,NW),J=1,NR)
      PUNCH 1002,((X(I,J),I=1,NW1),J=1,NR)
      PUNCH 1002,((Y(I,J),I=1,NW1),J=1,NR)
      PUNCH 1002,((Z(I,J),I=1,NW1),J=1,NR)
      GO TO 1
   32 DO 35  J=1,NR1
      TX1 = X(1,J)
      TY1 = Y(1,J)
      TZ1 = Z(1,J)
      DO 33 I=2,NW1
      TX2 = TY1
      TY2 = TY1
      TZ2 = TZ1
      TX1 = X(I,J)
      TY1 = Y(I,J)
      TZ1 = Z(I,J)
      X(I,J) = TX2+XLAM*U(I-1,J)*DPSI
      Y(I,J) = TY2+XLAM*V(I-1,J)*DPSI
      Z(I,J) = TZ2+XLAM*W(I-1,J)*DPSI
```

```
      IF(X(I,J)*SAT+Z(I,J)*(CAT+H.GT.A(I,J))GO TO 33
      X(I,J) = (X(I,J)*CAT-Z(I,J)*SAT)*CAT-(H-A(I,J))*SAT
      Z(I,J) = -((H-A(I,J))*CAT+(X(I,J)*CAT-Z(I,J)*SAT)*SAT)
   33 CONTINUE
      XJ = FLOAT(J-1)*TPNB
      X(I,J) = COS(PSI+XJ)
      Y(I,J) = SIN(PSI+XJ)
      Z(I,J) = 0.0
   35 CONTINUE
      DO 38  J=1,NB1
      JPS = MOD(NPS+(NA*(J-1))/NB+NAB,NA)
      IF(JPS.EQ.0) JPS = NA
      JPS1 = JPS-1
      IF(JPS1.EQ.0)JPS1 = NA
      SEG1 = SEG(1,J)
      GAM1 = GAMA(1,J)
      TA1 = A(1,J)
   36 DO 37  I=2,NN
      GAM2 = GAM1
      GAM1 = GAMA(I,J)
      GAMA(I,J) = GAM2
      SEG2 = SEG1
      SEG1 = SEG(I,J)
      SEG(I,J) = SQRT((X(I,J)-X(I+1,J))**2+(Y(I,J)-Y(I+1,J))**2+(Z(I,J)-
     1           Z(I+1,J))**2)
      TA2 = TA1
      TA1 = A(I,J)
      A(I,J) = TA2*SQRT(SEG2/SEG(I,J))
   37 CONTINUE
      SEG(1,J) = SQRT((X(1,J)-X(2,J))**2+(Y(1,J)-Y(2,J))**2+(Z(1,J)-
     1           Z(2,J))**2)
      A(1,J) = A1(JPS)
      GAMA(1,J) = (GAMB(JPS)+GAMB(JPS1))/2.0
   38 CONTINUE
      GO TO 13
      END
```

```
$IBFTC 777DT   LIST,REF
C     HELICOPTER WAKE VORTICITY WITH GROUND EFFECTS - SUBROUTINE IOOUT
      SUBROUTINE IOOUT
      COMMON X(340,5),Y(340,5),Z(340,5),U(340,5),V(340,5),W(340,5),
     1       GAMA(340,5),SEG(340,5),GAMB1(100),AI(100),A(340,5),PI,RAD,
     2        VMB,XMCL,XMSL,NB,NBW,NA,NW,NOPT,NTAPE,NPRINT,NOVCH,PSIO,
     3        XMU,XLAM,ALPHAT,DINT,PSIF,XNA,DPSI,NB1,NW1,XNW,XNR,TPNB,
     4        SAT,CAT,C1,C2,PSI,TPI,XI,T1,T2,XJ,NPS,JPS,IPS,IPS1,XXX,YYY,
     5        ZZZ,IST,IND,IFLG,SIG1,SIG2,SIG3,GGG,DEN,XNU1,XNU2,XNU3,TR1,
     6        XMY,XMY,XM7,SIG4,SIG5,RR,SQI1,SE,SQI,SG,BE,LPS,SEG1,SEG2,
     7        SUM,LNCT,XIPT(100),YIPT(100),ZIPT(100),VX(100),VY(100),
     8        VZ(100),NXPT,NAP,RADIP,RB,H,WORAP,SAT2,CAT2,SA2T,CA2T,THCAT
     9        ,THSAT
    1 WRITE(6,1000)NB,NBW,NA,PSIO,PSIF,XLAM,XMU,ALPHAT,RR,H
 1000 FORMAT(1H1,40X33HHELICOPTER WAKE VORTICITY PROGRAM //45X31HNUMBER
     1OF BLADES                =I11 /45X31HNUMBER OF REVOLUTIONS OF WAKE =
     2 I11 /45X31HNUMBER OF AZIMUTH STATIONS     =I11
     3      /45X,23HPSI (INITIAL)          =
     3          F11.3,8H DEGREES /45X23HPSI (FINAL)              =F11.3,
     4 8H DEGREES /45X23HLAMBDA                    =F12.5 /45X23HMU
     5            =F12.5 /45X23HALPHAT                    =F11.3,8H DEGREES /
     6       45X23HR/3                       =F11.3/
     7       45X23H4                         =F11.3)
    2 DPS = 360.0/FLOAT(NA)
      PS = 0.0
      WRITE(6,1001)
 1001 FORMAT(//40X33HPSI,15X22H  STRENGTH OF BLADE 1 ,14X22HCORE SIZE AT
     1BLADE 1 )
    3 DO 4  I=1,NA
      WRITE(6,1002)PS,GAMB1(I),AI(I)
 1002 FORMAT(F35.3,F40.5,F35.5)
      PS = PS+DPS
    4 CONTINUE
      RETURN
      END
```

```
$IBFTC ZZOUTP  LIST,REF
C     HELICOPTER WAKE VORTICITY WITH GROUND EFFECTS - SUBROUTINE OUTPUT
      SUBROUTINE OUTPUT
      COMMON X(340,5),Y(340,5),Z(340,5),U(340,5),V(340,5),W(340,5),
     1       GAMA(340,5),SEG(340,5),GAMBI(100),AL(100),A(340,5),PI,RAD,
     2        VMP,XMCL,XMSL,NB,NRW,NA,NW,NUPT,NTAPE,NPRINT,NOVCH,PSIO,
     3        XMU,XLAM,ALPHAT,PINT,PSIF,XMA,DPSI,NP1,NW1,XMW,XNR,TPNB,
     4        SAT,CAT,C1,C2,PSI,TPI,X1,T1,T2,XJ,NPS,JPS,IPS,IPS1,XXX,YYY,
     5        ZZZ,IST,IND,IFLG,SIG1,SIG2,SIG3,GGG,DEN,XMU1,XMU2,XMU3,IR1,
     6        XMY,XMY,XM7,SIG4,SIG5,RR,SQI1,SF,SQI,SG,BF,IPS,SEG1,SEG2,
     7        SUM,LNCT,XIPT(100),YIPT(100),ZIPT(100),VX(100),VY(100),
     8        VZ(100),NXPT,NAB,FACTR,RB,H,WGRAP,SAT2,CAT2,SA2T,CA2T,THCAT
     9        ,THSAT
    1 ILINE = 0
      PSIO = PSI/RAD
      DPSID = DPSI/RAD
    2 DO 5 J=1,NB1
      IF(ILINE.EQ.0) WRITE(6,1000)NB,NA,NRW,XLAM,XMU,ALPHAT,DPSID,PSID
 1000 FORMAT(1H1,44X28HHELICOPTER WAKE VORTICITY DISTRIBUTION //13X
     1       15HNO. OF BLADES = I2,23X25HNO. OF AZIMUTH STATIONS = I3,
     2       21X21HNO. OF REV. OF WAKE = I2 /9X8HLAMBDA =F12.5,15X4HMU =
     3       F12.5,12X9HALPHA T = F7.3,5H DEG. 11X11HDELTA PSI = F7.3,
     4       5H DEG. //55X5HPSI = F8.3,8H DEGREES )
    3 WRITE(6,1002)J
 1002 FORMAT( /59X12HBLADE NUMBER I2 / )
    4 WRITE(6,1003)(I,X(I,J),Y(I,J),Z(I,J),U(I,J),V(I,J),W(I,J),
     1                GAMA(I,J),A(I,J),I=1,NW1,NPRINT)
 1003 FORMAT( 4X5HSTAT.,10X1HX,14X1HY,14X1HZ,14X2HVX,13X2HVY,13X2HVZ,
     1       10X8HSTRENGTH, 6X9HCORE SIZE /(I8,F19.5,7E15.5) )
      ILINE = ILINE + NW1/MAXO(NPRINT,1)+3
      IF (ILINE.GE.LNCT) ILINE = 0
    5 CONTINUE
      IF(NXPT.EQ.0) GO TO 6
      IF(ILINE.EQ.0)WRITE(6,1000)NB,NA,NRW,XLAM,XMU,ALPHAT,DPSID,PSID
      WRITE(6,1004)(XIPT(I),YIPT(I),ZIPT(I),VX(I),VY(I),VZ(I),I=1,NXPT)
 1004 FORMAT( /53X26HVELOCITIES AT OTHER POINTS //19X1HX,14X1HY,14X1HZ,
     1       14X2HVX,13X2HVY,13X2HVZ/ /(F26.5,5E15.5 ) )
    6 RETURN
      END
```

```
$IBFTC ZZVLCT  LIST,REF
C     HELICOPTER WAKE VORTICITY WITH GROUND EFFECTS - SUBROUTINE VLCTY
      SUBROUTINE VLCTY
      COMMON X(340,5),Y(340,5),Z(340,5),U(340,5),V(340,5),W(340,5),
     1       GAMA(340,5),SEG(340,5),GAMSI(100),AI(100),A(340,5),PI,RAD,
     2        VMP,XMCL,XMSL,NB,NRW,NA,NW,NOPT,NTAPE,NPRINT,NDVCH,PSIO,
     3        XMU,XLAM,ALPHAT,PINT,PSIF,XNA,DPSI,NBI,NWI,XNW,XNB,TPNB,
     4        SAT,CAT,C1,C2,PSI,TPI,XI,T1,T2,XJ,NPS,JPS,IPS,IPS1,XXX,YYY,
     5        ZZZ,IST,IND,IFLG,SIG1,SIG2,SIG3,GGG,DEN,XNU1,XNU2,XNU3,IR1,
     6        XVX,XMY,XMZ,SIG4,SIG5,RR,SQI1,SF,SQI,SG,BF,LPS,SEG1,SEG2,
     7        SUM,LNCT,XIPT(100),YIPT(100),ZIPT(100),VX(100),VY(100),
     8        VZ(100),NXPT,NAB,FACTR,BB,H,WOBAR,SAT2,CAT2,SA2T,CA2T,THCAT
     9        ,THSAT
      DIMENSION GAMB(100)
      EQUIVALENCE(GAMB1,GAMB)
    1 DO 7  I=1,NXPT
      XXX = XIPT(I)
      YYY = YIPT(I)
      ZZZ = ZIPT(I)
      VX(I) = 0.0
      VY(I) = 0.0
      VZ(I) = 0.0
  130 DO 135  LL=1,NB
      XXBR = X(1,LL)*CA2T-Z(1,LL)*SA2T-THSAT
      YYBR = Y(1,LL)
      ZZBR = -(Z(1,LL)*CA2T+X(1,LL)*SA2T+THCAT)
      XXBR1 = X(2,LL)*CA2T-Z(2,LL)*SA2T-THSAT
      YYBR1 = Y(2,LL)
      ZZBR1 = -(Z(2,LL)*CA2T+X(2,LL)*SA2T+THCAT)
      SGBR1 = SQRT((XXX-XXBR)**2+(YYY-YYBR)**2+(ZZZ-ZZBR)**2)
  131 DO 134  IBR=1,NW
      SGBR2 = SQRT((XXX-XXBR1)**2+(YYY-YYBR1)**2+(ZZZ-ZZBR1)**2)
      SEGSQ = SEG(IBR,LL)**2
      HM1 = SGBR1**2+SGBR2**2
      IF (HM1.GT.SEGSQ) GO TO 132
      HM2 = .25*((SGBR1+SGBR2)**2-SEGSQ)*(SEGSQ-(SGBR1-SGBR2)**2)/SEGSQ
      IF (HM2.GT.A(IBR,LL)**2)GO TO 132
      GGG = -GAMA(IBR,LL)/SEG(IBR,LL)
      GO TO 133
  132 GGG = -GAMA(IBR,LL)*(SGBR1+SGBR2)/(SGBR1*SGBR2*((SGBR1+SGBR2)**2
     1       -SEGSQ))
  133 XNU1 = (YYY-YYBR1)*(ZZBR-ZZBR1)-(ZZZ-ZZBR1)*(YYBR-YYBR1)
      XNU2 = (ZZZ-ZZBR1)*(XXBR-XXBR1)-(XXX-XXBR1)*(ZZBR-ZZBR1)
      XNU3 = (XXX-XXBR1)*(YYBR-YYBR1)-(YYY-YYBR1)*(XXBR-XXBR1)
      VX(I) = VX(I)+XNU1*GGG
      VY(I) = VY(I)+XNU2*GGG
      VZ(I) = VZ(I)+XNU3*GGG
      SGBR1 = SGBR2
      XXBR = XXBR1
      YYBR = YYBR1
      ZZBR = ZZBR1
      XXBR1 = X(IBR+2,LL)*CA2T-Z(IBR+2,LL)*SA2T-THSAT
      YYBR1 = Y(IBR+2,LL)
      ZZBR1 = -(Z(IBR+2,LL)*CA2T+X(IBR+2,LL)*SA2T+THCAT)
```

```
  134 CONTINUE
  135 CONTINUE
    2 DO 5  J=1,NB1
      SIG2 = SQRT((XIPT(I)-X(1,J))**2+(YIPT(I)-Y(1,J))**2+(ZIPT(I)-
     1        Z(1,J))**2)
    3 DO 4  K=1,NW
      SIG1 = SIG2
      SIG2 = SQRT((XIPT(I)-X(K+1,J))**2+(YIPT(I)-Y(K+1,J))**2+(ZIPT(I)-
     1        Z(K+1,J))**2)
      SEGSQ = SEG(K,J)**2
      HM1 = SIG1**2+SIG2**2
      IF(HM1.GT.SEGSQ)GO TO 30
      HM2 = .25*((SIG1+SIG2)**2-SEGSQ)*(SEGSQ-(SIG1-SIG2)**2)/SEGSQ
      IF(HM2.GT.A(K,J)**2)GO TO 30
      GGG = GAMA(K,J)/SEG(K,J)
      GO TO 31
   30 GGG = GAMA(K,J)*(SIG1+SIG2)/(SIG1*SIG2*((SIG1+SIG2)**2-SEGSQ))
   31 XNU1 = (YIPT(I)-Y(K,J))*(Z(K,J)-Z(K+1,J))-(ZIPT(I)-Z(K,J))*
     1        (Y(K,J)-Y(K+1,J))
      XNU2 = (ZIPT(I)-Z(K,J))*(X(K,J)-X(K+1,J))-(XIPT(I)-X(K,J))*
     1        (Z(K,J)-Z(K+1,J))
      XNU3 = (XIPT(I)-X(K,J))*(Y(K,J)-Y(K+1,J))-(YIPT(I)-Y(K,J))*
     1        (X(K,J)-X(K+1,J))
      VX(I) = VX(I)+XNU1*GGG
      VY(I) = VY(I)+XNU2*GGG
      VZ(I) = VZ(I)+XNU3*GGG
    4 CONTINUE
    5 CONTINUE
      SIG1 = SQRT(XIPT(I)**2+YIPT(I)**2+ZIPT(I)**2)
      XXBR = -THSAT
      YYBR = 0.0
      ZZBR = -THCAT
      SGBR1 = SQRT((XXX-XXBR)**2+(YYY-YYBR)**2+(ZZZ-ZZBR)**2)
      DO 6  L=1,NB
      LPS = MOD(NBS+(NA*(L-1)))/NB+NAB,NA)
      IF(LPS.EQ.0) LPS = NA
      XXBR1 = X(1,L)*CA2T-THSAT
      YYBR1 = Y(1,L)
      ZZBR1 = -X(1,L)*SA2T-THCAT
      XNU11 = (YYBR-YYY)*(ZZBR1-ZZBR)+(ZZZ-ZZBR)*(YYBR1-YYBR)
      XNU21 = (ZZBR-ZZZ)*(XXBR1-XXBR)+(XXX-XXBR)*(ZZBR1-ZZBR)
      XNU31 = (XXBR-XXX)*(YYBR1-YYBR)+(YYY-YYBR)*(XXBR1-XXBR)
      SGBR2 = SQRT((XXX-XXBR1)**2+(YYY-YYBR1)**2+(ZZZ-ZZBR1)**2)
      GGG1 =GAMB(LPS)*(SGBR1+SGBR2)/(SGBR1*SGBR2*((SGBR1+SGBR2)**2-1.0))
      VX(I) = VX(I)-GGG1*XNU11
      VY(I) = VY(I)-GGG1*XNU21
      VZ(I) = VZ(I)-GGG1*XNU31
      XNU1 = -YIPT(I)*Z(1,L)+ZIPT(I)*Y(1,L)
      XNU2 = -ZIPT(I)*X(1,L)+XIPT(I)*Z(1,L)
      XNU3 = -XIPT(I)*Y(1,L)+YIPT(I)*X(1,L)
      SIG2 = SQRT((XIPT(I)-X(1,L))**2+(YIPT(I)-Y(1,L))**2+(ZIPT(I)-
     1        Z(1,L))**2)
      DEN = SIG1*SIG2*((SIG1+SIG2)**2-1.0)
      IF(DEN.EQ.0.0) DEN = .001
```

```
      GGG = GAMP1(LPS)*(SIG1+SIG2)/DEN
      VX(I) = VX(I)+XNU1*GGG
      VY(I) = VY(I)+XNU2*GGG
      VZ(I) = VZ(I)+XNU3*GGG
    6 CONTINUE
      VX(I) = VX(I)+XMCL
      VZ(I) = VZ(I)-XMSL
    7 CONTINUE
      RETURN
      END
```

REFERENCES

1. Brady, W. G. and Crimi, P. Representation of Propeller Wakes by Systems of Finite Core Vortices Cornell Aeronautical Laboratory Report No. BB-1665-S-2 (ONR Contract Nonr 3691(00) February 1965 DDC No. AD 612007

2. Trenka, A. R. Development of a Method for Predicting the Performance and Stresses of VTOL-Type Propellers USAAVLABS TR 66-26 Cornell Aeronautical Laboratory Report No. BB-1846-S-1 1966 DDC No. AD 635-951

3. Crimi, P. Theoretical Prediction of the Flow in the Wake of a Helicopter Rotor Part I - Development of Theory and Results of Computations Cornell Aeronautical Laboratory Report No. BB-1994-S-1 September 1965 DDC No. AD 629-782

4. Crimi, P. Theoretical Prediction of the Flow in the Wake of a Helicopter Rotor Part II - Formulation and Application of the Rotor-Wake-Flow Computer Program Cornell Aeronautical Laboratory Report No. BB-1994-S-2 September 1965 DDC No. AD 629-783

5. Piziali, R. A. and DuWaldt, F. A. A Method for Computing Rotary Wing Air Load Distribution in Forward Flight Cornell Aeronautical Laboratory Report BB-1495-S-1 TCREC TR 62-44 November 1962

6. Fradenburgh, E. A. Flow Field Measurements for a Hovering Rotor Near the Ground Paper presented at AHS 5th Annual Western Forum, Los Angeles, California September 25-26 1958

7. Payne, P. R. Helicopter Dynamics and Aerodynamics MacMillan New York 1959

8. Burpo, F. and Lynn, R. Measurement of Dynamic Air Loads on a Full-Scale Semirigid Rotor TCREC TR62-42 December 1962

9. McCloud, J. and Biggers, J. Full-Scale Wind-Tunnel Tests of a Medium-Weight Utility Helicopter at Forward Speeds NASA TN D-1887 May 1963

10. Lamb, H. Hydrodynamics Sixth Edition Dover, New York 1945

11. Durand, W. F. Aerodynamic Theory Volume II Page 329 Dover, New York 1963

UNCLASSIFIED

Security Classification

DOCUMENT CONTROL DATA - R&D

(Security classification of title, body of abstract and indexing annotation must be entered when the overall report is classified)

1. ORIGINATING ACTIVITY (Corporate author) Cornell Aeronautical Laboratory, Inc. Buffalo, New York 14221	2a. REPORT SECURITY CLASSIFICATION Unclassified 2b GROUP

3. REPORT TITLE

Wakes of Lifting Propellers (Rotors) in Ground Effect

4. DESCRIPTIVE NOTES (Type of report and inclusive dates)

Final Report, February 1965 - May 1966

5. AUTHOR(S) (Last name, first name, initial)

DuWaldt, F. A.

6. REPORT DATE	7a. TOTAL NO. OF PAGES	7b. NO. OF REFS
November 1966	92	11

8a. CONTRACT OR GRANT NO.	9a. ORIGINATOR'S REPORT NUMBER(S)
Nonr 3691(00) b. PROJECT NO. RF012-01-01 c. NR 212-163 d.	BB-1665-S-3 9b. OTHER REPORT NO(S) (Any other numbers that may be assigned this report)

10. AVAILABILITY/LIMITATION NOTICES

Distribution of this document is unlimited.

11. SUPPLEMENTARY NOTES	12. SPONSORING MILITARY ACTIVITY
	Office of Naval Research Air Programs, Naval Applications Group Washington, D. C. 20360

13. ABSTRACT

This is a summary report that presents the development of a wake model for a lifting propeller (rotor) in ground effect and the computational procedure used to determine the spacial distribution of wake vorticity and the induced velocity field accompanying that vorticity distribution.

Sample calculations for a two-bladed rotor were carried out on an IBM 7044 computer. Locations of wake vortical elements and the associated induced velocities at selected field points are presented for advance ratios of 0, 0.02, 0.05, and 0.10 for an H/R (ratio of rotor height above ground to rotor radius) of 1.0. Also, a few results for a hovering case with H/R = 0.5 are presented. A calculated root-mean-square velocity map is compared with measured hovering data (time averaged) and good agreement is obtained in the outer half of the slipstream. The implications of computed results with respect to the flow field at a horizontal stabilizer or tail rotor are noted as examples of the use of the model.

The wake vortex model used for these calculations is a distorted continuous helix emanating from each blade tip. For purposes of numerical calculation of mutual vortex interference effects, the continuous vortex is approximated by short straight-line filaments. For purposes of numerical calculation of self-induced effects (that is, the effect of an element on itself), the local element curvature and the core diameter are estimated. The Fortran statements of the computer program are presented in the Appendix.

DD FORM 1 JAN 64 1473

UNCLASSIFIED

Security Classification

14. KEY WORDS	LINK A		LINK B		LINK C	
	ROLE	WT	ROLE	WT	ROLE	WT
Fluid mechanics Aerodynamics Propellers Rotors Vortices Wake						

INSTRUCTIONS

1. ORIGINATING ACTIVITY: Enter the name and address of the contractor, subcontractor, grantee, Department of Defense activity or other organization *(corporate author)* issuing the report.

2a. REPORT SECURITY CLASSIFICATION: Enter the overall security classification of the report. Indicate whether "Restricted Data" is included. Marking is to be in accordance with appropriate security regulations.

2b. GROUP: Automatic downgrading is specified in DoD Directive 5200.10 and Armed Forces Industrial Manual. Enter the group number. Also, when applicable, show that optional markings have been used for Group 3 and Group 4 as authorized.

3. REPORT TITLE: Enter the complete report title in all capital letters. Titles in all cases should be unclassified. If a meaningful title cannot be selected without classification, show title classification in all capitals in parenthesis immediately following the title.

4. DESCRIPTIVE NOTES: If appropriate, enter the type of report, e.g., interim, progress, summary, annual, or final. Give the inclusive dates when a specific reporting period is covered.

5. AUTHOR(S): Enter the name(s) of author(s) as shown on or in the report. Enter last name, first name, middle initial. If military, show rank and branch of service. The name of the principal author is an absolute minimum requirement.

6. REPORT DATE: Enter the date of the report as day, month, year, or month, year. If more than one date appears on the report, use date of publication.

7a. TOTAL NUMBER OF PAGES: The total page count should follow normal pagination procedures, i.e., enter the number of pages containing information.

7b. NUMBER OF REFERENCES: Enter the total number of references cited in the report.

8a. CONTRACT OR GRANT NUMBER: If appropriate, enter the applicable number of the contract or grant under which the report was written.

8b, 8c, & 8d. PROJECT NUMBER: Enter the appropriate military department identification, such as project number, subproject number, system numbers, task number, etc.

9a. ORIGINATOR'S REPORT NUMBER(S): Enter the official report number by which the document will be identified and controlled by the originating activity. This number must be unique to this report.

9b. OTHER REPORT NUMBER(S): If the report has been assigned any other report numbers *(either by the originator or by the sponsor)*, also enter this number(s).

10. AVAILABILITY/LIMITATION NOTICES: Enter any limitations on further dissemination of the report, other than those imposed by security classification, using standard statements such as:

(1) "Qualified requesters may obtain copies of this report from DDC."

(2) "Foreign announcement and dissemination of this report by DDC is not authorized."

(3) "U. S. Government agencies may obtain copies of this report directly from DDC. Other qualified DDC users shall request through _____."

(4) "U. S. military agencies may obtain copies of this report directly from DDC. Other qualified users shall request through _____."

(5) "All distribution of this report is controlled. Qualified DDC users shall request through _____."

If the report has been furnished to the Office of Technical Services, Department of Commerce, for sale to the public, indicate this fact and enter the price, if known.

11. SUPPLEMENTARY NOTES: Use for additional explanatory notes.

12. SPONSORING MILITARY ACTIVITY: Enter the name of the departmental project office or laboratory sponsoring *(paying for)* the research and development. Include address.

13. ABSTRACT. Enter an abstract giving a brief and factual summary of the document indicative of the report, even though it may also appear elsewhere in the body of the technical report. If additional space is required, a continuation sheet shall be attached.

It is highly desirable that the abstract of classified reports be unclassified. Each paragraph of the abstract shall end with an indication of the military security classification of the information in the paragraph, represented as *(TS), (S), (C), or (U).*

There is no limitation on the length of the abstract. However, the suggested length is from 150 to 225 words.

14. KEY WORDS. Key words are technically meaningful terms or short phrases that characterize a report and may be used as index entries for cataloging the report. Key words must be selected so that no security classification is required. Identifiers, such as equipment model designation, trade name, military project code name, geographic location, may be used as key words but will be followed by an indication of technical context. The assignment of links, rules, and weights is optional.